A Cumulants Approach To Studying Quantum Advantage

Masterarbeit

zur Erlangung des akademischen Grades
Master of Science
(MSc)

eingereicht an der
Fakultät für Mathematik, Informatik und Physik
der Universität Innsbruck

von
Johannes Kerber, BSc

Hauptbetreuer:
Univ.-Prof. Dr. Helmut Ritsch
Zweitbetreuer:
Dr. Laurin Ostermann

Institut für Theoretische Physik
Innsbruck, 20.August, 2024

Abstract

The fundamental theorem of arithmetic states that every integer larger than one can be uniquely represented as a product of prime numbers. The procedure of finding these prime numbers is called factorization. In contrast to multiplication the factorization problem is challenging to solve. The reason is probably its NP-complete nature, which remains to be proven. Especially, the factors of bi-primes, which can be represented as a product of two primes, are very difficult to determine. Indeed, the most powerful supercomputer with the most efficient classical factorization algorithm is incapable of solving the factorization problem for sufficiently large bi-primes. This is due the fact that all known non-quantum factorization algorithms possess exponential time-complexity-growth. Hence, the factorization procedure is of great interest in the field of encryption. The factoring-based encryption methods, referred to as RSA-cryptosystems, follow a simple but powerful procedure which will be discussed in more detail later.

In this thesis we first consider the bi-prime factorization problem as an optimization problem in binary representation. Harvesting quantum mechanics, we exchange the classical bits with qubits. This allows us to translate the classical optimization problem into a quantum mechanical one, which provides a factorization Hamiltonian. We use quantum annealing based on the adiabatic transfer from an initial Hamiltonian to the factorization Hamiltonian to solve the problem. Measurements on the classical bits described by quantum mechanical observables solve the bi-prime factorization problem and give the correct factors, i.e., the correct prime numbers. This is true for certain adiabatic conditions. We compute the correct factors for multiple different cases. We also find a bi-prime, where the factors cannot be determined with high probability. Increasing the adiabatic evolution-time of the quantum annealing process results in worse solutions.
The larger the bi-prime, the higher the count of qubits which manifests in an increase of computation time. Approximating the full quantum dynamics by utilizing the Ehrenfest theorem together with the so-called generalized cumulant expansion method can reduce the computation time. The Ehrenfest theorem is used to obtain a system of non-autonomous nonlinear and coupled ordinary differential equations (ODEs) in first order consisting of averages with orders from one up to infinity. An average of order n is the average of the product of n considered observables. The cumulant expansion is utilized to truncate the Ehrenfest ODE system and simultaneously provides a way to discard certain or all quantum dynamical correlations. The latter is the first-order cumulant expansion and known

as mean-field expansion. The mean-field expansion is expected to produce a quantum advantage for the bi-prime factorization problem. Indeed, the mean-field approach, which we call the first-order cumulant approach, reveals features, which can be understood as hints for a possible quantum advantage. The mean-field expansion provides the correct solutions for very small bi-primes as fast as the full quantum dynamics. However, increasing the bi-primes shows that the mean-field expansion requires a longer adiabatic evolution-time to acquire the correct factors. For the largest investigated bi-prime the correct solution is never found using the first-order expansion but the results give a hint that using a sufficiently long evolution-time should provide the correct factors. Since the generalized cumulant expansion method is used, it is possible to allow certain quantum correlations. This is achieved by increasing the expansion order. We assume that the higher-order expansions approach more and more the full quantum dynamics, which is reached at orders equal to or higher the total bit-number of the bi-prime. The assumption turns out to be false, since one receives divergent solutions for these expansion orders. The origins of the divergences are not clear. We introduce a thorough discussion, where these divergences possibly come from.

Zusammenfassung

Der Fundamentalsatz der Arithmetik besagt, dass jede natürliche Zahl größer Eins eindeutig als Produkt von Primzahlen geschrieben werden kann. Dieses Produkt wird als Primfaktorzerlegung bezeichnet und wir nennen das Procedere, welches die korrekten Primzahlen bestimmt, das Faktorisierungsverfahren. Im Gegensatz zur Multiplikation wird das Faktorisieren von natürlicher Zahlen mit Anwachsen der Zahlengröße sehr herausfordernd, da es wahrscheinlich NP-complete ist. Dies gilt noch zu beweisen. Besonders schwierig ist das Faktorisieren von Fastprimzahlen zweiter Ordnung, auch Semiprimzahlen genannt. Solch eine Zahl kann nur als Produkt von zwei Primzahlen repräsentiert werden. Für genügend große Semiprimzahlen wird das Faktorisieren immens aufwendig, sodass die Berechnung der Faktoren sogar für den besten klassischen Faktorisierungsalgorithmus auf dem stärksten Supercomputer zeit-technisch impraktikabel ist. Dies ist der Fall, weil alle klassischen Faktorisierungsalgorithmen eine exponentiell anwachsende Zeitkomplexität besitzen. Daher ist das Semiprimzahlfaktorisierungsverfahren von großem Interesse für Internetkryptographie. Die Verschlüsselungsmethoden werden RSA-Verschlüsselungen genannt und basieren auf ein einfaches, aber sehr mächtiges, Verfahren, welches später detaillierter besprochen wird.

In dieser Arbeit betrachten wir das Semiprimzahlfaktorisierungsproblem zunächst als Optimierungsproblem in Binärdarstellung und übersetzen dieses dann anschließend in die Quantenmechanik. Dafür werden die klassische Bits mit Qubits ausgetauscht. Somit erhalten wir von einem klassischen ein quantenmechanisches Optimierungsproblem, welches durch einen Faktorisierungshamiltonian beschrieben wird. Wir setzten Quantum Annealing in Form eines adiabatischen Transfers von einem Anfangshamiltonian in den Faktorisierungshamiltonian um. Dies löst anschließend das Semiprimzahlfaktorisierungsproblem. Die klassischen Bits werden dann über Messungen entsprechender Observablen bestimmt. Diese Messungen liefern die korrekten Bits unter speziellen adiabatischen Voraussetzungen. Die richtigen Faktoren werden für verschiedene Semiprimzahlen bestimmt. Wir besprechen ebenfalls eine Semiprimzahl, wo die Lösungen nicht mit großer Wahrscheinlichkeit bestimmt werden können und diese sogar abnimmt, wenn die adiabatischen Evolutionszeit des Quantum-Annealing-Prozesses verlängert wird.
Es gilt, je größer die Semiprimzahl, desto größer die Zahl von Qubits. Das wirkt sich enorm auf die Berechnungszeit aus. Wir approximieren die volle Quantendynamik, indem das Ehrenfest Theorem zusammen mit der verallgemeinerten Kumulantenentwicklung

umgesetzt wird. Dies reduziert die Berechnungszeit. Das Ehrenfest Theorem kann verwendet werden, um ein nicht-autonomes nichtlineares gekoppeltes gewöhnliches Differentialgleichungssystem (GDGL System) erster Ordnung zu erhalten, wo die Variablen durch Erwartungswerte von erster bis unendlicher Ordnung gegeben sind. Ein Erwartungswert n-ter Ordnung bezeichnet den Erwartungswert des Produkts von n zu untersuchenden Observablen. Die Kumulantenentwicklung stellt eine Möglichkeit zur Verfügung, das Ehrenfest System auf eine gewisse Größe zu reduzieren und somit bestimmte oder alle quantendynamischen Korrelationen zu vernachlässigen. Das Letztere ist die Kumulantenentwicklung 1. Ordnung und wird als die Molekularfeldnäherung (mean-field approach) bezeichnet. Diese Näherung wird verwendet, um die Existenz eines möglichen Quantenvorteils nachzuweisen. In der Tat weisen die Lösungen der Molekularfeldnäherung bestimmte Eigenschaften auf, welche auf einen Quantenvorteil für das Semiprimzahlenfaktorisierungsproblem hindeuten. Die Molekularfeldlösungen geben die korrekten Faktoren für sehr kleine Semiprimzahlen gleich schnell wie die volle Quantendynamik, jedoch benötigt das klassische Verfahren für größer werdenden Zahlen längere Evolutionszeiten. Für die größte untersuchte Semiprimzahl wurden keine korrekten Faktoren gefunden. Aber man findet den Hinweis, dass für hinreichend große Zeiten die richtige Lösung erlangt werden sollte. Weil wir die verallgemeinerte Kumulantenentwicklung verwenden, können wir mit steigender Ordnung mehr und mehr Quantenkorrelationen in die Lösung mit einfließen lassen. Wir nehmen an, dass die Lösung bei einer Zunahme der Entwicklungsordnung sich mehr und mehr der vollen Quantendynamik, welche für Entwicklungsordnungen größer gleich der Anzahl der totalen Bit-Zahl oder höher entspricht, annähert. Es stellt sich heraus, dass die Annahme nicht zutrifft, da für die meisten Semiprimzahlen divergierende Lösungen erhalten werden. Der Ursprung der Divergenzen ist nicht klar. Daher führen wir eine genaue Besprechung und Analyse der auftretenden Divergenzen durch.

Danksagung

Zunächst möchte ich mich bei meinen Eltern, meinen Schwestern und meinem Bruder bedanken, die mich stets bei meinen Entscheidungen und auf meinem Lebensweg unterstützt haben. Ohne sie wäre mein Studium nicht möglich gewesen. Dafür bin ich ihnen unendlich dankbar. Auch bedanke ich mich beim Rest meiner Familie, der mich stetig unterstützt.

Besonderen Dank gebührt meinem Betreuer Prof. Helmut Ritsch, der mir die Arbeit über dieses spannende Thema überhaupt ermöglichte und der mit seinen hilfreichen Ideen und Ansätzen den Fortschritt der Arbeit garantierte.

Auch möchte ich mich bei den Mitgliedern der Arbeitsgruppe bedanken, die mich sehr herzlich aufgenommen und unterstützt haben. Insbesondere möchte ich mich bei Laurin Ostermann und Elias A. Starchl bedanken, die mir stets bei der Lösungsfindung von Problemen zur Seite standen und mich mit ihren sehr lehrreichen Antworten auf meine Fragen bereicherten.

Abschließend bedanke ich mich bei meinen wundervollen Freunden. Speziellen Dank gebührt meinen Freunden, die mir bereits von klein auf zur Seite stehen. Ohne sie wäre dieser Lebensweg ebenfalls nicht möglich gewesen. Auch bedanke ich mich bei meinen Freunden, welche ich während des Studiums kennen gelernt habe. Ohne ihre Motivation und Begeisterung wäre das Studium nur halb so unterhaltsam gewesen.

Contents

Chapter 1

Introduction

It is claimed, that *Carl Friedrich Gauß* once said [1]:

> Mathematics is the queen of the sciences - and number theory is the queen of mathematics.

Number theory, more commonly known under its older name arithmetic, is a branch of pure mathematics. It is referred to as the study of integers and arithmetic functions. The fundamental theorem of arithmetic states, that every positive integer larger than one can be represented uniquely as a product of prime numbers [2, 3]. These integers are called composite. It is well-known that multiplication of given factors to a product can be done rather easily, whereas the factorization of a product into its factors is difficult. To obtain the factors for small integers it is enough to use pencil and paper. We can utilize classical factoring-algorithms, e.g. sieve of Eratosthenes, Fermat's or Euler's factorization method, to determine the factors of large integers [4, 5, 6]. However, if the integers under consideration are sufficiently large the known classical algorithms become exponentially slower and we need quantum algorithms, e.g., Shor's algorithm [7], introduced by Peter Shor in 1994, to receive the factors with polynomial growth of time. Indeed, all known classical factoring-algorithms possess an exponentially growing time complexity, whereas Shor's algorithm scales polynomially. Not all factorization problems are equally hard to solve. A particularly difficult one is the bi-prime factorization. Bi-primes are composite integers which can be represented by two prime numbers. In the case of the prime numbers being large, randomly chosen and of similar size but not too close for Fermat's factorization method [5] to be efficient, the factorization of the product can be unfeasible for even the fastest classical prime factoring algorithm executed on the fastest classical computer. This knowledge provides a perfect starting point to develop factoring-based encryption methods such as RSA key encryption or RSA digital signature [8]. RSA encryption methods are widely utilized, e.g., Internet encryption such as SSH-RSA key encryption for secure access of remote servers. The procedure is the following [9]. Two large prime numbers a and b with large differences are chosen randomly and are kept secret. These numbers are then

multiplied with each other which provides a bi-prime ω. This bi-prime ω is released as part of the public key. Inserting ω into Carmichael's totient function gives an integer $\lambda(\omega)$ which is kept secret. An integer e is released as another part of the public key, where $1 < e < \lambda(\omega)$ and $\gcd(e, \lambda(\omega)) = 1$. The numbers $e, \lambda(\omega)$ are called coprimes. Furthermore, d is the modular multiplicative inverse, which is kept secrete as the private key exponent. Quantum algorithms could render RSA encryption methods useless. Since the discovery of Shor's algorithm, physicists have tried to find more efficient quantum algorithms to solve the bi-prime factorization problem [10]. Especially, quantum algorithms running on an adiabatic quantum computer [11] are promising, because the principle of adiabatic quantum computation could be more attainable in near future. Some examples are given in [12, 13].

An interesting question is now, whether one can find a quantum advantage for the bi-prime factorization problem using an annealing approach. Thus, one should derive a classical algorithm based on a well-known quantum algorithm [12, 13] for the factorization problem and compare the performance between the two algorithms. If the quantum algorithm provided the factors faster than the classical one, we would see a quantum advantage. For an adiabatic quantum algorithm, the full quantum dynamics can be obtained by using the time-dependent Schrödinger equation [14]. This can be transformed into a quantum inspired classical algorithm by using mean-field methods or higher order cumulant expansions. Therefore, we utilize Ehrenfest's theorem [15] as well as the generalized cumulant expansion method [16]. These two methods are implemented in a package called *QuantumCumulants.jl* [17] in the programming language *Julia*. We utilize QuantumCumulants.jl to derive the classical solutions for different bi-primes and undergo a thorough examination of the results. The solutions are the measurements of later defined projectors, thus, the results of both classical and quantum algorithms are classical. However, for clarity, we refer to the solution of the classical algorithm as the classical solution. To discard all quantum mechanical effects, we expand the problem in the first-order of the generalized cumulant expansion method. The full quantum dynamics is obtained by using the package QuantumOptics.jl [18]. Indeed, comparing the first-order cumulant expansion solution with the results utilizing the full quantum dynamics provides hints for a possible quantum advantage. Since we can increase the order of expansion, we can permit more and more quantum correlations until we end up at the full quantum-dynamical description. The full quantum dynamics is reached at the expansion order which is equal or larger the total number of qubits. The results are, in a sense, investigations of a domain where quantum effects appear. We acquire results, which need to be examined more carefully. Considering bi-primes and adiabatic evolution-times, where correct factors are obtained by both the classical and the quantum algorithm, the solutions evolve divergent oscillations. We found two exceptions which we discuss in this thesis as well. We call the expectation values of the projectors of a given solution divergent if the expectation values are much larger than one or much smaller than zero. These are the boundaries that label the results as physical reasonable.

Chapter 2

Theoretical Concepts

In this chapter we introduce all the fundamental theoretical concepts and frameworks which are necessary to formulate the mathematical bi-prime factorization problem in classical as well as full quantum-mechanical terms.

First, we introduce the concept of bi-primes. We continue by describing the bi-prime factorization as an optimization problem. Afterwards, the optimization is being translated into a quantum-mechanical framework. The properties of quantum mechanics are harnessed by describing the problem in terms of qubits. The adiabatic theorem provides a full quantum dynamical description to receive the correct factors of a given bi-prime by using Schrödinger's equation. In chapter 3, we observe that for most of the investigated bi-primes the factors are correct, but the bi-prime 95 reveals an unsual behavior that results in providing the wrong factors. We examine this case further by utilizing the entropy of entanglement and the bipartite quantum mutual information. Afterwards, we introduce the cumulants approach, which allows to obtain a classical approximation of the full quantum dynamics. The formulation of the cumulants approach requires the discussion of the Ehrenfest theorem, the generalized cumulant expansion method as well as a short introduction to QuantumCumulants.jl.

For the entire discussion, we set $\hbar = 1$, where $\hbar$ denotes the reduced Planck's constant.

2.1 The Factorization Problem

The fundamental theorem of arithmetic states that every integer larger than 1 can be factorized and represented uniquely by a product of two or more prime numbers [2, 3]. To acquire the respective prime numbers of a given integer, one needs special procedures generally known as prime factorization methods. In the following subsection 2.1.1 we introduce a mathematical formulation for describing bi-primes.

2.1.1 Bi-primes

We consider a bi-prime $\omega \in \mathbb{N}$ with $\omega = ab$, where a and b are prime numbers. The binary representation [19] is a simple way to describe ω as a sum of $n \in \mathbb{N}$ terms of shape $\omega_m 2^m$ where $\omega_m \in \{0, 1\}$ and $m \in \{0, 1, \cdots, n-1\}$. The values ω_m are called binary-digits or bits. Here, n is the number of terms necessary to construct the value ω. We call n the total number of bits. Let ω be a n-bit integer, then, the binary representation of ω has the shape

$$\omega = \sum_{m=0}^{n-1} \omega_m 2^m. \tag{2.1}$$

Thus, the integer ω can be written as $\omega = [\omega_{n-1} \cdots \omega_1 \omega_0]$ in a short way. The two primes a and b possess total bit numbers $k, l \in \mathbb{N}$, respectively, such that $\omega = ab$. The binary representations are given by

$$a = \sum_{i=0}^{k-1} a_i 2^i \qquad\qquad b = \sum_{j=0}^{l-1} b_j 2^j, \tag{2.2}$$

where $a_i, b_j \in \{0, 1\}$. The bi-prime relation is given by

$$\omega = \sum_{m=0}^{n-1} \omega_m 2^m = \sum_{i=0}^{k-1} \sum_{j=0}^{l-1} a_i b_j 2^{i+j} = ab. \tag{2.3}$$

It is clear, that the total bit-number of ω is either $n = k + l$ or $n = k + l - 1$ (This applies if the largest bit-digit of ω fulfills $\omega_{n-1} = 0$). The bit-digits a_i, b_j can be determined by describing the problem as an optimization problem. This is done in subsection 2.1.2. For the sake of convenience, we consider for further investigations only $n = k + l$ and $k > n/2$. The partition $(k, l = n - k)$ is usually not known in advance. For an arbitrary integer the correct value of k lies somewhere in the domain $[n/2 + 1, \cdots, n]$ [12]. Since we want to find a quantum advantage for the bi-prime factorization problem, we consider only primes, where k and l are already known.

2.1.2 Factorization as an Optimization Problem

In mathematics, optimization is a tool for finding extrema of a specific function $f(\mathbf{x})$ by varying the entries x_i of $\mathbf{x} = (x_1, x_2, \cdots, x_n) \in \mathbb{R}^n$, where $\mathbf{x}$ is referred to as an event and x_i are called decision variables [20]. We call $f(\mathbf{x})$ a cost function if the wanted extrema are minima. The optimization problem of $f(\mathbf{x})$ is often considered as a decision problem. The

event is then a function of difference between estimated and true values. Optimization can be used, e.g., for parameter estimation. This allows to determine the correct bit-configurations of a and b to solve the bi-prime factorization problem.

We start with the optimization problem by considering the integers in decimal representation. The natural equation $\omega = ab$ provides an ideal form for defining a cost function for bi-prime factorization. Let f_ω be the cost function, where ω denotes the examined bi-prime. We know, that $\omega - ab = \omega - ba = 0$. It would be convenient to find a cost function f_ω, that possesses minima for the tuples (a, b) and (b, a). Fortunately, we can define:

$$\begin{aligned} f_\omega : \mathbb{N}^2 &\to \mathbb{N} \\ (x, y) &\mapsto (\omega - xy)^2. \end{aligned} \tag{2.4}$$

The square in Equation 2.4 ensures that $f_\omega(x, y)$ is non-negative. This is a convention of cost functions [20]. The global minima can mathematically be derived by

$$\nabla f_\omega \stackrel{!}{=} 0 \implies (x, y) = (a, b) \wedge (x, y) = (b, a). \tag{2.5}$$

Hence, f_ω vanishes at the global minima and fulfills exactly the condition above. The plot in Figure 2.1 visualizes this for the example $\omega = 15$.

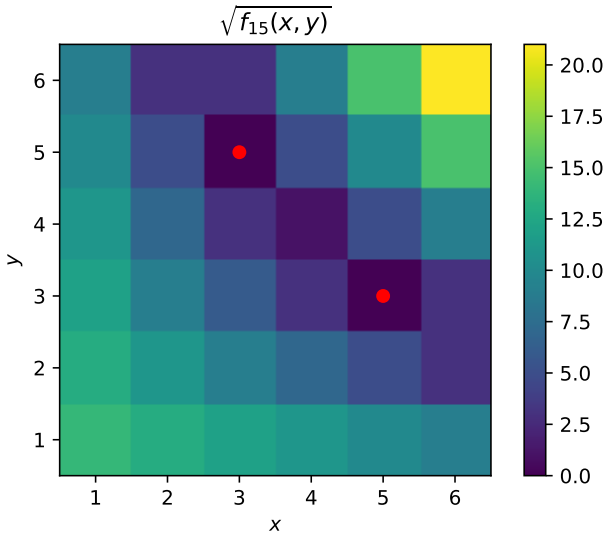

Figure 2.1: Determination of the minima of $f_{15}(x, y) = (15 - xy)^2$ indirectly by visualizing $\sqrt{f_{15}(x, y)}$. The red dots indicate the locations of the minima, i.e., $(x, y) = (3, 5) \wedge (x, y) = (5, 3)$, thus, the solutions for $15 = ab$. The colormap shows $\sqrt{f_{15}(x, y)}$.

The specific form of $f_\omega(x, y)$ is also known as *quadratic loss function*. The factorization of bi-primes is now described as an optimization problem. Since our goal is to harness the properties of quantum mechanics, we want to describe the optimization problem to determine the correct factors a and b using qubits instead of classical bits. This requires the classical cost function to be in terms of classical bits, which can be acquired by considering the integers now in binary representation introduced in subsection 2.1.1. The bi-prime relation reads

$$\omega[\omega_{n-1} \cdots \omega_1 \omega_0] = a[a_{k-1} \cdots a_1 a_0] \cdot b[b_{l-1} \cdots a_1 b_0], \tag{2.6}$$

where $k > n/2 > l$. This implies that only the lower triangular part in Figure 2.1 is important for the discussion in this thesis. The solution is always unique. We can write Equation 2.4 in terms of the bit-digits of a and b:

$$f_\omega(a_0, a_1, \cdots, a_{k-1}, b_0, b_1, \cdots, b_{l-1}) = (\omega - a(a_0, a_1, \cdots, a_{k-1}) \cdot b(b_0, b_1, \cdots, b_{l-1}))^2, \tag{2.7}$$

where we have now n unknown bit-digits. Minimizing Equation 2.7 provides the correct bit-configurations for a and b, hence, solves the bi-prime factorization problem. In section 2.2 we show how the classical optimization problem can be translated into a quantum theoretical model with quantum bits of information.

2.2 Adiabatic Quantum Computation

It is clear, that the optimization problem in subsection 2.1.2 is non-trivial to solve. The fundamental idea of solving the bi-prime factorization problem is to transform the cost function in Equation 2.4 into a quantum mechanical object which can be solved by utilizing the principle of adiabatic quantum computation (AQC) [11]. It provides a way to obtain the, e.g. , ground state of a difficult problem Hamiltonian by using the adiabatic theorem of quantum mechanics. The bi-prime factorization problem in quantum mechanics is a quantum algorithm suited to run on an adiabatic quantum computer. A process of solving an optimization problem by utilizing quantum mechanics is called quantum annealing. This is introduced more precisely in subsection 2.2.2. First, we want to discuss the adiabatic theorem in subsection 2.2.1.

2.2.1 Adiabatic Theorem

The statement of the adiabatic theorem was originally expressed by M. Born and V. Fock in their general proof of the theorem [21] in 1928:

> A physical system remains in its instantaneous eigenstate if a given perturbation is acting on it slowly enough and if there is a gap between the eigenvalue and the rest of the Hamiltonian's spectrum.

Since the considered initial and target Hamiltonians are time-independent, we discuss the adiabatic theorem only for this case. However, we keep in mind that a general description exists [21]. Let $\hat{H}_\mathrm{p}$ be the time-independent Hamiltonian of a physical system under consideration, e.g., a system of n qubits on a 2^n-dimensional Hilbert space $\mathcal{H} \cong \mathbb{C}^{2^n}$, where the eigenstates are unknown. We introduce another time-independent initial Hamiltonian $\hat{H}_0$ on the same Hilbert space $\mathcal{H}$. The eigenenstates and eigenenergies of $\hat{H}_0$ are well-known. We can define a time-dependent Hamiltonian $\hat{H}(t)$ with $t \in [0, T]$ of the shape

$$\hat{H}(t) = \left(1 - \frac{t}{T}\right) \hat{H}_0 + \left(\frac{t}{T}\right) \hat{H}_\mathrm{p} \tag{2.8}$$

$$\hat{H}(s) = (1 - s)\, \hat{H}_0 + s\hat{H}_\mathrm{p}, \qquad s \equiv \frac{t}{T}, s \in [0, 1] \tag{2.9}$$

such that a smooth transition from the initial Hamiltonian $\hat{H}_0$ to the target Hamiltonian $\hat{H}_\mathrm{p}$ is possible. The parameter T denotes the evolution time. Let a time-dependent state $|\psi(t)\rangle \in \mathcal{H}$ be given. The state $|\psi(t)\rangle$ is governed by the time-dependent Schrödinger equation. We assume $|\psi(0)\rangle = |\mathrm{GS}_0\rangle$, where $|\mathrm{GS}_0\rangle$ denotes the ground state of $\hat{H}_0$. According to the adiabatic theorem, the state fulfills $|\psi(T)\rangle \approx |\mathrm{GS}_p\rangle$ with $|\mathrm{GS}_p\rangle$ being the ground state of $\hat{H}_\mathrm{p}$ if the following two conditions are valid. The overall evolution time T is large enough, such that $\hat{H}(t)$ is slowly varying and if there exists a gap larger than 0 between the ground state energy and the rest of the Hamiltonian's spectrum. These two conditions

for $\hat{H}(t)$ prevent the system to undergo a transition from the ground state to an excited state. We want to discuss the statement of the adiabatic theorem more thoroughly.

A time-dependent eigenstate $|\psi(t)\rangle$ of a Hamiltonian $\hat{H}(t)$, acting on a N-dimensional Hilbert space, is subject to the following Schrödinger equation:

$$\hat{i}\frac{d}{dt}|\psi(t)\rangle = \hat{H}(t)|\psi(t)\rangle, \tag{2.10}$$

where $\hat{i}$ denotes the imaginary unit. We define $s = t/T$ and introduce the instantaneous eigenstates and eigenvalues

$$\hat{H}(s)|\phi_i(s)\rangle = E_i(s)|\phi_i(s)\rangle, \tag{2.11}$$

where $E_0(s) \leq E_1(s) \leq \cdots \leq E_{N-1}(s)$. We assume $|\psi(0)\rangle = |\phi_0(0)\rangle$, hence, $|\psi(0)\rangle$ is instantaneously in the ground state of $\hat{H}(0)$ and s is varying sufficiently slowly. Then, the adiabatic theorem states if $\exists \Delta E_1(s) = |E_1(s) - E_0(s)| > 0, \forall s \in [0,1]$, the following is valid [11]:

$$\lim_{T\to\infty} |\langle\phi_0(s=1)|\psi(T)\rangle| = 1. \tag{2.12}$$

The state $|\psi(t)\rangle$ remains very close to the instantaneous ground states of $\hat{H}(t)$. This allows to derive the validity condition for arbitrary states [14]:

$$R(T) = \frac{\max_{s\in[0,1]} |\overbrace{\langle\phi_j(s)|\left(\partial_s|\phi_i(s)\rangle\right)}^{\substack{\text{measure of speed of rotation}\\ \text{of eigenvectors in } \mathcal{H}}}|}{\Delta_{\min}}\frac{1}{T} = \frac{\max_{s\in[0,1]} |\langle\phi_j(s)|\partial_s\hat{H}(s)|\phi_i(s)\rangle|}{\Delta_{\min}^2}\frac{1}{T} \ll 1, \tag{2.13}$$

where $\Delta_{\min} = \min_{\substack{s\in[0,1]\\ i\neq j}} |E_i(s) - E_j(s)|$ quantifies the minimal gap. In Equation 2.13 we can see that $R(T)$ possesses an $1/T$ proportionality. This allows us to estimate the domain for T where the adiabatic theorem is valid. The application is performed in chapter 3.

2.2.2 Quantum Annealing

The optimization process of obtaining an ideal parameter result by utilizing quantum physics in the form of an energy minimization problem is widely used and finds application in many different areas such as natural sciences, economics or technologies [22, 23, 24]. This is called quantum annealing. Here, one prepares all (candidate) states usually in a ground state consisting of states in superposition of equal weight. The state is then evolved by using the adiabatic theorem (see subsection 2.2.1) which results in receiving the ground state of a problem under consideration [11].

In our discussion we employ the classical bi-prime factoring optimization problem and translate it into a quantum-mechanical framework. Therefore, we consider the cost function f_ω in Equation 2.7 given by

$$f_\omega(a_0, a_1, \cdots, a_k, b_0, b_1, \cdots b_l) = (\omega - a(a_0, a_1, \cdots, a_k)b(b_0, b_1, \cdots b_l))^2, \tag{2.14}$$

where we assume a consists of $k+1$ and b of $l+1$ bits, which are denoted by $a_0, a_1, \cdots, a_k$ and $b_0, b_1, \cdots b_l$, respectively. These parameters need to be optimized in order to solve the bi-prime factorization problem. The new cost function in Equation 2.14 provides the starting point to construct a factorization target Hamiltonian $\hat{H}_\mathrm{p}$ in terms of qubits. We assume for the rest of the investigation in this thesis $a_0 = 1 = b_0$. This is a simplification which restricts us to only considering odd bi-primes ω. Hence, the number of bits of a and b reduces to k and l, respectively. We end up with $n = k + l$ bit-digit parameters $a_1, \cdots, a_k, b_1, \cdots b_l$, which we need to determine. We refer to those parameters as classical dynamical bits. The n classical dynamical bits become n dynamical spin-1/2 objects and are denoted as vectors $|a_i\rangle_i \in \mathcal{H}_i$ and $|b_j\rangle_{j+k} \in \mathcal{H}_{j+k}$, where $\mathcal{H}_m \cong \mathbb{C}^2$, $i \in \{1, \cdots, k\}$, $j \in \{1, \cdots, l\}$ and $m \in \{1, \cdots, k, k+1, \cdots, k+l\}$. The basis vectors of $\mathcal{H}_m$ posses the form

$$|0\rangle_m = \begin{pmatrix} 1 \\ 0 \end{pmatrix} \qquad\qquad |1\rangle_m = \begin{pmatrix} 0 \\ 1 \end{pmatrix}. \tag{2.15}$$

We can construct an arbitrary state $|\psi\rangle$

$$|\psi\rangle = \bigotimes_{m=1}^{n} (c_{0,m} |0\rangle_m + c_{1,m} |1\rangle_m) \tag{2.16}$$

$$= |a_1\rangle_1 \otimes \cdots \otimes |a_k\rangle_k \otimes |b_1\rangle_{k+1} \otimes \cdots \otimes |b_l\rangle_{k+l} \tag{2.17}$$

$$= \bigotimes_{i=1}^{k} |a_i\rangle_i \otimes \bigotimes_{j=1}^{l} |b_j\rangle_{j+k}, \tag{2.18}$$

where $c_{0,m}$ and $c_{1,m}$ are normalization weights. The representation of ω lives in a 2^n-dimensional Hilbert space $\mathcal{H} \cong \mathbb{C}^{2^n}$. The bit-digits a_i, b_j can be evaluated by introducing the projectors

$$\hat{P}_{m,-} = \underbrace{\mathbb{1}_{2\times2} \otimes \cdots \otimes \mathbb{1}_{2\times2}}_{m-1} \otimes \frac{\mathbb{1}_{2\times2} - \sigma_z}{2} \otimes \underbrace{\mathbb{1}_{2\times2} \otimes \cdots \otimes \mathbb{1}_{2\times2}}_{n-m} \tag{2.19}$$

$$= \frac{\mathbb{1} - \sigma_z^{(m)}}{2}, \tag{2.20}$$

where $\sigma_z^{(m)}$ is the z- Pauli matrix and $\mathbb{1}$ is the identity acting on the m-th sub-Hilbert space $\mathcal{H}_m$. The minus sign in $\hat{P}_{m,-}$ indicates that the z- Pauli matrix is subtracted. In quantum information theory the notation is given by $\hat{P}_{m,-} = |1\rangle_m \langle 1| = \hat{P}_{m,1} = \hat{\Pi}_{m,1}$ and $\hat{P}_{m,+} = |0\rangle_m \langle 0| = \hat{P}_{m,0} = \hat{\Pi}_{m,0}$ [25]. In this thesis we employ the "$\pm$"- notation, because this is more convenient in chapter 4. The operators $\hat{P}_{i,-}, \hat{P}_{j+k,-}$ fulfill the eigenvalue equations

$$\hat{P}_{i,-} |\psi\rangle = a_i |\psi\rangle , \tag{2.21}$$

$$\hat{P}_{j+k,-} |\psi\rangle = b_j |\psi\rangle . \tag{2.22}$$

This allows to introduce the two prime numbers a and b, defined in Equation 2.2, as observables $\hat{a}$ and $\hat{b}$ in binary representation:

$$\hat{a} = \mathbb{1} + \sum_{i=1}^{k} 2^i \hat{a}_i = \mathbb{1} + \sum_{i=1}^{k} 2^i \hat{P}_{i,-}, \tag{2.23}$$

$$\hat{b} = \mathbb{1} + \sum_{j=1}^{l} 2^j \hat{b}_j = \mathbb{1} + \sum_{j=1}^{l} 2^j \hat{P}_{k+j,-}. \tag{2.24}$$

The expectation values of the observable $\hat{a}$ is then the value of the classical a

$$\langle \hat{a} \rangle = \langle \psi | \hat{a} | \psi \rangle = 1 + \sum_{i=1}^{k} 2^i \langle \psi | \hat{a}_i | \psi \rangle = 1 + \sum_{i=1}^{k} 2^i a_i = a. \tag{2.25}$$

The same applies for $\hat{b}$. The above mathematical framework permits the transformation of the cost function in Equation 2.14 to the target Hamiltonian $\hat{H}_\mathrm{p}$ of the shape

$$\hat{H}_\mathrm{p} = \Omega(\omega\mathbb{1} - \hat{a}\hat{b})^2 = (\omega\mathbb{1} - \hat{a}\hat{b})^2, \tag{2.26}$$

where we set the frequency $\Omega = 1/s$. The final states should ideally be either in $|0\rangle_m$ or $|1\rangle_m$. Thus, it is useful to prepare the qubits in an simultaneous superposition of both basis states (weighted equally) which is called the $|+\rangle_m$ state. The $|+\rangle_m = 1/\sqrt{2}(|0\rangle_m + |1\rangle_m)$ can also be written as $|0\rangle_{m,x}$, where the x stands for the x-direction in the Bloch sphere representation. Hence, $|+\rangle_m$ is the unit vector in x-direction. The qubits are forced into $|0\rangle_m$ or $|1\rangle_m$ during the transition process. Depending on the situation, all the qubits can be prepared in the $|+\rangle_m$ state if we consider an initial Hamiltonian, e.g., with an external magnetic field aligned in x-direction, which is mathematically expressed by

$$\hat{H}_0 = -\sum_{m=1}^{n} \xi_m \sigma_x^{(m)}. \tag{2.27}$$

Here, $\xi_m = \xi \in \mathbb{R}$ and $\sigma_x^{(m)}$ is the x-Pauli matrix. The setup is shown in Figure 2.2.

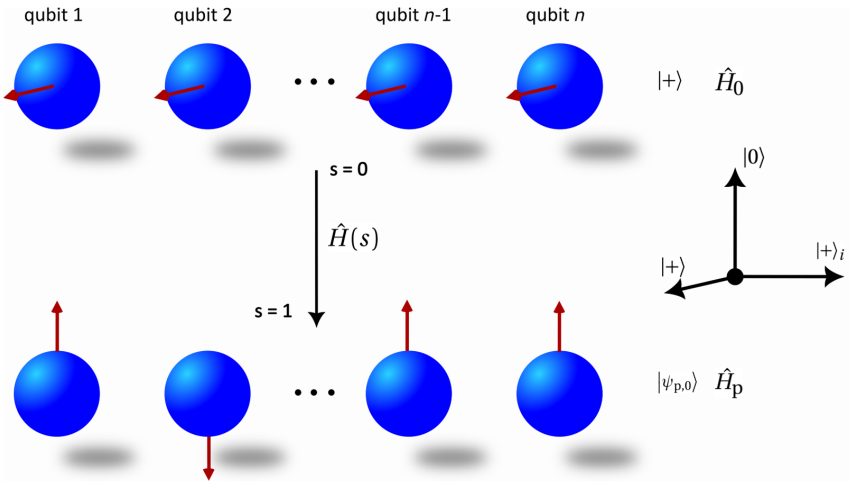

Figure 2.2: The physical realization of $\hat{H}(s)$. At $s = 0$, all the spins are aligned in x-direction. During the evolution $\hat{H}(s = 0) \to \hat{H}(s = 1)$, the spins rearrange towards $|0\rangle_m$ or $|1\rangle_m$. The state $|\psi_{\mathrm{p},0}\rangle$ stands for the ground state of $\hat{H}_\mathrm{p}$.

The ground state of the $n \times n$ matrix $\hat{H}_0$ can be determined straight forwardly and is given by the non-entangled state

$$|+\rangle = \bigotimes_{m=1}^{n} \frac{|0\rangle_m + |1\rangle_m}{\sqrt{2}}. \tag{2.28}$$

We sketch the derivation of the ground state for $n = 2$. The Hamiltonian in matrix form has the shape:

$$\hat{H}_0 = \xi \begin{pmatrix} 0 & -1 & -1 & 0 \\ -1 & 0 & 0 & -1 \\ -1 & 0 & 0 & -1 \\ 0 & -1 & -1 & 0 \end{pmatrix}. \tag{2.29}$$

The eigenvalues are $\{0, \pm 2\xi\}$, where 0 possess the algebraic multiplicity $\mu = 2$. The eigenvector corresponding to the ground state energy $E_0 = -2\xi$ is determined by

$$\xi \begin{pmatrix} 0 & -1 & -1 & 0 \\ -1 & 0 & 0 & -1 \\ -1 & 0 & 0 & -1 \\ 0 & -1 & -1 & 0 \end{pmatrix} \cdot \begin{pmatrix} \psi_1 \\ \psi_2 \\ \psi_3 \\ \psi_4 \end{pmatrix} = -2\xi \begin{pmatrix} \psi_1 \\ \psi_2 \\ \psi_3 \\ \psi_4 \end{pmatrix} \tag{2.30}$$

$$\Rightarrow \psi_2 + \psi_3 = 2\psi_1 = 2\psi_4 \wedge \psi_1 + \psi_4 = 2\psi_2 = 2\psi_3, \tag{2.31}$$

where $\psi_1, \psi_2, \psi_3, \psi_4 \in \mathbb{R}$. The normalized eigenvector is given by $|\psi_0\rangle = 1/\sqrt{2^2} \cdot (1,1,1,1)^T = |+\rangle_1 \otimes |+\rangle_2$. Using the theory in subsection 2.2.1, we consider $\hat{H}(s)$ with the initial Hamiltonian above $\hat{H}(0) = \hat{H}_0$ and rewrite Equation 2.10 in terms of s:

$$\hat{i}\frac{d}{ds} |\psi(s)\rangle = T\hat{H}(s) |\psi(s)\rangle, \tag{2.32}$$

where $|\psi(0)\rangle = |+\rangle$. We can now plot the three lowest eigenenergies of the spectrum of $\hat{H}(s)$ for $\omega = 15$ as an example, where $\xi = 10$. This can be seen in Figure 2.3.

In Figure 2.3 it is obvious that one of the two requirements of the adiabatic theorem is fulfilled. We have $\forall s \in [0,1]$ a non-zero gap between ground state and the rest of the spectrum. Hence, the condition of validity in Equation 2.13 has the form $R(T) = \text{const}/T \ll 1$. The second requirement can be estimated by plotting $R(T)$. This is done in chapter 3.

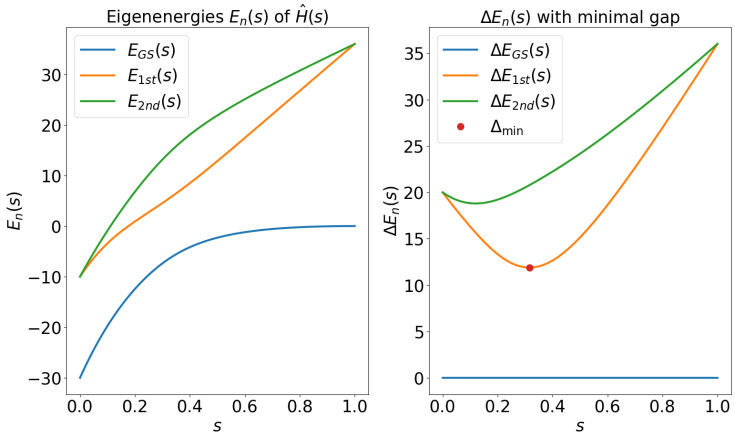

Figure 2.3: Left: Lowest three eigenenergies of $\hat{H}(s)$. The ground state energy reaches zero at $s = 1$. This means that at $s = 1$ we achieve the energy minimization of $\hat{H}_{\text{p}}$. Right: Gaps between ground state energy and the rest of the spectrum. Since we have a non-zero gap between ground state energy and the rest of the spectrum $\forall s \in [0, 1]$, the first condition of the adiabatic theorem is valid. The evolution time is given in time-units and the energy in inverse time-units.

2.3 Entropy of Entanglement

We can expand the examination of our full quantum description by introducing the *Entropy of Entanglement* [26]. It is a measure to express the quantum entanglement between two subsystems of a composite two-part quantum system. Let Ω be an entire quantum system, where $\Omega = A \cup B$ with $A = \{a_1, \cdots, a_k\}$ and $B = \{b_1, \cdots, b_l\}$. The subsystems A and B define the composite two-part quantum system. The entropy of entanglement of A or B is then the *von Neumann entropy* of the reduced density matrix ρ_A or ρ_B, respectively.

Let $\mathcal{I}_\Omega = \mathcal{I}_\mathrm{A} \cup \mathcal{I}_\mathrm{B}$ be the index set of the entire quantum system, where $\mathcal{I}_\mathrm{A} = \{1, \cdots, k\}$ and $\mathcal{I}_\mathrm{B} = \{k+1, \cdots, k+l\}$. One could say that we consider a quantum system, where the first k qubits correspond to the bit-digits of an integer a and the last l qubits correspond to an integer b. For further investigation, we choose the subsystem A. We receive the respective time-dependent density matrix $\rho_\mathrm{A}(t)$ as follows:

$$\rho_\mathrm{A}(t) = \mathrm{Tr}_\mathrm{B}(\rho(t)), \tag{2.33}$$

where $\rho(t)$ denotes the density matrix of the entire system Ω. The *von Neumann entanglement entropy* $S_\mathrm{A}(t)$ can be expressed by

$$S_\mathrm{A}(t) = -\mathrm{Tr}(\rho_\mathrm{A}(t)\log\rho_\mathrm{A}(t)). \tag{2.34}$$

For pure states, the von Neumann entropy is a measure for the entanglement between the subsystem A and its complement $\bar{A} = B$. One could compute the entropy of entanglement for each qubit as well. We will not discuss this here, since this goes beyond the scope of this thesis. To quantify the amount of quantum correlations between two finite subsystems A and B we introduce a second measure called the *bipartite quantum mutual information (QMI)* [27], defined as

$$I(t) = S_\mathrm{A}(t) + S_\mathrm{B}(t) - S(t). \tag{2.35}$$

We use the two discussed measures for obtaining information for a more precise discussion in chapter 3.

2.4 Concepts Underlying The Cumulants Approach

A wave function $|\psi(t)\rangle \in \mathcal{H}$ of a time-dependent quantum-mechanical Hamiltonian $\hat{H}(t)$ is governed by the Schrödinger equation [15]

$$\hat{i}\frac{\partial}{\partial t}|\psi(t)\rangle = \hat{H}(t)\,|\psi(t)\rangle\,. \tag{2.36}$$

The time-dependence of $|\psi(t)\rangle$ is subject to the unitary time-evolution operator

$$\hat{U}(t,t_0) = \exp\left\{-\hat{i}\int_{t_0}^{t} dt'\hat{H}(t')\right\}, \qquad U^\dagger U = \mathbb{1} = UU^\dagger \tag{2.37}$$

where t_0 denotes the initial time. The solution of Equation 2.36 is given by

$$|\psi(t)\rangle = \hat{U}(t,t_0)\,|\psi(t_0)\rangle\,. \tag{2.38}$$

We call this mathematical treatment of the wave function the Schrödinger picture [15]. In the Schrödinger picture all observables $\mathcal{O}_{\mathrm{S}}(t)$ acting on the Hilbert space $\mathcal{H}$ are time-independent in a sense that no explicit time-dependence is induced by a time-evolution operator. Such a time-independent operator could be, e.g., a Hamiltonian containing a time-dependent potential $\hat{V}(t)$. We choose a complete and an orthonormal set of wave functions $\{|\psi_i(t)\rangle\}$ subject to Equation 2.36, which allows to write

$$|\psi(t)\rangle = \sum_i c_i\,|\psi_i(t)\rangle = \sum_i c_i\hat{U}(t,t_0)\,|\psi_i(t_0)\rangle\,, \tag{2.39}$$

where $c_i = \langle\psi_i(t)|\psi(t)\rangle$. Furthermore, we introduce the density operator $\rho(t)$, utilized in section 2.3, as

$$\rho(t) = |\psi(t)\rangle\,\langle\psi(t)| = \sum_{i,j} c_i c_j^*\,|\psi_i(t)\rangle\,\langle\psi_j(t)|\,. \tag{2.40}$$

Applying projective measurements [28] allows to write the density matrix as

$$\rho(t) = \sum_i p_i\,|\psi_i(t)\rangle\,\langle\psi_i(t)|\,, \tag{2.41}$$

where for the probability applies $p_i = |c_i|^2$. Now, we can express the measurement of an arbitrary observable $\mathcal{O}_{\mathrm{S}}(t)$ in terms of the density matrix

$$\langle \mathcal{O}_{\mathrm{S}}(t) \rangle = \sum_i |c_i|^2 \langle \psi_i(t)| \mathcal{O}_{\mathrm{S}}(t) |\psi_i(t)\rangle = \mathrm{Tr}(\mathcal{O}_{\mathrm{S}}(t)\rho(t)) \tag{2.42}$$

Equation 2.42 provides the opportunity to introduce the so-called *Ehrenfest theorem*, a key equation in this thesis.

2.4.1 Ehrenfest Theorem

By applying the time derivative on Equation 2.42, we obtain the following expression:

$$\frac{d}{dt}\langle \mathcal{O}_{\mathrm{S}}(t) \rangle = \frac{d}{dt}\mathrm{Tr}(\mathcal{O}_{\mathrm{S}}(t)\rho(t)) = \mathrm{Tr}\left(\frac{d\mathcal{O}_{\mathrm{S}}(t)}{dt}\rho(t)\right) + \mathrm{Tr}\left(\mathcal{O}_{\mathrm{S}}(t)\frac{d\rho(t)}{dt}\right) \tag{2.43}$$

$$= \left\langle \frac{\partial \mathcal{O}_{\mathrm{S}}(t)}{\partial t} \right\rangle + \mathrm{Tr}\left(\mathcal{O}_{\mathrm{S}}(t)\frac{d\rho(t)}{dt}\right). \tag{2.44}$$

We continue by computing

$$\frac{d\rho(t)}{dt} = \sum_i p_i \frac{d}{dt}(|\psi_i(t)\rangle \langle \psi_i(t)|) = \sum_i p_i \left(\frac{d|\psi_i(t)\rangle}{dt}\langle \psi_i(t)| + |\psi_i(t)\rangle \frac{d\langle \psi_i(t)|}{dt}\right) \tag{2.45}$$

$$= -\hat{i}\sum_i p_i \left(\hat{H}(t)|\psi_i(t)\rangle\langle\psi_i(t)| - |\psi_i(t)\rangle\langle\psi_i(t)|\hat{H}(t)\right) \tag{2.46}$$

$$\frac{d\rho(t)}{dt} = -\hat{i}[\hat{H}(t), \rho(t)], \tag{2.47}$$

where $[\cdot,\cdot]$ denotes the commutator. We inserted Equation 2.36 and its daggered counterpart into Equation 2.46. Equation 2.47 is known as the *von Neumann equation* [29]. Plugging in the von Neumann equation into Equation 2.44 yields

$$\frac{d}{dt}\langle \mathcal{O}_{\mathrm{S}}(t) \rangle = -\hat{i} \cdot \mathrm{Tr}\left(\mathcal{O}_{\mathrm{S}}(t)[\hat{H}(t), \rho(t)]\right) + \left\langle \frac{\partial \mathcal{O}_{\mathrm{S}}(t)}{\partial t} \right\rangle \tag{2.48}$$

$$= -\hat{i} \cdot \mathrm{Tr}\left(\mathcal{O}_{\mathrm{S}}(t)\hat{H}(t)\rho(t) - \mathcal{O}_{\mathrm{S}}(t)\rho(t)\hat{H}(t)\right) + \left\langle \frac{\partial \mathcal{O}_{\mathrm{S}}(t)}{\partial t} \right\rangle \tag{2.49}$$

$$\overset{\text{c.p.}}{=} -\hat{i} \cdot \mathrm{Tr}\left([\mathcal{O}_{\mathrm{S}}(t), \hat{H}(t)]\rho(t)\right) + \left\langle \frac{\partial \mathcal{O}_{\mathrm{S}}(t)}{\partial t} \right\rangle \tag{2.50}$$

$$\frac{d}{dt}\langle \mathcal{O}_{\mathrm{S}}(t) \rangle = \hat{i}\left\langle [\hat{H}(t), \mathcal{O}_{\mathrm{S}}(t)] \right\rangle + \left\langle \frac{\partial \mathcal{O}_{\mathrm{S}}(t)}{\partial t} \right\rangle, \tag{2.51}$$

where c.p. stands for the application of the trace's cyclic property. The Equation 2.51 is the mathematical formulation of the *Ehrenfest theorem* and supports the important correspondence principle [14]. The correspondence principle connects the quantum mechanical commutator structure with the Poissonian structure of classical mechanics:

$$\underbrace{\{\hat{A},\hat{B}\}}_{\text{Poisson brackets}} \rightarrow \frac{1}{\hat{i}} \underbrace{[\hat{A},\hat{B}]}_{\text{commutator}} . \tag{2.52}$$

Therefore, the Equation 2.47 is often referred to as the quantum Liouville equation. Equation 2.51 can also be expressed in the Heisenberg picture [15]:

$$\langle \mathcal{O}_{\mathrm{S}}(t)\rangle = \langle \mathcal{O}_{\mathrm{S}}(t)\rangle_{\mathrm{S}} = \mathrm{Tr}(\mathcal{O}_{\mathrm{S}}(t)\rho(t)) = \mathrm{Tr}(\mathcal{O}_{\mathrm{S}}(t)\hat{U}(t,t_0)\rho(t_0)\hat{U}^{\dagger}(t,t_0)) \tag{2.53}$$

$$= \mathrm{Tr}(\underbrace{\hat{U}^{\dagger}(t,t_0)\mathcal{O}_{\mathrm{S}}(t)\hat{U}(t,t_0)}_{\mathcal{O}_{\mathrm{H}}(t)}\rho(t_0)) = \langle \mathcal{O}_{\mathrm{H}}(t)\rangle_{\mathrm{H}}. \tag{2.54}$$

The Ehrenfest equation then takes the form

$$\frac{d}{dt}\langle \mathcal{O}_{\mathrm{H}}(t)\rangle_{\mathrm{H}} = \hat{i}\left\langle [\hat{H}_{\mathrm{H}}(t), \mathcal{O}_{\mathrm{H}}(t)]\right\rangle_{\mathrm{H}} + \left\langle \frac{\partial \mathcal{O}_{\mathrm{H}}(t)}{\partial t}\right\rangle_{\mathrm{H}} \tag{2.55}$$

In the Heisenberg picture the wave functions are time-independent $|\psi(t)\rangle_{\mathrm{H}} = |\psi(t_0)\rangle_{\mathrm{S}}$ and the operators obtain a time-dependence induced by a unitary evolution operator $\hat{U}(t,t_0)$. In this thesis we only consider Equation 2.51. From Equation 2.25 we recognize, that we can use Equation 2.51 to derive a system of non-autonomous nonlinear coupled ordinary differential equations (ODEs) of first order which allows to determine the time-evolution of the classical bit expectation values $a_i = \langle \hat{a}_i\rangle$ and $b_j = \langle \hat{b}_j\rangle$ directly. However, the term $\hat{i}\left\langle [\hat{H}(t), \mathcal{O}_{\mathrm{S}}(t)]\right\rangle$ makes the entire calculations more difficult. The completeness of the Ehrenfest system requires higher-order averages which implies a fast growth of the system size. We derive the mathematics and discuss the problem of completeness of the Ehrenfest system more precisely in chapter 4. The full quantum dynamics can be computed by solving Equation 2.36 for $\hat{H}(t)$ numerically and calculating the expectation value $\mathcal{O}_{\mathrm{S}}(t)$, according to

$$\langle \mathcal{O}_{\mathrm{S}}(t)\rangle = \langle \psi(t)|\, \mathcal{O}_{\mathrm{S}}(t)\, |\psi(t)\rangle . \tag{2.56}$$

Quantum annealing is more conveniently performed by solving the Schrödinger equation, however solving the Ehrenfest system can reduce computation time. The occurring averages in the Ehrenfest system can be expanded by utilizing the general cumulant expansion

method. This allows to suspend certain quantum physical effects such as quantum entanglement. Discarding all quantum-dynamical correlations by expanding the full quantum dynamics in first-order yields a classical solution. This solution is called the mean-field approach. If the classical solution coincided with the quantum dynamical description for an arbitrary n qubit system, it would rule out a quantum advantage for the bi-prime factorization.

2.4.2 Generalized Cumulant Expansion Method

The generalized cumulant expansion method was introduced by R.Kubo in 1962 [16]. In probability theory a random variable X is defined as a measurable function $X : \Omega \to E$, where Ω denotes a sample space with possible outcomes and E is a measurable space. Here, Ω needs to be subject to a measure-theoretic definition [30]. A joint cumulant of n ordered random variables $X_1, X_2, \cdots, X_n$ is defined as the coefficient in the Maclaurin series of the multivariate cumulant generating function [31] and it can be expressed combinatorially by the following abstract equation [16, 17]:

$$\langle X_1 X_2 \cdots X_n \rangle_{\mathrm{c}} = \sum_{p \in P(\mathcal{I})} (|p| - 1)!(-1)^{|p|-1} \prod_{B \in p} \left\langle \prod_{i \in B} X_i \right\rangle . \tag{2.57}$$

The joint cumulant is denoted by $\langle \cdot \rangle_{\mathrm{c}}$. In the above we define the index set $\mathcal{I} = \{1, 2, \cdots, n\}$ with all possible partitions $P(\mathcal{I})$. Then, $p \in P(\mathcal{I})$ is a possible partition with $B \in p$ its elements. For simplicity, we choose n to be finite, but in general n could be infinite as well. As an example we set $n = 3$. The index set is given by $\mathcal{I} = \{1, 2, 3\}$ with partitions $P(\mathcal{I}) = \{\{1, 2, 3\}, \{1, \{2, 3\}\}, \{2, \{1, 3\}\}, \{3, \{1, 2\}\}, \{\{1\}, \{2\}, \{3\}\}\}$. Utilizing Equation 2.57 yields for the joint cumulant expression

$$\langle X_1 X_2 X_3 \rangle_{\mathrm{c}} = \langle X_1 X_2 X_3 \rangle - \langle X_1 \rangle \langle X_2 X_3 \rangle - \langle X_2 \rangle \langle X_1 X_3 \rangle - \langle X_3 \rangle \langle X_1 X_2 \rangle + 2 \langle X_1 \rangle \langle X_2 \rangle \langle X_3 \rangle \tag{2.58}$$

The joint cumulant can be thought of as a general measure of correlations of random variables [17]. One recognizes, that it is an expansion of expectation values of correlations up to order n, where the n-th order term, $\langle X_1 X_2 \cdots X_n \rangle$, only appears once. The key assumption of the generalized cumulant expansion method is Theorem 1 in [16]. It states that the relation $\langle X_1 X_2 \cdots X_n \rangle_{\mathrm{c}} = 0$ is assumed to hold if the random variables $X_1 X_2 \cdots X_n$ (or any subset of them) are statistically independent [16, 17]. Let the random variables $X_1 X_2 \cdots X_n$ be chosen such that Theorem 1 holds, then, we can rearrange Equation 2.57. This allows to obtain an expression of the n-th order average $\langle X_1 X_2 \cdots X_n \rangle$ depending only on averages of order $n - 1$ or less. It has the following combinatorial form [17]:

$$\langle X_1 X_2 \cdots X_n \rangle = \sum_{p \in P(\mathcal{I}) \setminus \mathcal{I}} (|p|-1)!(-1)^{|p|} \prod_{B \in p} \left\langle \prod_{i \in B} X_i \right\rangle. \tag{2.59}$$

We receive an expression where the n-th-order average can be expressed as a sum of products of averages of orders up to $n-1$. This is a recursive formula. Returning to the example with $n = 3$ we present the first- as well as second-order expansion of the third-order average:

$$\langle X_1 X_2 X_3 \rangle \overset{\text{2nd order}}{=} \langle X_1 \rangle \langle X_2 X_3 \rangle + \langle X_2 \rangle \langle X_1 X_3 \rangle + \langle X_3 \rangle \langle X_1 X_2 \rangle - 2\langle X_1 \rangle \langle X_2 \rangle \langle X_3 \rangle \tag{2.60}$$

$$\langle X_1 X_2 X_3 \rangle \overset{\text{1st order}}{=} \langle X_1 \rangle \langle X_2 \rangle \langle X_3 \rangle. \tag{2.61}$$

We say that the order of a considered average can be determined by $\max_{i \in B} |i|$. Equation 2.59 is another key equation in this thesis. Applied to Equation 2.51 one obtains an approximated description of the bi-prime factorization problem.

The assumption $\langle X_1 X_2 \cdots X_n \rangle_c(s) = 0$ for all $s \in [0,1]$, which provides the recursive formula in Equation 2.59, allows to define the following relation:

$$\langle X_1 X_2 \cdots X_n \rangle_c(s) = \langle X_1 X_2 \cdots X_n \rangle_S(s) - \langle X_1 X_2 \cdots X_n \rangle_{C,o}(s), \tag{2.62}$$

where $\langle X_1 X_2 \cdots X_n \rangle_S(s)$ is a n-th order average obtained by Equation 2.56 and $\langle X_1 X_2 \cdots X_n \rangle_{C,o}(s)$ is given by Equation 2.59 up to an order o. This relation is used in section 6.4.

2.4.3 QuantumCumulants.jl

QuantumCumulants.jl [17, 32] is a Julia package, where the theory of section 2.4 is implemented. A precise description provides [17]:

> QuantumCumulants.jl is a package for the symbolic derivation of mean-field equations for quantum mechanical operators in Julia. The equations are derived using fundamental commutation relations of operators. When averaging these equations they can be automatically expanded in terms of cumulants to an arbitrary order (generalized mean-field approximation). This results in a closed set of symbolic differential equations, which can also be solved numerically.
>
> For the application of commutation relations QuantumCumulants.jl implements a simple noncommutative algebra, where any commutation relations are applied immediately. All other symbolic simplification and rewriting is done using the Symbolics.jl package.

To obtain a numerical solution, equations derived with QuantumCumulants.jl can be converted to ModelingToolkit.jl and subsequently solved with DifferentialEquations.jl.

QuantumCumulants.jl turns out to be very useful in the fields of quantum optics as well as quantum information. We utilize QuantumCumulants.jl to our bi-prime factorization problem. Analogously to the examples presented in [17], we assume that with increasing expansion order the results become better and better until the solutions coincide with the full quantum-dynamical description. We will see that the problem under consideration is not as banal as this assumption. This is discussed in chapter 5 and in chapter 6.

2.5 Jacobi Matrix of Ehrenfest ODE Systems

Let $\mathcal{J}_{\mathbf{x}(s_0)}\mathbf{f}(\mathbf{x}(s), s)$ be the Jacobi matrix [33] of a given nonlinear non autonomous ordinary differential equation (ODE) system of first-order of the shape

$$\frac{d\mathbf{x}(s)}{ds} = \mathbf{f}(\mathbf{x}(s), s) \tag{2.63}$$

with $\mathbf{x}(s) \in \mathbb{C}^N$ the system variables depending on $s \in [0, 1]$ and $\mathbf{x}(s_0)$ fixed at s_0. Here, N denotes the system size. The Jacobi matrix, often referred to as Jacobian, can be useful to clarify if a the system under consideration becomes stiff. Therefore, one computes the eigenvalues $\lambda_i(s) \in \Lambda(s) = \{\lambda_1(s), \cdots, \lambda_N(s)\}$ of $\mathcal{J}_{\mathbf{x}(s)}\mathbf{f}(\mathbf{x}(s), s)\ \forall s$, where $\lambda_i(s) \in \mathbb{C}$. The Jacobian can be expressed mathematically by

$$\mathcal{J}_{\mathbf{x}(s)}\mathbf{f}(\mathbf{x}(s), s) = \left[\frac{\partial \mathbf{f}(\mathbf{x}(s), s)}{\partial x_1(s)}, \cdots, \frac{\partial \mathbf{f}(\mathbf{x}(s), s)}{\partial x_N(s)}\right] = \begin{pmatrix} \frac{\partial f_1(\mathbf{x}(s),s)}{\partial x_1(s)} & \cdots & \frac{\partial f_1(\mathbf{x}(s),s)}{\partial x_N(s)} \\ \vdots & \ddots & \vdots \\ \frac{\partial f_N(\mathbf{x}(s),s)}{\partial x_1(s)} & \cdots & \frac{\partial f_N(\mathbf{x}(s),s)}{\partial x_N(s)} \end{pmatrix}. \tag{2.64}$$

Considering now the Ehrenfest systems of the cumulants approach in this thesis, the system size N depends on the expansion order and on the number of dynamical qubits. For a qubit system with n dynamical qubits, we use the two transition operators $\sigma_{\pm}^{(i)}$ as well as the projector $\hat{P}_{i,-}$ acting on each sub-Hilbert space $\mathcal{H}_i$ with $i \in \{1, 2, \cdots, n\}$ instead of the commoly used Pauli operators $\sigma_x^{(i)}, \sigma_y^{(i)}, \sigma_z^{(i)}$. In the case of an Ehrenfest system in arbitrary cumulant expansion we define $\mathbf{x}(s) = (\langle\sigma_+^{(1)}\rangle, \langle\hat{P}_{1,-}\rangle, \langle\sigma_-^{(1)}\rangle, \langle\sigma_+^{(2)}\rangle, \cdots \langle\sigma_+^{(1)}\sigma_+^{(2)}\rangle, \cdots, \langle\sigma_+^{(1)}\sigma_+^{(2)}\sigma_+^{(3)}\rangle, \cdots)(s)$. The higher-order averages are necessary expressions to receive a complete ODE system (see chapter 4). For example, the vector $\mathbf{x}(s)$ for n qubits in first-, second- and third-order expansion possesses the lengths:

$$N \overset{1^{\text{st}}}{=} 3n \tag{2.65}$$

$$N \overset{2^{\text{nd}}}{=} \frac{3n}{2}(3n - 1) \tag{2.66}$$

$$N \overset{3^{\text{rd}}}{=} \frac{3n}{2}(5 - 6n + 3n^2). \tag{2.67}$$

The derivation of the above formulas is given in section A.1. We use the Jacobian to acquire more information about the stiffness of the considered systems in section 6.3.

In section 6.3, we also try to approximate the Jacobian from the Schrödinger expectation values, i.e., the expectation values obtained by using the time-dependent state $|\psi(s)\rangle$ governed by Equation 2.32. This helps to examine if the Jacobian eigenvalues stay finite for

the full quantum expectation values. We start by recalling the expectation values of a Schrödinger operator:

$$\langle \hat{O}_i(s) \rangle = \langle \hat{O}_i \rangle_s = \langle \psi(s) | \, \hat{O}_i \, | \psi(s) \rangle = \langle \psi(s_0) | \, \hat{U}^\dagger(s, s_0) \hat{O}_i \hat{U}(s, s_0) \, | \psi(s_0) \rangle \,, \tag{2.68}$$

where $\hat{O}_i$ are operator products consisting of $\sigma_\pm^{(m)}$ and $\hat{P}_{m,-}$ with $m \in \{1, 2, \cdots, n\}$. We write the Ehrenfest system of size N as

$$\frac{d}{ds}\mathbf{O}(s) = \mathbf{f}(\mathbf{O}(s), s) = \mathbf{f}(\langle \hat{O}_1 \rangle_s, \cdots, \langle \hat{O}_N \rangle_s; s) \tag{2.69}$$

and calculate the following partial differentiation

$$\frac{\partial f_i}{\partial \langle \hat{O}_j \rangle_s} \approx \frac{f_i(\langle \hat{O}_1 \rangle_s, \cdots, \langle \hat{O}_j \rangle_{s+\tau}, \cdots, \langle \hat{O}_N \rangle_s; s) - f_i(\langle \hat{O}_1 \rangle_s, \cdots, \langle \hat{O}_N \rangle_s; s)}{\langle \hat{O}_j \rangle_{s+\tau} - \langle \hat{O}_j \rangle_s}, \tag{2.70}$$

where τ is small. Going one time-step $s \to s + \tau$ changes the dynamical system $\mathbf{f}$ in each component. By considering the $s+\tau$ time-step in the j-th component in the above formula the partial derivative $\partial f_i(\mathbf{O}(s), s)/\partial \langle \hat{O}_j \rangle_s$ is approximated linearly. One receives, then, the approximation of the Jacobian

$$\mathcal{J}_{\mathbf{O}(s)}\mathbf{f}(\mathbf{O}(s), s) \approx \begin{pmatrix} \frac{\partial f_1(\mathbf{O}(s),s)}{\partial \langle \hat{O}_1 \rangle_s} & \cdots & \frac{\partial f_1(\mathbf{O}(s),s)}{\partial \langle \hat{O}_N \rangle_s} \\ \vdots & \ddots & \vdots \\ \frac{\partial f_N(\mathbf{O}(s),s)}{\partial \langle \hat{O}_1 \rangle_s} & \cdots & \frac{\partial f_N(\mathbf{O}(s),s)}{\partial \langle \hat{O}_N \rangle_s} \end{pmatrix}. \tag{2.71}$$

Chapter 3

Quantum Dynamics

In this chapter we want to compute the full quantum dynamical solutions of the bi-prime factorization problem. Therefore, we implement the theory of bi-prime factorization in section 2.1 together with the quantum adiabatic computation in section 2.2 in Julia utilizing a framework for open quantum dynamics called *QuantumOptics.jl* [18]. We investigate different integers ω with qubit number n where we already know the partition (k, l). The different ω are presented in Table 3.1.

Table 3.1: Qubit numbers $n = k + l$ for different $\omega = ab$, where k and l denote the number of bit digits of a and b, which are given in binary representation $[\cdot]$ as well.

ω	$n = k + l$	a	b
15[1111]	$3 = 2 + 1$	5[101]	3[11]
21[10101]	$3 = 2 + 1$	7[111]	3[11]
33[100001]	$4 = 3 + 1$	11[1011]	3[11]
39[100111]	$4 = 3 + 1$	13[1101]	3[11]
51[110011]	$5 = 4 + 1$	17[10001]	3[11]
57[111001]	$5 = 4 + 1$	19[10011]	3[11]
93[1011101]	$6 = 4 + 1$	31[11111]	3[11]
95[1011111]	$6 = 4 + 2$	19[10011]	5[101]
265[100001001]	$7 = 5 + 2$	53[110101]	5[101]

The adiabatic theorem requires two conditions. For $s \in [0, 1]$, a minimal energy gap in the spectrum of the Hamiltonian $\Delta_{\min} > 0$ must exist and the transition from initial Hamiltonian $\hat{H}_0$ to the target Hamiltonian $\hat{H}_\mathrm{p}$ has to be sufficiently slow, hence, T needs to be large enough. The function $R(T)$ in Equation 2.13 is a mathematical representation of these two conditions. Before we continue, we want to find a valid domain for T. Thus, we plot $R_\omega(T)$ for $\omega \in \{15, 21, 33, 39, 51, 57\}$. The results are depicted in Figure 3.1.

Figure 3.1 shows the typical behavior of $R_\omega(T) \propto 1/T$, which is encoded in Equation 2.13. In general, the larger T, the smaller $R_\omega(T)$ where the relation $R_\omega(T) \ll 1$ is eventually

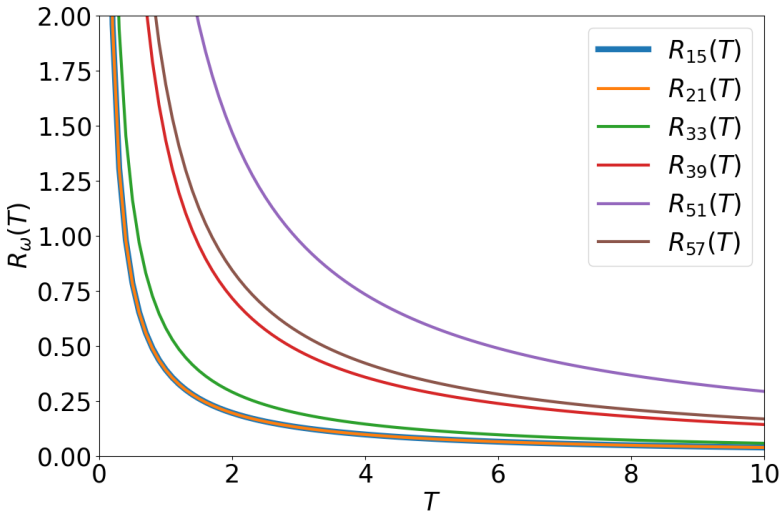

Figure 3.1: Adiabaticity condition $R_\omega(T)$ as function of the evolution time $T \in [0, 10]$ for different bi-primes ω. We denote the corresponding integer as subscripts. The bi-primes 15 and 21 are three-qubit systems, 33 and 39 are four-qubit systems and 51 and 57 are five-qubit systems.

fulfilled. All considered integers satisfy $R_\omega(T) < 1$ at $T = 10$. However, it is not quite clear if $R_\omega(T) \ll 1$ is fulfilled. For a more precise analysis we list the values $R_\omega(10)$ in Table 3.2.

Table 3.2: Values of $R_\omega(T = 10)$, where ω denotes the corresponding bi-prime.

ω	15	21	33	39	51	57
$R_\omega(10)$	0.0392	0.0391	0.0581	0.1433	0.2936	0.1687

Increasing the number n of qubits in our system implies a more complicated target Hamiltonian $\hat{H}_\mathrm{p}$. Thus, we assume that T needs to be increased as well, such that a correct solution can be obtained. Figure 3.1 and Table 3.2 prove this assumption to be correct, however, it seems that $R_\omega(T)$ is also dependent on the internal structure of $\hat{H}_\mathrm{p}$, since $R_{15}(10) > R_{21}(10)$ and $R_{51}(10) > R_{57}(10)$. The latter is satisfied for $\forall T \in [0, 10]$. For large integer factorization the evolution time T can individually be estimated. This implies a possibility to reduce computation time. There is still the question: when is the relation $R_\omega(T) \ll 1$ fulfilled? One can introduce the overlap probabilities $|\langle \mathrm{GS_p}|\psi(s)\rangle|^2$ and $|\langle \phi_0(s)|\psi(s)\rangle|^2$ which are called *fidelity* and *"the remaining in the ground state" (remaining ground state population)*, respectively. Here, $|\psi(s)\rangle$ is the state subject to the Schrödinger equation in Equation 2.32, $|\phi_0(s)\rangle$ denotes the instantaneous ground state of $\hat{H}(s)$ and $|\mathrm{GS_p}\rangle$ is the exact ground state of the $\hat{H}_\mathrm{p}$, hence, the solution of the bi-prime problem. The fidelity gives the probability that $|\psi(s)\rangle$ evolves into the correct final state

$|\mathrm{GS_p}\rangle$ and the other overlap shows the probability, that no transition to an excited state has taken place during the evolution. We consider $\omega = 15$ with $T \in \{0.1, 0.5, 1, 10\}$ as an example. The fidelity as well as the *remaining in the ground state* are shown in Figure 3.2.

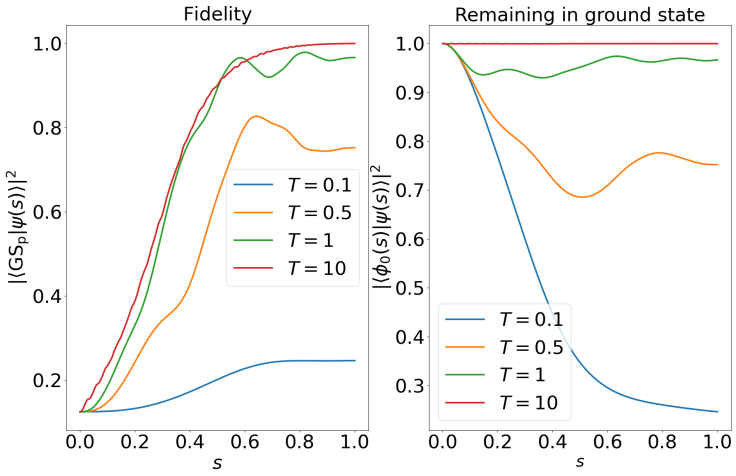

Figure 3.2: The fidelity and the *remaining in the ground state* for the cases $\omega = 15$ at different evolution times $T \in \{0.1, 0.5, 1, 10\}$.

We can observe in Figure 3.2 that $T = 0.1$ yields a low probability to end up in the exact state $|\mathrm{GS_p}\rangle$, which implies a high probability of a transition to an excited state. This is expected, because the numerical value in Figure 3.1 is given by $R_{15}(0.1) = 3.9197 > 1$. The adiabatic theorem is not valid for this case. If we consider $T = 0.5$ at $s = 1$ the fidelity gives a probability above 70%, that the correct result is obtained. We see for $T = 1$ the fidelity is over 90% and for $T = 10$ we get $\approx 100\%$. Therefore, the larger T, the higher the fidelity. The *remaining in the ground state* shows that the overlap probability becomes more and more constant for growing T. We assume for $\omega \in \{15, 21, 33, 39, 51, 57\}$ a value $T = 10$ to be a good choice. In a further step the measurements of the projectors $\hat{a}_i$ and $\hat{b}_j$ are determined, where $\omega = 15$. The measurements are plotted in Figure 3.3.

Figure 3.3 reflects the discussion above. We can follow the entire measurements in dependence of s, where we obtain the expectation values of the classical bits a_i and b_j by utilizing $\langle\psi(s=1)|\,\hat{a}_i\,|\psi(s=1)\rangle = a_i$ and $\langle\psi(s=1)|\,\hat{b}_j\,|\psi(s=1)\rangle = b_j$. At $T = 0.1$ the adiabatic transition is too fast. The numerical values of a_1, a_2 and b_1 lie somewhere between 0 and 1 at $s = 1$. If one executes the measurements multiple times, one will obtain $7[111] \times 3[11] = 21$, which is the wrong solution. Increasing the evolution time T results in better and, eventually, correct solutions. The *blue* line approaches zero, whereas orange and green go to one as can be observed in Figure 3.3. Thus, the quantum dynamics of the factorization problem provides the correct result.

Now, we want to examine all the bi-primes in Table 3.1. We plot again the expectation values of the projectors. The results for $\omega \in \{15, 21, 33, 39, 51, 57\}$ are visualized in Fig-

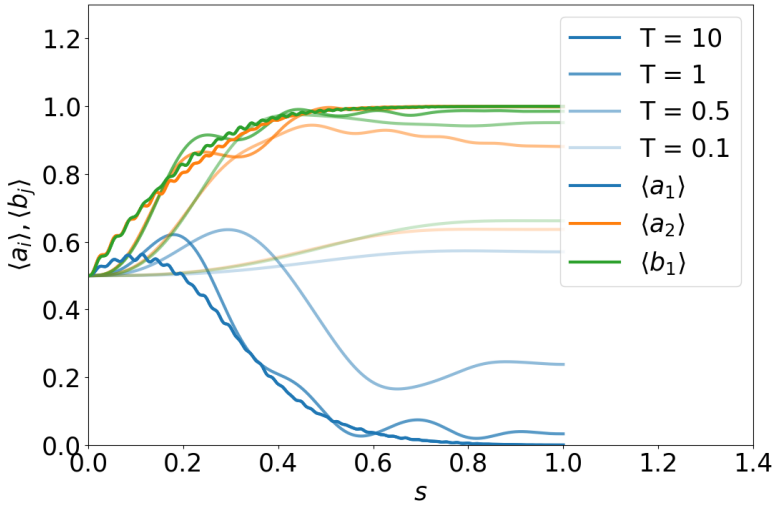

Figure 3.3: Measurements of $\hat{a}_i$ and $\hat{b}_j$ for a given ω at $T \in \{0.1, 0.5, 1, 10\}$. The line opacities correspond to different T. The colors indicate the evolution of a considered measurement for a projector during $0 \leq s \leq 1$, where one should receive either one or zero for every measurement at $s = 1$. This can be understood by writing the bi-prime in bit-digit representation of the form $15[1111] = \omega = a \cdot b = 5[101] \times 3[11]$. The black digits are always one, since we assume $a_0 = 1 = b_0$. The colored ones are the expectation values of the dynamical qubits at $s = 1$.

ure 3.4, for $\omega \in \{93, 95\}$ in Figure 3.5 and for $\omega = 265$ in Figure 3.10. We choose $T = 10$ for all bi-primes $\omega \in \{15, 21, 33, 39, 51, 57\}$, according to the discussion in Figure 3.1 and Table 3.2. The overall evolution time T for larger bi-primes is estimated accordingly.

In Figure 3.4, we compute the factorization solutions for the three-, four- and five-qubit-systems (except $\omega = 93$). Obviously, the results provide correct bit-digits in all six cases. However, we recognize that the larger systems partially contain small deviations from zero, e.g. $\langle a_3(s) \rangle > 0, \forall s \in [0, 1]$ in Figure 3.4f. These are typical signs, that one uses a rather fast adiabatic transition for the corresponding problem. The deviations can be resolved by increasing T. This is visualized for $\omega = 265$ in Figure 3.10. In Figure 3.5 we consider systems consisting of five (93) and six (95) qubits. We increase T to $T = 100$, which should be enough at first glance.

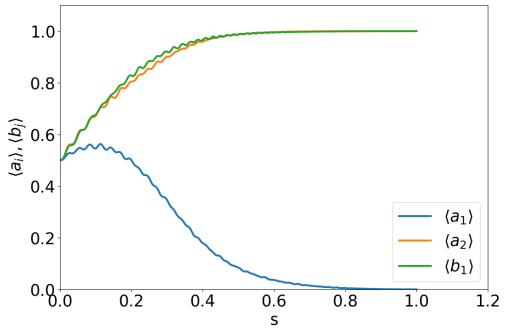

(a) $\omega = 15[1111] = 5[101] \times 3[11]$

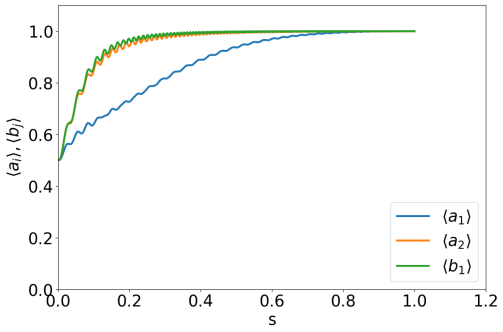

(b) $\omega = 21[10101] = 7[111] \times 3[11]$

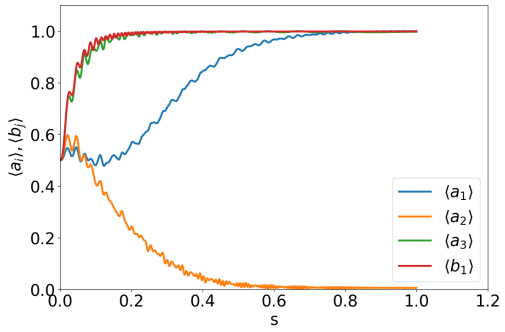

(c) $\omega = 33[100001] = 11[1011] \times 3[11]$

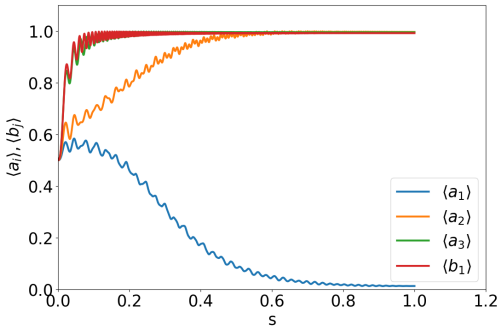

(d) $\omega = 39[100111] = 13[1101] \times 3[11]$

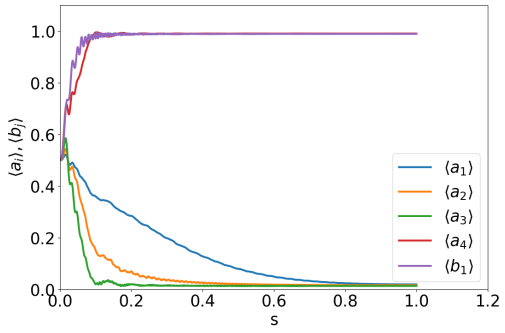

(e) $\omega = 51[110011] = 17[10001] \times 3[11]$

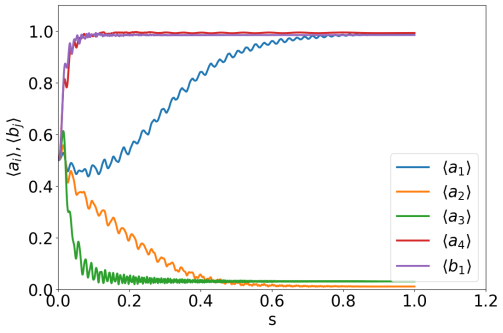

(f) $\omega = 57[111001] = 19[10011] \times 3[11]$

Figure 3.4: Quantum dynamics for $\omega \in \{15, 21, 33, 39, 51, 57\}$. The colored bit-digits indicate the respective expectation values. The bit-digit values are the numerical values at the end of the evolution at $s = 1$. We set $T = 10$.

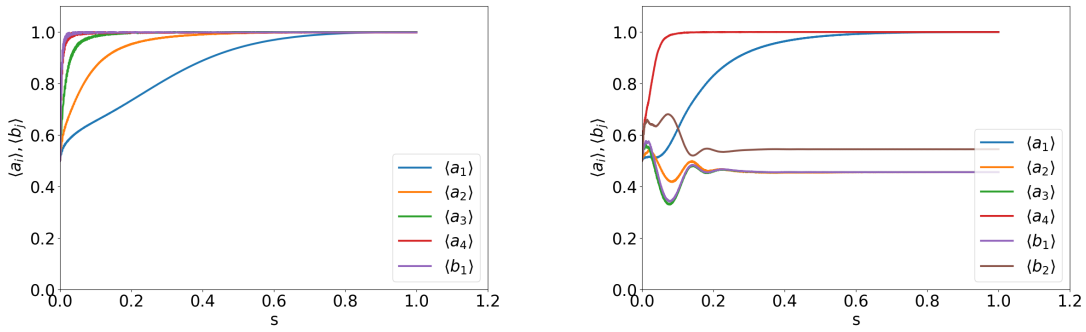

(a) $\omega = 93[1011101] = 31[11111] \times 3[11]$ (b) $\omega = 95[1011111] = 19[10011] \times 5[101]$

Figure 3.5: Expectation values of the observables $\hat{a}_i$ and $\hat{b}_j$ for $\omega \in \{93, 95\}$. The adiabatic transition with $T = 100$ for $\omega = 93$ provides the correct factors a and b, whereas for $\omega = 95$ at $T = 100$ the values $\langle a_2\rangle, \langle a_3\rangle, \langle b_1\rangle, \langle b_2\rangle$ are in the vicinity of 0.5 with $s \in [0.2, 1]$.

In Figure 3.5, we recognize that $\omega = 95$ is a special case for the bi-prime factorization problem utilizing quantum annealing. To understand this, we plot the partial spectrum as well as the gaps of $\hat{H}(s)$ with $\hat{H}_\mathrm{p} = (95\mathbb{1} - \hat{a}\hat{b})^2$ presented in Figure 3.6.

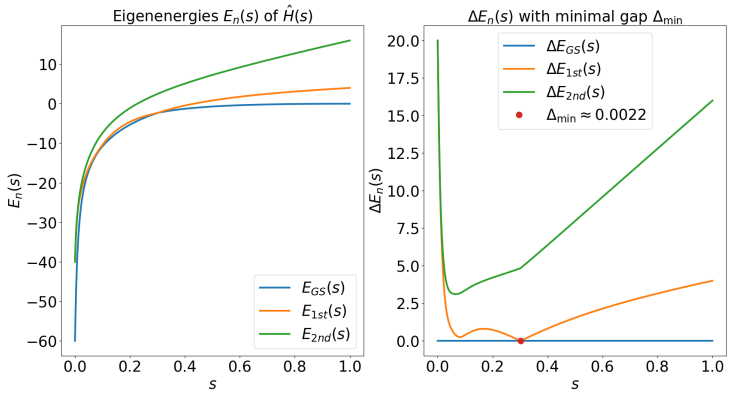

Figure 3.6: Energy spectrum $E_n(s)$ up to the second excited energy as well as their energy differences to the ground state energy $\Delta E_n(s)$. The red dot indicates the location of the minimal gap $\Delta_{\min} \approx 0.0022$.

The minimal gap $\Delta_{\min} \approx 0.0022$ in Figure 3.6 is relatively small, which implies a large prefactor in Equation 2.13. Therefore, the overall evolution-time T should be chosen much larger. We can estimate the approximate value for T by using Equation 2.13. Assuming the constant to be 1 we receive $1/\Delta^2_{\min} \approx 1/0.0022^2 \approx 206612 \ll T$. It turns out that the cases with very small minimum gap need to be treated differently, which is discussed in [12]. Since we do not want to go too deep into the discussion of $\omega = 95$, we simply increase T a little more and plot the fidelity and the *remaining in ground state* in Figure 3.7.

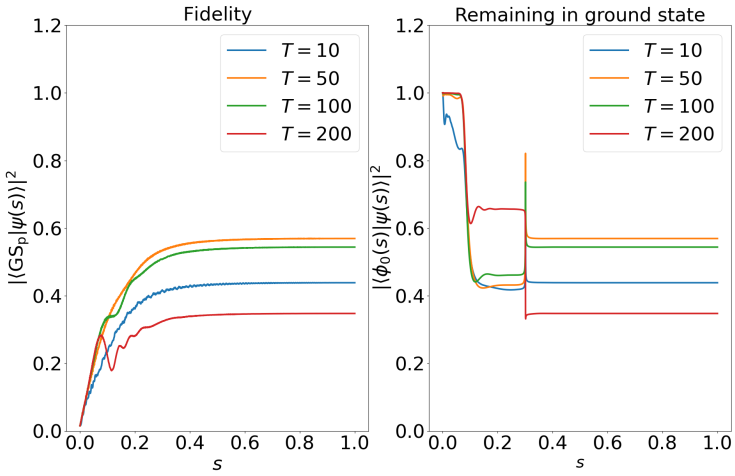

Figure 3.7: Fidelity as well as the *remaining in the ground state* are presented for $\omega = 95$ with $T \in \{10, 50, 100, 200\}$. For $10 \ll T < 100$ the fidelity is slightly above 50% where increasing T results in a drop of the probability below 40%. The *remaining in the ground state* drops rapidly for $s > 0.1$ and manifests plateaus in the same way as the fidelity.

In Figure 3.7, it is clear that with increasing T the fidelity shrinks. We set $T = 500$ and plot the measurements of $\hat{a}_i$ and $\hat{b}_j$ presented in Figure 3.8.

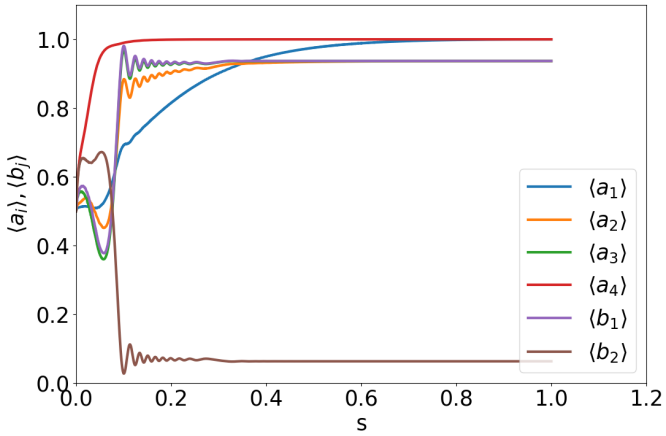

Figure 3.8: Bit-digit expectation values for $\omega = 95$ at $T = 500$. The acquired bit-digits provide the factors a and b, which solve 93, i.e., $\omega = 95[1011111] \neq 31[11111] \times 3[011] = 93[1011101]$.

In the case of $\omega = 95$ at $T = 500$ the measurements solve the factorization problem for $\omega = 93$. Vice versa, this is not the case, since $\hat{H}(s)$ for 93 has a much larger minimal gap. The direct implication is given in Figure 3.5a. Since this is a quite interesting behavior, we

want to investigate $\omega = 95$ a little further. Therefore, we utilize the entropy of entanglement (EE) and the bipartite quantum mutual information (QMI) from section 2.3. The results are shown in Figure 3.9.

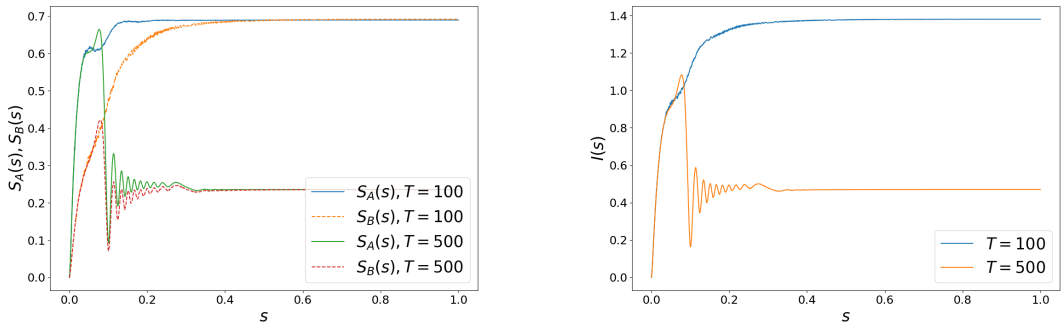

(a) EE (b) QMI

Figure 3.9: Entropy of entanglement (EE) as well as the bipartite quantum mutual information (QMI) for the case $\omega = 95$ at $T \in \{100, 500\}$ and $s \in [0, 1]$. For EE we plot the von Neumann entropies $S_{\mathrm{A}}(s)$ and $S_{\mathrm{B}}(s)$ of the subsystems $A = \{\hat{a}_1, \cdots, \hat{a}_k\}$ and $B = \{\hat{b}_1, \cdots, \hat{b}_l\}$, respectively. The QMI is then computed by $I(s) = S_{\mathrm{A}}(s) + S_{\mathrm{B}}(s) - S(s)$, where $S(s)$ is the von Neumann entropy of the entire system.

We observe in Figure 3.9 that for EE the entropies $S_{\mathrm{A}}(s)$ and $S_{\mathrm{B}}(s)$ have a plateau at $(0.4 < s < 1)$ in the vicinity of 0.7 at $T = 100$. The plateau values drop then to a value around 0.24 when increasing to $T = 500$. Hence, the larger T, the smaller the entropy of quantum entanglement. At the plateaus both entropies are nearly the same, i.e. $S_{\mathrm{A}}(s) \approx S_{\mathrm{B}}(s)$ and imply $S(s) \approx 0$. We have in this case a pure state. Here, the quantum mutual information QMI is then given by $I(s) \approx S_{\mathrm{A}}(s) + S_{\mathrm{B}}(s) \approx 2S_{\mathrm{A}}(s) \approx 2S_{\mathrm{B}}(s)$. The increase of T provides eventually the wrong solution, simultaneously the degree of quantum entanglement decreases and the expectation values approach zero or one which implies a more classical solution.

Now, we consider $\omega = 265$, which is a seven-qubit-system. The measurement results of the bit-digits are given in Figure 3.10.

Figure 3.10 provides the correct solution for the bi-prime problem $\omega = 265$. The expectation values, which have their plateau slightly below one or slightly above zero, approach more and more the respective values if the overall evolution-time is increased.

In this section, we have shown that the quantum mechanical energy minimization problem discussed in chapter 2, indeed, provides correct solutions for the bi-prime factorization problem. However, there are solutions, which are not unambiguous. These cases are beyond the scope of this discussion. This chapter has shown that the quantum dynamics obtained with the underlying quantum algorithm provides the correct factors, except $\omega = 95$. We now want to compute the solutions by considering the expanded Ehrenfest systems.

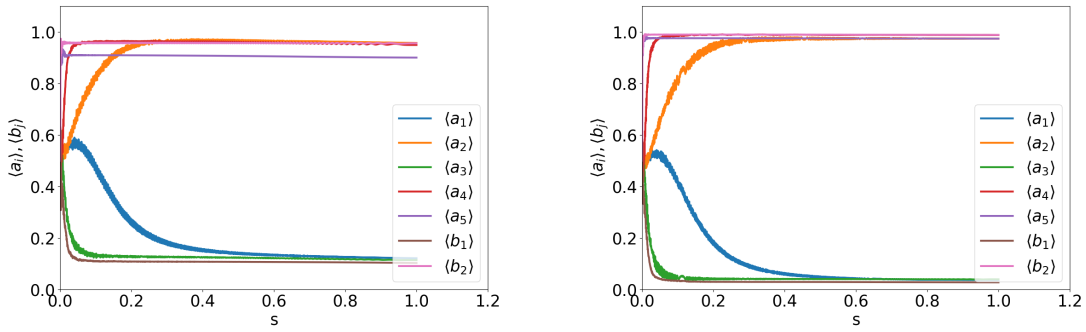

(a) $T = 100$ (b) $T = 200$

Figure 3.10: The factorization problem of $\omega = 265[100001001] = 53[110101] \times 5[101]$. Considering the problem at $T = 100$ shows that the plateaus for the bit-digits approaching zero remain between 0.1 and 0.2. Analogously, $\langle a_5 \rangle$ possesses a plateau between 0.9 and 1. Increasing to $T = 200$ shifts these plateaus towards the classical values zero and one.

Before using QuantumCumulants.jl, we mathematically derive the commutator relations for $\omega = 15$ in first- and second-order.

Chapter 4

Cumulants Approach to Bi-prime Factorization

In this chapter we use the fundamental theoretical concepts from section 2.4 to compute the commutator relations as well as explicitly derive the Ehrenfest system of ordinary differential equations (ODEs) for the bi-prime factorization problem in first- as well as second-order expansion. The obtained system can then be solved numerically. Since the developers of Quantum Cumulants.jl claim that the package is in early stages of development, this mathematical derivation serves as a comparison [17, 32].

4.1 First-Order Expansion

Let $\hat{\mathcal{O}}_m(t)$ be an operator acting on the m-th sub-Hilbert space $\mathcal{H}_m$. According to Equation 2.51, the Ehrenfest theorem is given by

$$\frac{d}{dt}\langle\hat{\mathcal{O}}_m(t)\rangle = \hat{i}\left\langle[\hat{H}(t),\hat{\mathcal{O}}_m(t)]\right\rangle + \left\langle\frac{\partial\hat{\mathcal{O}}_m(t)}{\partial t}\right\rangle, \tag{4.1}$$

where $\hat{H}(t)$ is the time-dependent Hamiltonian of the adiabatic transition from the initial Hamiltonian $\hat{H}_0$ to the target Hamiltonian $\hat{H}_\mathrm{p}$ in Equation 2.8. Hence, $\hat{H}(t)$ has the form

$$\hat{H}(t) = \underbrace{-\sum_{i=1}^{n}\xi\sigma_x^{(i)}}_{=\hat{H}_0}\left(1-\frac{t}{T}\right) + \underbrace{(\omega\mathbb{1}-\hat{a}\hat{b})^2}_{=\hat{H}_\mathrm{p}}\left(\frac{t}{T}\right). \tag{4.2}$$

We assume $\hat{\mathcal{O}}_m(t)$ to be time-independent, i.e. $\hat{\mathcal{O}}_m$, which results in the simplification of the Ehrenfest theorem:

$$\frac{d}{dt}\langle\hat{\mathcal{O}}_m(t)\rangle = \hat{i}\left\langle[\hat{H}(t),\hat{\mathcal{O}}_m]\right\rangle. \tag{4.3}$$

One continues by simplifying the commutator expression in the above equation. Since we only consider odd ω we know that the first bit digits of $\hat{a}$ and $\hat{b}$ will always be equal to 1, where $\hat{a}$ has $k+1$ bit digits and $\hat{b}$ possesses $l+1$ bits. From subsection 2.2.2 the system has $n = k + l$ dynamical qubits. The commutator can be written as

$$[\hat{H}(t),\hat{\mathcal{O}}_m] = -\sum_{i=1}^{n}\xi[\sigma_x^{(i)},\hat{\mathcal{O}}_m]\left(1-\frac{t}{T}\right) + [(\omega\mathbb{1}-\hat{a}\hat{b})^2,\hat{\mathcal{O}}_m]\left(\frac{t}{T}\right). \tag{4.4}$$

We know from subsection 2.4.2, that expectation values of multiple observables become the product of expectation values of each observable. Hence, the construction of the ODE system requires $\hat{\mathcal{O}}_m$ only to be an expression consisting of Pauli matrices, such that the derived ODE system is complete. QuantumCumulants.jl uses for the derivation, by default, the transition operators $\sigma_\pm$ as well as the projector $\hat{P}_-$, i.e., we define $\hat{\mathcal{O}}_m$ as an element of the following set:

$$\hat{\mathcal{O}}_m \in \bigcup_{r=1}^{n}\{\sigma_+^{(r)},\sigma_-^{(r)},\hat{P}_{r,-}\} = \bigcup_{i=1}^{k}\{\sigma_+^{(i)},\sigma_-^{(i)},\hat{P}_{i,-}\}\cup\bigcup_{j=1}^{l}\{\sigma_+^{(j+k)},\sigma_-^{(j+k)},\hat{P}_{j+k,-}\} = A\cup B. \tag{4.5}$$

The set includes then all necessary operators for a complete system in first-order cumulant expansion. This approach is equivalent to the one, which considers Pauli-matrices for the c-number system. The Pauli-matrices can be written by

$$\begin{aligned}\sigma_\pm^{(i)} &= \frac{1}{2}\left(\sigma_x^{(i)} \pm \hat{i}\sigma_y^{(i)}\right) = (\sigma_\mp^{(i)})^\dagger\\ \Rightarrow \sigma_x^{(i)} &= \sigma_+^{(i)} + \sigma_-^{(i)},\\ \Rightarrow \sigma_y^{(i)} &= -\hat{i}(\sigma_+^{(i)} - \sigma_-^{(i)}).\end{aligned} \tag{4.6}$$

Equation 4.4 then takes the form

$$\begin{aligned}[\hat{H}(t),\hat{\mathcal{O}}_m] &= -\sum_{i=1}^{n}\xi[\sigma_+^{(i)}+\sigma_-^{(i)},\hat{\mathcal{O}}_m]\left(1-\frac{t}{T}\right) + [(\omega\mathbb{1}-\hat{a}\hat{b})^2,\hat{\mathcal{O}}_m]\left(\frac{t}{T}\right)\\ &= -\sum_{i=1}^{n}\xi([\sigma_+^{(i)},\hat{\mathcal{O}}_m]+[\sigma_-^{(i)},\hat{\mathcal{O}}_m])\left(1-\frac{t}{T}\right) + [(\omega\mathbb{1}-\hat{a}\hat{b})^2,\hat{\mathcal{O}}_m]\left(\frac{t}{T}\right).\end{aligned} \tag{4.7}$$

We continue by computing the following commutator relations:

$$[\sigma_+^{(i)}, \hat{\mathcal{O}}_m] = \delta_{i,m} \begin{cases} 0, & , \hat{\mathcal{O}}_m = \sigma_+^{(m)} \\ (\mathbb{1} - 2\hat{P}_{i,-}), & , \hat{\mathcal{O}}_m = \sigma_-^{(m)} \\ \sigma_+^{(i)} & , \hat{\mathcal{O}}_m = \hat{P}_{m,-} \end{cases} \tag{4.8}$$

$$[\sigma_-^{(i)}, \hat{\mathcal{O}}_m] = \delta_{i,m} \begin{cases} -(\mathbb{1} - 2\hat{P}_{i,-}), & , \hat{\mathcal{O}}_m = \sigma_+^{(m)} \\ 0, & , \hat{\mathcal{O}}_m = \sigma_-^{(m)} \\ -\sigma_-^{(i)} & , \hat{\mathcal{O}}_m = \hat{P}_{m,-} \end{cases} \tag{4.9}$$

Furthermore, one writes the commutator

$$[(\omega\mathbb{1} - \hat{a}\hat{b})^2, \hat{\mathcal{O}}_m] = -2\omega[\hat{a}\hat{b}, \hat{\mathcal{O}}_m] + [\hat{a}^2\hat{b}^2, \hat{\mathcal{O}}_m], \tag{4.10}$$

where the property $[\hat{a}, \hat{b}] = 0$ implies $(\hat{a}\hat{b})^2 = \hat{a}\hat{b}\hat{a}\hat{b} = \hat{a}^2\hat{b}^2$. Since only the dynamical qubits are being considered, we use the definition of $\hat{a}$ and $\hat{b}$ from Equation 2.23 and Equation 2.24, respectively. The observables possess the shape:

$$\hat{a} = \mathbb{1} + \sum_{i=1}^{k} 2^i \hat{P}_{i,-}, \tag{4.11}$$

$$\hat{b} = \mathbb{1} + \sum_{j=1}^{l} 2^j \hat{P}_{k+j,-}. \tag{4.12}$$

The squared expressions are given by

$$\begin{aligned} \hat{a}^2 &= \mathbb{1} + 2\sum_{i=1}^{k} 2^i \hat{P}_{i,-} + \sum_{i,i'=1}^{k} 2^{i+i'} \hat{P}_{i,-}\hat{P}_{i',-} \\ \overset{\hat{P}_{i,-}^2 = \hat{P}_{i,-}}{\hookrightarrow} &= \mathbb{1} + 2\sum_{i=1}^{k} 2^i \hat{P}_{i,-} + \sum_{i=1}^{k} 2^{2i} \hat{P}_{i,-} + \sum_{\substack{i,i'=1 \\ i\neq i'}}^{k} 2^{i+i'} \hat{P}_{i,-}\hat{P}_{i',-} \\ &= \mathbb{1} + \sum_{i=1}^{k} 2^{i+1}(1 + 2^{i-1})\hat{P}_{i,-} + \sum_{\substack{i,i'=1 \\ i\neq i'}}^{k} 2^{i+i'} \hat{P}_{i,-}\hat{P}_{i',-}. \end{aligned} \tag{4.13}$$

A similar equation can be determined for $\hat{b}^2$:

$$\hat{b}^2 = \mathbb{1} + \sum_{j=1}^{l} 2^{j+1}(1+2^{j-1})\hat{P}_{j+k,-} + \sum_{\substack{j,j'=1 \\ j\neq j'}}^{l} 2^{j+j'}\hat{P}_{j+k,-}\hat{P}_{j'+k,-}. \tag{4.14}$$

We return to Equation 4.10 and notice that the operator $\hat{\mathcal{O}}_m$ can either commute with $\hat{a}$ or $\hat{b}$. This requires the case distinctions utilizing the index sets $\mathcal{I}_A = \{1, \cdots, k\}$ and $\mathcal{I}_B = \{k+1, \cdots, k+l\}$. Let $m \in \mathcal{I}_A$, hence, $[\hat{b}, \hat{\mathcal{O}}_m] = 0$. This assumption yields

$$\begin{aligned}
[(\omega\mathbb{1} - \hat{a}\hat{b})^2, \hat{\mathcal{O}}_m] &= -2\omega[\hat{a}, \hat{\mathcal{O}}_m]\hat{b} + [\hat{a}^2, \hat{\mathcal{O}}_m]\hat{b}^2 \\
&= -2\omega\sum_{i=1}^{k} 2^i[\hat{P}_{i,-}, \hat{\mathcal{O}}_m]\hat{b} + \sum_{i=1}^{k} 2^{i+1}(1+2^{i-1})[\hat{P}_{i,-}, \hat{\mathcal{O}}_m]\hat{b}^2 \\
&+ \sum_{\substack{i,i'=1 \\ i\neq i'}}^{k} 2^{i+i'} \underbrace{[\hat{P}_{i,-}\hat{P}_{i',-}, \hat{\mathcal{O}}_m]}_{=\hat{P}_{i,-}[\hat{P}_{i',-},\hat{\mathcal{O}}_m]+[\hat{P}_{i,-},\hat{\mathcal{O}}_m]\hat{P}_{i',-}} \hat{b}^2 \\
&= -2\omega\sum_{i=1}^{k} 2^i[\hat{P}_{i,-}, \hat{\mathcal{O}}_m]\hat{b} + \sum_{i=1}^{k} 2^{i+1}(1+2^{i-1})[\hat{P}_{i,-}, \hat{\mathcal{O}}_m]\hat{b}^2 \\
&+ 2\sum_{\substack{i,i'=1 \\ i\neq i'}}^{k} 2^{i+i'}[\hat{P}_{i,-}, \hat{\mathcal{O}}_m]\hat{P}_{i',-}\hat{b}^2 \\
[(\omega\mathbb{1} - \hat{a}\hat{b})^2, \hat{\mathcal{O}}_m] &= -2^{m+1}\omega[\hat{P}_{m,-}, \hat{\mathcal{O}}_m]\hat{b} + 2^{m+1}(1+2^{m-1})[\hat{P}_{m,-}, \hat{\mathcal{O}}_m]\hat{b}^2 \\
&+ 2^{m+1}[\hat{P}_{m,-}, \hat{\mathcal{O}}_m]\sum_{\substack{i=1 \\ i\neq m}}^{k} 2^i\hat{P}_{i,-}\hat{b}^2.
\end{aligned} \tag{4.15}$$

A similar expression can be acquired for $m \in \mathcal{I}_B$:

$$\begin{aligned}
[(\omega\mathbb{1} - \hat{a}\hat{b})^2, \hat{\mathcal{O}}_m] &= -2^{m-k+1}\omega\hat{a}[\hat{P}_{m,-}, \hat{\mathcal{O}}_m] + 2^{m-k+1}(1+2^{m-k-1})\hat{a}^2[\hat{P}_{m,-}, \hat{\mathcal{O}}_m] \\
&+ 2^{m-k+1}\hat{a}^2[\hat{P}_{m,-}, \hat{\mathcal{O}}_m]\sum_{\substack{j=1 \\ j\neq m-k}}^{l} 2^j\hat{P}_{j+k,-},
\end{aligned} \tag{4.16}$$

where the commutator $[\hat{P}_{m,-}, \hat{\mathcal{O}}_m]$ leads to a three-case distinction:

$$[\hat{P}_{m,-}, \hat{\mathcal{O}}_m] = \begin{cases} -\sigma_+^{(m)}, & \hat{\mathcal{O}}_m = \sigma_+^{(m)} \\ 0, & \hat{\mathcal{O}}_m = \hat{P}_{m,-} \\ \sigma_-^{(m)}, & \hat{\mathcal{O}}_m = \sigma_-^{(m)}. \end{cases} \tag{4.17}$$

Assuming $\langle \mathbb{1} \rangle = 1$ and let $m \in \mathcal{I}_A$. Then, the Ehrenfest system of ODEs for $\hat{\mathcal{O}}_m$ are given by

$$\begin{aligned} \frac{d}{dt}\langle \hat{\mathcal{O}}_m \rangle = &-\hat{i}\xi(\langle [\sigma_+^{(m)}, \hat{\mathcal{O}}_m] \rangle + \langle [\sigma_-^{(m)}, \hat{\mathcal{O}}_m] \rangle) \left(1 - \frac{t}{T}\right) \\ &- \hat{i} 2^{m+1} \Big(\omega \langle [\hat{P}_{m,-}, \hat{\mathcal{O}}_m] \hat{b} \rangle - (1 + 2^{m-1}) \langle [\hat{P}_{m,-}, \hat{\mathcal{O}}_m] \hat{b}^2 \rangle \\ &- \sum_{\substack{i=1 \\ i \neq m}}^{k} 2^i \langle [\hat{P}_{m,-}, \hat{\mathcal{O}}_m] \hat{P}_{i,-} \hat{b}^2 \rangle \Big) \left(\frac{t}{T}\right). \end{aligned} \tag{4.18}$$

Furthermore, we know that $\hat{\mathcal{O}}_m \in A$ which provides

$$\begin{aligned} \frac{d}{dt}\langle \sigma_\pm^{(m)} \rangle = &\pm \hat{i}\xi(1 - 2\langle \hat{P}_{m,-} \rangle) \left(1 - \frac{t}{T}\right) \\ &\pm \hat{i} 2^{m+1} \Big(\omega \langle \sigma_\pm^{(m)} \hat{b} \rangle - (1 + 2^{m-1}) \langle \sigma_\pm^{(m)} \hat{b}^2 \rangle - \sum_{\substack{i=1 \\ i \neq m}}^{k} 2^i \langle \sigma_\pm^{(m)} \hat{P}_{i,-} \hat{b}^2 \rangle \Big) \left(\frac{t}{T}\right) \end{aligned} \tag{4.19}$$

$$\frac{d}{dt}\langle \hat{P}_{m,-} \rangle = -\hat{i}\xi(\langle \sigma_+^{(m)} \rangle - \langle \sigma_-^{(m)} \rangle) \left(1 - \frac{t}{T}\right). \tag{4.20}$$

Analogously for $m \in \mathcal{I}_B$:

$$\begin{aligned} \frac{d}{dt}\langle \sigma_\pm^{(m)} \rangle = &\pm \hat{i}\xi(1 - 2\langle \hat{P}_{m,-} \rangle) \left(1 - \frac{t}{T}\right) \\ &\pm \hat{i} 2^{m-k+1} \Big(\omega \langle \hat{a} \sigma_\pm^{(m)} \rangle - (1 + 2^{m-k-1}) \langle \hat{a}^2 \sigma_\pm^{(m)} \rangle - \sum_{\substack{i=1 \\ j \neq m-k}}^{l} 2^l \langle \hat{a}^2 \sigma_\pm^{(m)} \hat{P}_{j+k,-} \rangle \Big) \left(\frac{t}{T}\right) \end{aligned} \tag{4.21}$$

$$\frac{d}{dt}\langle \hat{P}_{m,-} \rangle = -\hat{i}\xi(\langle \sigma_+^{(m)} \rangle - \langle \sigma_-^{(m)} \rangle) \left(1 - \frac{t}{T}\right). \tag{4.22}$$

We present now the procedure of the *cumulants approach* in first-order expansion. Therefore, we return to $m \in \mathcal{I}_{\mathrm{A}}$ and consider Equation 4.19. All averages consist of sums of *sub-averages*, i.e. averages which contain the fundamental operators $\sigma_{\pm}$ and $\hat{P}_{-}$. In the cumulant-approach all these sub-averages with order higher than one are expanded by utilizing Equation 2.59. The sub-averages can be identified as

$$\langle \sigma_{\pm} \hat{b} \rangle = \langle \sigma_{\pm} \rangle + \sum_{j=1}^{l} 2^{j} \langle \sigma_{\pm} \hat{P}_{j+k,-} \rangle \tag{4.23}$$

$$\langle \sigma_{\pm} \hat{b}^{2} \rangle = \langle \sigma_{\pm} \rangle + \sum_{j=1}^{l} 2^{j+1}(1-2^{j-1}) \langle \sigma_{\pm} \hat{P}_{j+k,-} \rangle + \sum_{\substack{j,j'=1 \\ j \neq j'}}^{l} 2^{j+j'} \langle \sigma_{\pm} \hat{P}_{j+k,-} \hat{P}_{j'+k,-} \rangle \tag{4.24}$$

$$\langle \sigma_{\pm} \hat{P}_{i,-} \hat{b}^{2} \rangle = \langle \sigma_{\pm} \hat{P}_{i,-} \rangle + \sum_{j=1}^{l} 2^{j+1}(1-2^{j-1}) \langle \sigma_{\pm} \hat{P}_{i,-} \hat{P}_{j+k,-} \rangle + \sum_{\substack{j,j'=1 \\ j \neq j'}}^{l} 2^{j+j'} \langle \sigma_{\pm} \hat{P}_{i,-} \hat{P}_{j+k,-} \hat{P}_{j'+k,-} \rangle \tag{4.25}$$

The first-order expansion of the sub-averages in Equation 4.23, Equation 4.24 and Equation 4.25 with order > 1 yields

$$\langle \sigma_{\pm} \hat{P}_{j+k,-} \rangle = \langle \sigma_{\pm} \rangle \langle \hat{P}_{j+k,-} \rangle \tag{4.26}$$

$$\langle \sigma_{\pm} \hat{P}_{j+k,-} \hat{P}_{j'+k,-} \rangle = \langle \sigma_{\pm} \rangle \langle \hat{P}_{j+k,-} \rangle \langle \hat{P}_{j'+k,-} \rangle \tag{4.27}$$

$$\langle \sigma_{\pm} \hat{P}_{i,-} \hat{P}_{j+k,-} \hat{P}_{j'+k,-} \rangle = \langle \sigma_{\pm} \rangle \langle \hat{P}_{i,-} \rangle \langle \hat{P}_{j+k,-} \rangle \langle \hat{P}_{j'+k,-} \rangle. \tag{4.28}$$

We call this procedure the mean-field approach. The mean-field approach is a purely classical solution, since all quantum mechanical correlations are discarded. Inserting all approximate expressions Equation 4.26-Equation 4.28 into Equation 4.23-Equation 4.25, keeping an eye on the subscripts, and plugging the resulting equations further into Equation 4.19 and Equation 4.20, yields a system of coupled nonlinear c-number ODEs. The system has $3 \cdot n$ equations and can be evaluated by, e.g., Julia or Mathematica.

4.2 Second-Order Expansion

The Ehrenfest system with second-order averages contains now the expectation values of two operators $\hat{\mathcal{O}}_{m_1}, \hat{\mathcal{O}}_{m_2} \in A \cup B$, where $m_1, m_2 \in \mathcal{I}_A \cup \mathcal{I}_B$. Hence, the system of ODEs possesses the shape

$$\frac{d}{dt}\langle(\hat{\mathcal{O}}_{m_1}\hat{\mathcal{O}}_{m_2})(t)\rangle = \hat{i}\left\langle[\hat{H}(t), \hat{\mathcal{O}}_{m_1}\hat{\mathcal{O}}_{m_2}]\right\rangle = \hat{i}\left\langle[\hat{H}(t), \hat{\mathcal{O}}_{m_1}]\hat{\mathcal{O}}_{m_2}\right\rangle + \hat{i}\left\langle\hat{\mathcal{O}}_{m_1}[\hat{H}(t), \hat{\mathcal{O}}_{m_2}]\right\rangle \tag{4.29}$$

Interestingly, the Ehrenfest system of n-order averages, i.e. expectation values of n observables, can always be reduced to a superposition of averages, where in each term only commutators of the shape $[\hat{H}(t), \mathcal{O}]$ appear. The mathematical expression has been proven in section A.2. This is very useful, since we can consider the entire set of results from section 4.1 for any order expansion. However, here we will focus on the second-order expansion.

For the sake of clarity, we only look at the left term on the right-hand side in Equation 4.29 and keep in mind, that for the right term the procedure is analogous:

$$\begin{aligned}\hat{i}\left\langle[\hat{H}(t), \hat{\mathcal{O}}_{m_1}]\hat{\mathcal{O}}_{m_2}\right\rangle = &-\hat{i}\xi(\langle[\sigma_+^{(m_1)}, \hat{\mathcal{O}}_{m_1}]\hat{\mathcal{O}}_{m_2}\rangle + \langle[\sigma_-^{(m_1)}, \hat{\mathcal{O}}_{m_1}]\hat{\mathcal{O}}_{m_2}\rangle)\left(1 - \frac{t}{T}\right) \\ &- \hat{i}2^{m_1+1}\Big(\omega\langle[\hat{P}_{m_1,-}, \hat{\mathcal{O}}_{m_1}]\hat{b}\hat{\mathcal{O}}_{m_2}\rangle - (1 + 2^{m_1-1})\langle[\hat{P}_{m_1,-}, \hat{\mathcal{O}}_{m_1}]\hat{b}^2\hat{\mathcal{O}}_{m_2}\rangle \\ &- \sum_{\substack{i=1 \\ i\neq m_1}}^{k} 2^i\langle[\hat{P}_{m_1,-}, \hat{\mathcal{O}}_{m_1}]\hat{P}_{i,-}\hat{b}^2\hat{\mathcal{O}}_{m_2}\rangle\Big)\left(\frac{t}{T}\right),\end{aligned} \tag{4.30}$$

where $\hat{\mathcal{O}}_{m_1} \in A$. Analogously for $\hat{\mathcal{O}}_{m_1} \in B$. Obviously, the commutators are all the same as in section 4.1, however, the averages have now one additional operator $\hat{\mathcal{O}}_{m_2}$ with $m_2 \in \mathcal{I}_A \cup \mathcal{I}_B$. Inserting the possible operators for $\hat{\mathcal{O}}_{m_1}$ as well as utilizing the commutator relations in Equation 4.8, Equation 4.9 and Equation 4.17 yields

$$\hat{i}\left\langle[\hat{H}(t),\sigma_{\pm}^{(m_1)}]\hat{\mathcal{O}}_{m_2}\right\rangle = \pm\hat{i}\xi(\langle\hat{\mathcal{O}}_{m_2}\rangle - \langle\sigma_{\pm}^{(m_1)}\hat{\mathcal{O}}_{m_2}\rangle)\left(1-\frac{t}{T}\right)$$
$$\pm\hat{i}2^{m_1+1}\Big(\omega\langle\sigma_{\pm}^{(m_1)}\hat{b}\hat{\mathcal{O}}_{m_2}\rangle - (1+2^{m_1-1})\langle\sigma_{\pm}^{(m_1)}\hat{b}^2\hat{\mathcal{O}}_{m_2}\rangle$$
$$-\sum_{\substack{i=1\\ i\neq m_1}}^{k} 2^i\langle\sigma_{\pm}^{(m_1)}\hat{P}_{i,-}\hat{b}^2\hat{\mathcal{O}}_{m_2}\rangle\Big)\left(\frac{t}{T}\right), \tag{4.31}$$

$$\hat{i}\left\langle[\hat{H}(t),\hat{P}_{m_1,-}]\hat{\mathcal{O}}_{m_2}\right\rangle = -\hat{i}\xi(\langle\sigma_{+}^{(m_1)}\hat{\mathcal{O}}_{m_2}\rangle - \langle\sigma_{-}^{(m_1)}\hat{\mathcal{O}}_{m_2}\rangle)\left(1-\frac{t}{T}\right). \tag{4.32}$$

The above equations look familiar. In Equation 4.19 and Equation 4.20, we have the same structure. Before we continue, we shall compute some multiplications of operators acting on the same sub-Hilbert space.

$$\begin{aligned}
\sigma_+\sigma_+ &= \hat{0}, & \sigma_+\hat{P}_- &= \sigma_+ & \sigma_+\sigma_-, &= \mathbb{1}_{2\times 2} - \hat{P}_- = \hat{P}_+\\
\hat{P}_-\sigma_+ &= \hat{0}, & \hat{P}_-\hat{P}_- &= \hat{P}_- & \hat{P}_-\sigma_-, &= \sigma_-\\
\sigma_-\sigma_+ &= \hat{P}_-, & \sigma_-\hat{P}_- &= \hat{0} & \sigma_-\sigma_-, &= \hat{0}.
\end{aligned} \tag{4.33}$$

The relations are also valid for the corresponding Heisenberg operators see section A.3. The above equations show that for $m_1 = m_2$ the two operators on the left-hand side in Equation 4.29 become one operator acting on the same sub-Hilbert space. Therefore, the equations simplify to terms of first order and are the same as in section 4.1 except now we expand up to second order. The cases $m_1 \neq m_2$ remain for further investigation. We must include the operator relations, such that we can obtain the correct solutions. This is done for the following sub-averages:

$$\langle \sigma_{\pm}^{(m_1)} \hat{P}_{j+k,-} \hat{\mathcal{O}}_{m_2} \rangle = \begin{cases} 0, & , \hat{\mathcal{O}}_{m_2} = \sigma_{+}^{(m_2)}, \mathrm{Con}_1 \\ \langle \sigma_{\pm}^{(m_1)} \hat{P}_{j+k,-} \rangle, & , \hat{\mathcal{O}}_{m_2} = \hat{P}_{m_2}, \mathrm{Con}_1 \\ \langle \sigma_{\pm}^{(m_1)} \sigma_{-}^{(j+k)} \rangle & , \hat{\mathcal{O}}_{m_2} = \sigma_{-}^{(m_2)}, \mathrm{Con}_1 \\ \langle \sigma_{\pm}^{(m_1)} \hat{P}_{j+k,-} \hat{\mathcal{O}}_{m_2} \rangle & , m_2 \neq j+k \end{cases} \tag{4.34}$$

$$\langle \sigma_{\pm}^{(m_1)} \hat{P}_{j+k,-} \hat{P}_{j'+k,-} \hat{\mathcal{O}}_{m_2} \rangle = \begin{cases} 0, & , \hat{\mathcal{O}}_{m_2} = \sigma_{+}^{(m_2)}, \mathrm{Con} \\ \langle \sigma_{\pm}^{(m1)} \hat{P}_{j+k,-} \hat{P}_{j'+k,-} \rangle, & , \hat{\mathcal{O}}_{m_2} = \hat{P}_{m_2,-}, \mathrm{Con} \\ \langle \sigma_{\pm}^{(m_1)} \sigma_{-}^{(j+k)} \hat{P}_{j'+k,-} \rangle & , \hat{\mathcal{O}}_{m_2} = \sigma_{-}^{(m_2)}, \mathrm{Con}_1 \\ \langle \sigma_{\pm}^{(m_1)} \hat{P}_{j+k,-} \sigma_{-}^{(j'+k)} \rangle & , \hat{\mathcal{O}}_{m_2} = \sigma_{-}^{(m_2)}, \mathrm{Con}_2 \\ \langle \sigma_{\pm}^{(m_1)} \hat{P}_{j+k,-} \hat{P}_{j'+k,-} \hat{\mathcal{O}}_{m_2} \rangle & , j \neq m_2 - k \neq j' \end{cases} \tag{4.35}$$

$$\langle \sigma_{\pm}^{(m_1)} \hat{P}_{i,-} \hat{P}_{j+k,-} \hat{P}_{j'+k,-} \hat{\mathcal{O}}_{m_2} \rangle = \begin{cases} 0, & , \hat{\mathcal{O}}_{m_2} = \sigma_{+}^{(m_2)}, (m_2 = i) \vee \mathrm{Con} \\ \langle \sigma_{\pm}^{(m1)} \hat{P}_{i,-} \hat{P}_{j+k,-} \hat{P}_{j'+k,-} \rangle, & , \hat{\mathcal{O}}_{m_2} = \hat{P}_{m_2,-}, (m_2 = i) \vee \mathrm{Con} \\ \langle \sigma_{\pm}^{(m_1)} \sigma_{-}^{(i)} \hat{P}_{j+k,-} \hat{P}_{j'+k,-} \rangle & , \hat{\mathcal{O}}_{m_2} = \sigma_{-}^{(m_2)}, m_2 = i \\ \langle \sigma_{\pm}^{(m_1)} \hat{P}_{i,-} \sigma_{-}^{(j+k)} \hat{P}_{j'+k,-} \rangle & , \hat{\mathcal{O}}_{m_2} = \sigma_{-}^{(m_2)}, \mathrm{Con}_1 \\ \langle \sigma_{\pm}^{(m_1)} \hat{P}_{i,-} \hat{P}_{j+k,-} \sigma_{-}^{(j'+k)} \rangle & , \hat{\mathcal{O}}_{m_2} = \sigma_{-}^{(m_2)}, \mathrm{Con}_2 \\ \langle \sigma_{\pm}^{(m_1)} \hat{P}_{i,-} \hat{P}_{j+k,-} \hat{P}_{j'+k,-} \hat{\mathcal{O}}_{m_2} \rangle & , j \neq m_2 - k \neq j' \wedge m_2 \neq i \end{cases} \tag{4.36}$$

where we use the relations from Equation 4.33 and we define the conditions $\mathrm{Con}_1 \equiv (m_2 = j + k)$ $\mathrm{Con}_2 \equiv (m_2 = j' + k)$ and $\mathrm{Con} = \mathrm{Con}_1 \vee \mathrm{Con}_2$. We assumed $m_1 \in \mathcal{I}_A$ and $m_2 \in \mathcal{I}_A \cup \mathcal{I}_B$ to acquire the above averages. To obtain, however, a complete ODE system, it is enough to note that $m_1 < m_2$. This can be justified by the fact, that operators acting on different sub-Hilbert spaces always commute, hence, we get equal equations for $m_1 > m_2$. We show this in section A.4. Therefore, only the case $m_1 \in \mathcal{I}_B \backslash \{k + l\}$ with $m_1 < m_2$ remains. First, we write down the modified Equation 4.31:

$$\begin{aligned} \hat{i} \left\langle [\hat{H}(t), \sigma_{\pm}^{(m_1)}] \hat{\mathcal{O}}_{m_2} \right\rangle &= \pm \hat{i} \xi (\langle \hat{\mathcal{O}}_{m_2} \rangle - \langle \sigma_{\pm}^{(m_1)} \hat{\mathcal{O}}_{m_2} \rangle) \left(1 - \frac{t}{T} \right) \\ &\pm \hat{i} 2^{m_1 - k + 1} \Big(\omega \langle \sigma_{\pm}^{(m_1)} \hat{a} \hat{\mathcal{O}}_{m_2} \rangle - (1 + 2^{m_1 - k - 1}) \langle \sigma_{\pm}^{(m_1)} \hat{a}^2 \hat{\mathcal{O}}_{m_2} \rangle \\ &- \sum_{\substack{i=1 \\ i \neq m_1 - k}}^{l} 2^j \langle \sigma_{\pm}^{(m_1)} \hat{a}^2 \hat{P}_{j+k,-} \hat{\mathcal{O}}_{m_2} \rangle \Big) \left(\frac{t}{T} \right). \end{aligned} \tag{4.37}$$

It is clear, that the sub-average of the above equations $\langle \sigma_{\pm}^{(m_1)} \hat{P}_{i,-} \hat{\mathcal{O}}_{m_2} \rangle$ and $\langle \sigma_{\pm}^{(m_1)} \hat{P}_{i,-} \hat{P}_{i',-} \hat{\mathcal{O}}_{m_2} \rangle$ stay the same. The last sub-average possesses the cases:

$$\langle\sigma_{\pm}^{(m_1)}\hat{P}_{i,-}\hat{P}_{i',-}\hat{P}_{j+k,-}\hat{\mathcal{O}}_{m_2}\rangle = \begin{cases} 0 & , \hat{\mathcal{O}}_{m_2} = \sigma_{+}^{(m_2)}, m_2 = j+k \\ \langle\sigma_{\pm}^{(m_1)}\hat{P}_{i,-}\hat{P}_{i',-}\hat{P}_{j+k,-}\rangle & , \hat{\mathcal{O}}_{m_2} = \hat{P}_{m_2,-}, m_2 = j+k \\ \langle\sigma_{\pm}^{(m_1)}\hat{P}_{i,-}\hat{P}_{i',-}\sigma_{-}^{(j+k)}\rangle & , \hat{\mathcal{O}}_{m_2} = \sigma_{-}^{(m_2)}, m_2 = j+k \\ \langle\sigma_{\pm}^{(m_1)}\hat{P}_{i,-}\hat{P}_{i',-}\hat{P}_{j+k,-}\hat{\mathcal{O}}_{m_2}\rangle & , m_2 \neq j+k \end{cases} \tag{4.38}$$

Now, we have all possible sub-average cases for the left term on the right-hand side in Equation 4.29. Analogously, we can do the same for the right term, however, in a shortened manner. Considering the term and inserting definitions of $\hat{\mathcal{O}}_{m_2}$, we receive

$$\begin{aligned} \hat{i}\left\langle\hat{\mathcal{O}}_{m_1}[\hat{H}(t),\sigma_{\pm}^{(m_2)}]\right\rangle &= \pm\hat{i}\xi(\langle\hat{\mathcal{O}}_{m_1}\rangle - \langle\hat{\mathcal{O}}_{m_1}\sigma_{\pm}^{(m_2)}\rangle)\left(1-\frac{t}{T}\right) \\ &\pm \hat{i}2^{m_2+1}\Big(\omega\langle\hat{\mathcal{O}}_{m_1}\sigma_{\pm}^{(m_2)}\hat{b}\rangle - (1+2^{m_2-1})\langle\hat{\mathcal{O}}_{m_1}\sigma_{\pm}^{(m_2)}\hat{b}^2\rangle \\ &- \sum_{\substack{i=1 \\ i\neq m_2}}^{k} 2^i\langle\hat{\mathcal{O}}_{m_1}\sigma_{\pm}^{(m_2)}\hat{P}_{i,-}\hat{b}^2\rangle\Big)\left(\frac{t}{T}\right), \end{aligned} \tag{4.39}$$

$$\hat{i}\left\langle\hat{\mathcal{O}}_{m_1}[\hat{H}(t),\hat{P}_{m_2,-}]\right\rangle = -\hat{i}\xi(\langle\hat{\mathcal{O}}_{m_1}\sigma_{+}^{(m_2)}\rangle - \langle\hat{\mathcal{O}}_{m_1}\sigma_{-}^{(m_2)}\rangle)\left(1-\frac{t}{T}\right). \tag{4.40}$$

with $m_2 \in \mathcal{I}_A$. We start once again with $m_1 \in \mathcal{I}_A$. We recognize that it is also important to distinguish between $\hat{\mathcal{O}}_{m_2} \in A$ and $\hat{\mathcal{O}}_{m_2} \in B$. Firstly, let $m_2 \in \mathcal{I}_A$ and $m_1 < m_2$. The sub-averages of the form $\langle\hat{\mathcal{O}}_{m_1}\sigma_{\pm}^{(m_2)}\hat{P}_{j+k,-}\rangle$ and $\langle\hat{\mathcal{O}}_{m_1}\sigma_{\pm}^{(m_2)}\hat{P}_{j+k,-}\hat{P}_{j'+k,-}\rangle$ remain the same. The five-operator sub-averages, however, consist of the cases:

$$\langle\hat{\mathcal{O}}_{m_1}\hat{P}_{i,-}\sigma_{\pm}^{(m_2)}\hat{P}_{j+k,-}\hat{P}_{j'+k,-}\rangle = \begin{cases} \langle\sigma_{+}^{(i)}\sigma_{\pm}^{(m_2)}\hat{P}_{j+k,-}\hat{P}_{j'+k,-}\rangle & , \hat{\mathcal{O}}_{m_1} = \sigma_{+}^{(m_1)}, m_1 = i \\ \langle\hat{P}_{i,-}\sigma_{\pm}^{(m_2)}\hat{P}_{j+k,-}\hat{P}_{j'+k,-}\rangle & , \hat{\mathcal{O}}_{m_1} = \hat{P}_{m_1,-}, m_1 = i \\ 0 & , \hat{\mathcal{O}}_{m_1} = \sigma_{-}^{(m_1)}, m_1 = i \\ \langle\hat{\mathcal{O}}_{m_1}\hat{P}_{i,-}\sigma_{\pm}^{(m_2)}\hat{P}_{j+k,-}\hat{P}_{j'+k,-}\rangle & , m_1 \neq i \end{cases} \tag{4.41}$$

Secondly, let $m_2 \in \mathcal{I}_B$ and $m_1 \in \mathcal{I}_A \cup \mathcal{I}_B$. Here, the sub-averages contain now two projectors living in the domain A and one in B. Thus, we obtain

$$\langle\hat{\mathcal{O}}_{m_1}\hat{P}_{i,-}\hat{P}_{i',-}\sigma_{\pm}^{(m_2)}\hat{P}_{j+k,-}\rangle = \begin{cases} \langle\sigma_{+}^{(i)}\hat{P}_{i',-}\sigma_{\pm}^{(m_2)}\hat{P}_{j+k,-}\rangle & , \hat{\mathcal{O}}_{m_1} = \sigma_{+}^{(m_1)}, \widetilde{\text{Con}}_1 \\ \langle\hat{P}_{i,-}\sigma_{+}^{(i')}\sigma_{\pm}^{(m_2)}\hat{P}_{j+k,-}\rangle & , \hat{\mathcal{O}}_{m_1} = \sigma_{+}^{(m_1)}, \widetilde{\text{Con}}_2 \\ \langle\hat{P}_{i,-}\hat{P}_{i',-}\sigma_{\pm}^{(m_2)}\sigma_{+}^{(j+k)}\rangle & , \hat{\mathcal{O}}_{m_1} = \sigma_{+}^{(m_1)}, m_1 = j+k \\ \langle\hat{P}_{i,-}\hat{P}_{i',-}\sigma_{\pm}^{(m_2)}\hat{P}_{j+k,-}\rangle & , \hat{\mathcal{O}}_{m_1} = \hat{P}_{m_1,-}, \widetilde{\text{Con}} \vee m_1 = j+k \\ 0 & , \hat{\mathcal{O}}_{m_1} = \sigma_{-}^{(m_1)}, \widetilde{\text{Con}} \vee m_1 = j+k \\ \langle\hat{\mathcal{O}}_{m_1}\hat{P}_{i,-}\sigma_{\pm}^{(m_2)}\hat{P}_{j+k,-}\hat{P}_{j'+k,-}\rangle & , \widetilde{\text{Con}}_1 \wedge \widetilde{\text{Con}}_2 \wedge m_1 = j+k \end{cases}, \tag{4.42}$$

where $\widetilde{\text{Con}}_1 \equiv (i = m_1)$, $\widetilde{\text{Con}}_2 \equiv (m_1 = i')$ and $\widetilde{\text{Con}} = \widetilde{\text{Con}}_1 \vee \widetilde{\text{Con}}_2$. This concludes the investigation of the sub-averages reduction. The final step is now the utilization of the *cumulants approach*. The expectation values above in second-order expansion contain at most five operators. For convenience, we introduce χ_r with $r \in \{3,4,5\}$. Here, r denotes the expansion order of the considered averages. Let us consider the examples:

$$\begin{aligned} \langle\hat{X}_1\hat{X}_2\hat{X}_3\rangle = \chi_3(\hat{X}_1,\hat{X}_2,\hat{X}_3) &= \langle\hat{X}_1\rangle\langle\hat{X}_2\hat{X}_3\rangle + \langle\hat{X}_2\rangle\langle\hat{X}_1\hat{X}_3\rangle + \langle\hat{X}_3\rangle\langle\hat{X}_1\hat{X}_2\rangle \\ &\quad - 2\langle\hat{X}_1\rangle\langle\hat{X}_2\rangle\langle\hat{X}_3\rangle \\ \langle\hat{X}_1\hat{X}_2\hat{X}_3\hat{X}_4\rangle = \chi_4(\hat{X}_1,\hat{X}_2,\hat{X}_3,\hat{X}_4) &= \langle\hat{X}_1\hat{X}_2\rangle\langle\hat{X}_3\hat{X}_4\rangle + \langle\hat{X}_1\hat{X}_3\rangle\langle\hat{X}_2\hat{X}_3\rangle \\ &\quad + \langle\hat{X}_1\hat{X}_4\rangle\langle\hat{X}_2\hat{X}_3\rangle - 2\langle\hat{X}_1\rangle\langle\hat{X}_2\rangle\langle\hat{X}_3\rangle\langle\hat{X}_4\rangle. \end{aligned}$$

The entire section is implemented in *Mathematica* which can be viewed in Appendix B for the toy-model $\omega = 15$ at $T = 5$.

Chapter 5

Results

In this chapter we present the first-order expansion results of ω listed in Table 3.1 utilizing the theory from section 2.4, where we ignore $\omega \in \{93, 95\}$. The approximated classical solutions are compared with the full quantum-dynamical results discussed in chapter 3. These comparisons provide hints of a possible quantum advantage for the bi-prime factorization problem. Higher-order cumulant expansions are investigated as well. Most results yield divergences, which inspire to a more precise discussion in chapter 6.

5.1 First-Order Expansion Results

We utilize *QuantumCumulants.jl* to receive the results of the mean-field approach for the three- $(15, 21)$, four- $(33, 39)$ and five-qubit-systems $(51, 57)$ in Figure 5.1. Here, we compare the results with the full quantum-dynamical solutions obtained in chapter 3.

First, we treat the case $\omega = 15$ in Figure 5.1. We see that the blue line of the mean-field expansion approaches zero, which corresponds to the expectation value of the classical bit-digit a_1. The other two converge to one. Hence, the classical results provide the same correct results as the quantum dynamics at $T = 10$. There are some visual differences to the quantum treatment, nevertheless the expansion model solves the problem without doubt. The same applies for $\omega = 21$ where all lines approach one, thus, we receive $7[111] \times 3[11]$. This solves the bi-prime factorization problem for the case under consideration. So far, no significant differences between quantum dynamics and the classical model can be observed considering a three-qubit system. We continue by looking at the four-qubit-systems, i.e., $\omega \in \{33, 39\}$. We start with the bi-prime $\omega = 33$, where we can immediately see that we obtain the correct results utilizing the classical model. A similar visual shape of the bit-digit expectation values solves the problem of $\omega = 39$. Now, we increase the system size to five qubits. These bi-primes are examined more carefully. Even for this system size, the classical model does not seem to have any significant disadvantages compared to the full quantum dynamics for both $\omega = 51$ and $\omega = 57$. However, we can observe that some

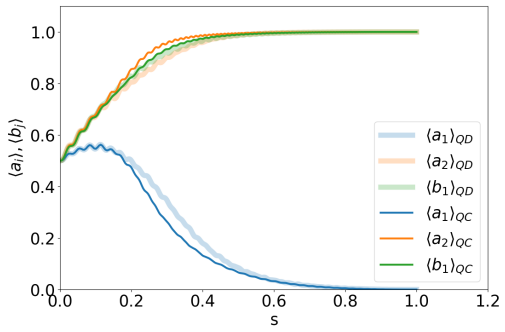

(a) $\omega = 15[1111] = 5[101] \times 3[11]$

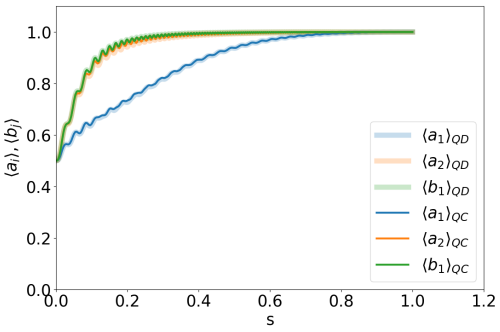

(b) $\omega = 21[10101] = 7[111] \times 3[11]$

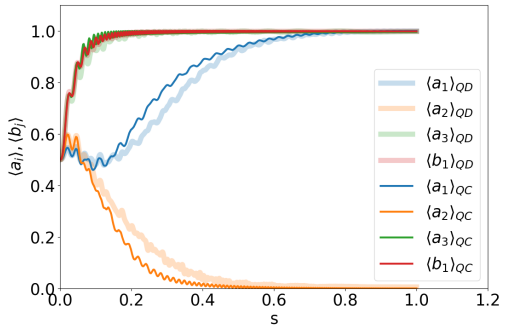

(c) $\omega = 33[100001] = 11[1011] \times 3[11]$

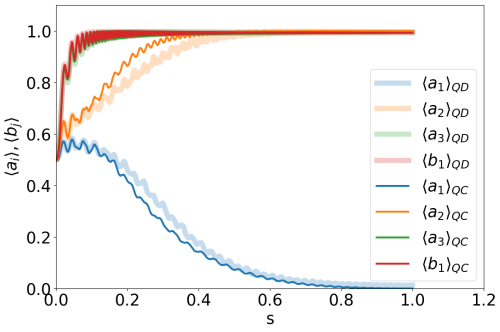

(d) $\omega = 39[100111] = 13[1101] \times 3[11]$

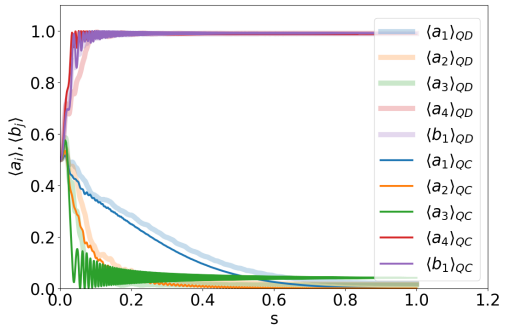

(e) $\omega = 51[110011] = 17[10001] \times 3[11]$

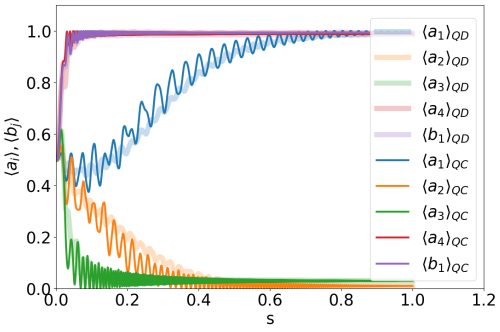

(f) $\omega = 57[111001] = 19[10011] \times 3[11]$

Figure 5.1: Comparison between classical model and the full quantum dynamics for $\omega \in \{15, 21, 33, 39, 51, 57\}$. The full quantum dynamics is denoted by QD and the cumulant expansion by QC. We set $T = 10$.

expectation values do not reach entirely the plateau at zero but manifest their equilibrium at a larger value. This is a sign that T should be chosen slightly larger than $T = 10$ for the classical model. This would be a hint of a possible quantum advantage for the bi-prime factorization problem. We examine now a 7-qubit system for a possible quantum advantage.

We investigate the bi-prime $\omega = 265$ which has 7 dynamical qubits with a 2^7 dimensional Hilbert space. The comparison between the full quantum dynamics and the classical results are visualized in Figure 5.2.

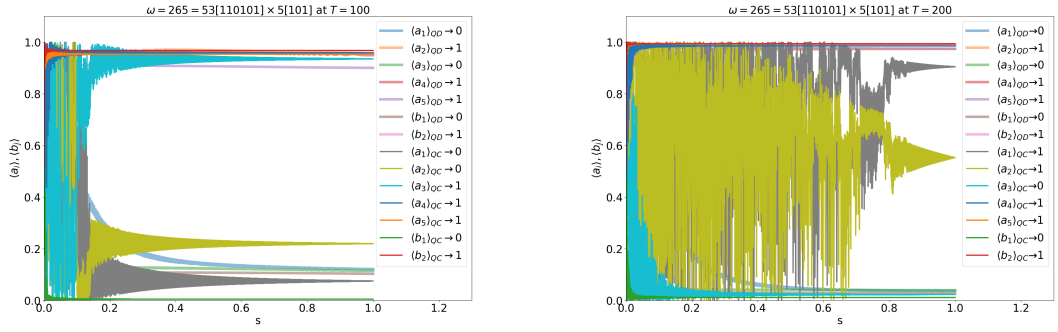

(a) (b)

Figure 5.2: Quantum dynamics (QD) as well as the cumulants approach (QC) with $\omega = 265$. The legend provides the rounded expectation values of the classical bit-digits received by the corresponding method.

According to Equation 2.13, the choice $T = 100$ implies a rather fast transition. The quantum dynamics reaches the plateaus neither for zero nor one for all expectation values in Figure 5.2a. Nevertheless, we get the correct bit-sequence utilizing the rounded numerical quantum-dynamical values at $s = 1$, whereas the mean-field approach yields the sequence of $\omega = 285$. Thus, the classical method fails. We increase T to $T = 200$ and receive now for the quantum dynamics numerical values closer to zero and one. The cumulants solution still gives the wrong sequence corresponding to the solution $\omega = 275$. We have found a case, where the factorization is solved faster by the quantum dynamical method. This is a direct hint that the mean-field approach requires a larger evolution time T than the full quantum dynamics for growing system size. We recall that T is the actual time necessary to solve a quantum algorithm on an adiabatic quantum computer. The comparison between classical and quantum solution provides insights about the importance of quantum effects to solve the factorization problem. The quantum advantage is given by looking at T, however, since we only have a classical computer we conclude as follows. We assume the comparisons in Figure 5.2 as a hint for a quantum advantage for the bi-prime factorization problem, because the real computation time for solving the problem on a classical computer tells us, that the results are evaluated faster using the cumulants approach in first-order than the actual quantum solution for the cases under consideration. At least for manageable system sizes, it is still efficient to choose T larger for the classical case to receive correct results.

5.2 Higher-Order Expansion Results

Since we utilize Equation 2.59, we can expand the quantum dynamics to higher-orders. In this section we show and discuss the results for $\omega \in \{15, 21, 33, 39\}$. The obtained results provide some interesting observations. It is important to mention, that we expand up to the order, which represents the full quantum dynamics. A given ω with n dynamical qubits has maximal order of n. This is a direct implication of the application of Equation 2.59. Thus, a three-qubit-system possesses maximal order 3 and a four-qubit-system has a maximal order 4. We apply again QuantumCumulants.jl to obtain the results in Figure 5.3 and in Figure 5.4

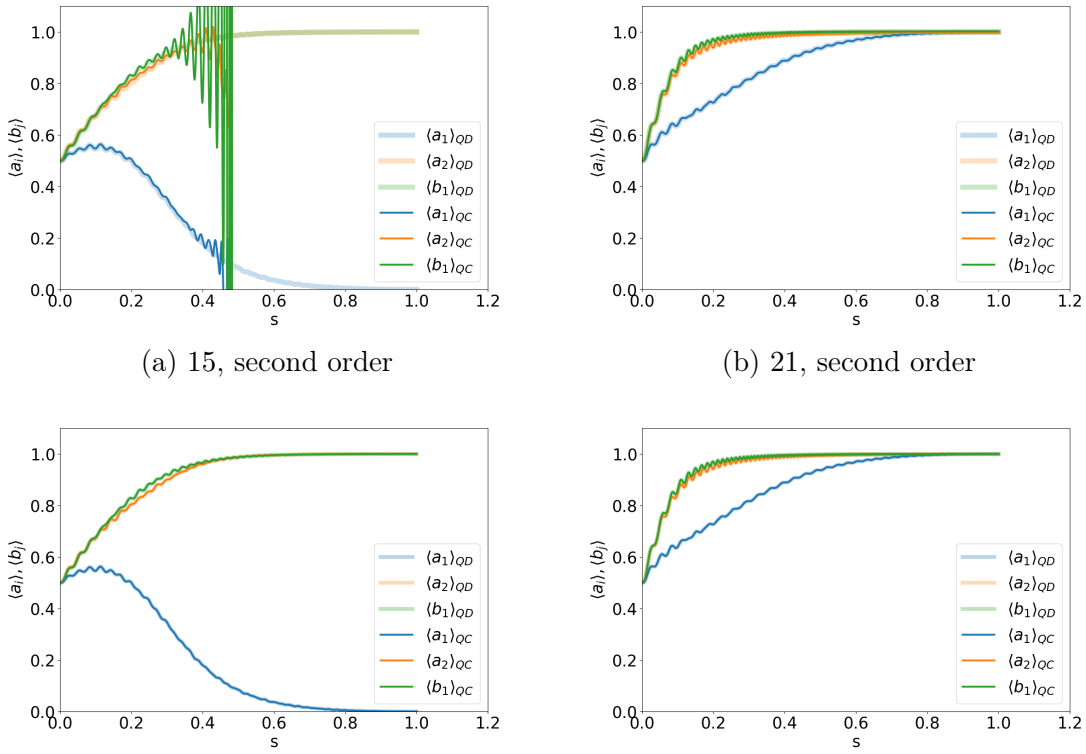

(a) 15, second order

(b) 21, second order

(c) 15, third order

(d) 21, third order

Figure 5.3: Solutions of $\omega = 15[1111] = 5[101] \times 3[11]$ and $\omega = 21[10101] = 7[111] \times 3[11]$ in second- and third- (maximal) order expansion, where $T = 10$. The non-full quantum dynamical solution shows a clear divergence for $\omega = 15$ in (a), whereas this is not the case for $\omega = 21$

In Figure 5.3, we observe that in second order expansion the case $\omega = 15$ yields a divergent solution, whereas $\omega = 21$ provides the correct result. In maximal order, we obtain the exact quantum dynamics for both factorization problems. At first glance, it is not entirely clear, where this divergent behavior of $\omega = 15$ could come from. We continue the examination by considering $\omega \in \{33, 39\}$ in Figure 5.4.

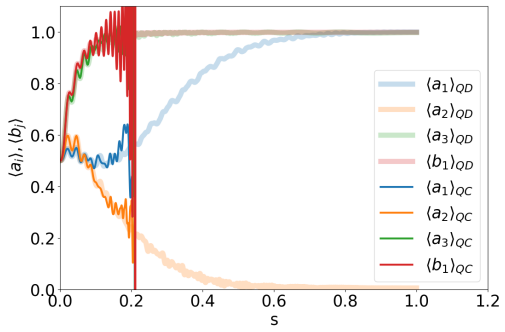

(a) 33, second order

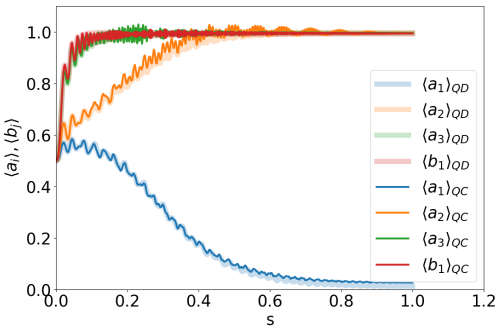

(b) 39, second order

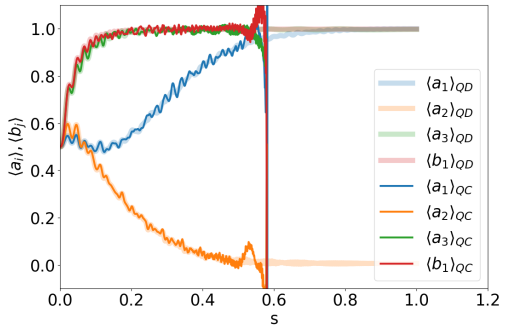

(c) 33, third order

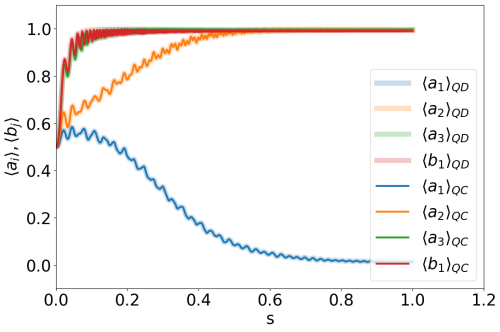

(d) 39, third order

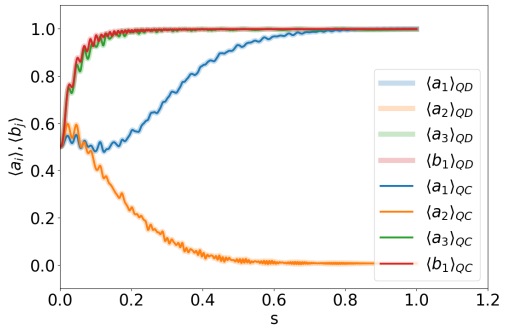

(e) 33, fourth order

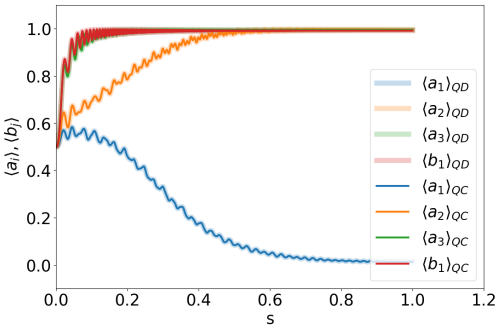

(f) 39, fourth order

Figure 5.4: Solutions of $\omega = 33[100001] = 11[1011] \times 3[11]$ and $\omega = 39[100111] = 13[1101] \times 3[11]$ in second-, third- and fourth- (maximal) order expansion. In (a) and (c) we observe the divergent non-full quantum dynamics for $\omega = 33$.

In Figure 5.4, we find divergent behaviors for $\omega = 33$ in second- and in third-order. The fourth-order expansion is again the full quantum dynamics. For $\omega = 39$ in second-order expansion we receive a good solution in the sense that the results are convergent. Nevertheless, we have some oscillations with values larger than one. The remaining cases for $\omega = 39$ are both correct. Comparing all cases with one another we recognize that the

divergent results seem only to appear in cumulant expansions with orders $1 < \text{order} < n$. Indeed, we have not found divergent solutions in the mean-field approximations so far. However, the integer $\omega = 39$ seems to be the last non-divergent case, because for the larger integers $\omega \in \{51, 57, 63, 85, 91, 93\}$ no stable second-order expansion solutions have been found. Apparently, for most bi-primes the annealing must either be classical or full quantum dynamical in order to give reasonable results. We discuss possible origins of the occurring divergences in Figure 5.3 and Figure 5.4 in chapter 6.

Chapter 6

Divergences

The divergences appearing in higher-order expansions seem to be quite exotic with unknown origin. There could be multiple different reasons why divergences occur in the results between the first- and the maximal-order expansion (see. section 5.2). In the scope of this thesis we tried many different approaches to resolve these divergences, assuming that the solutions of the bit-digit expectation values ought to be finite and between 0 and 1 for arbitrary expansion orders. This implies also the assumption that the generalized cumulant expansion method in arbitrary order works for the bi-prime factorization problem. The following list gives a short overview about what has been examined in detail.

Possible Problems: Model, Implementations and QuantumCumulants.jl

- Ensuring the correctness of our model as well as the implementations in the Julia programming language (e.g. toy-model in Appendix C) multiple times.
- Solving a given Ehrenfest ODE system requires an initial-value vector. It is well-known, that a small deviation of a given initial-value vector from the correct one can end up in major divergent solutions. By using the adiabatic Hamiltonian $\hat{H}(s)$ at $s = 0$ (see subsection 2.2.1), we can determine the correct initial-value vector (theoretical derivation in section A.5). The vector was computed in multiple different ways, which provided values coinciding with the theoretical expectations.
- The package *QuantumCumulants.jl* uses, by default, the transition operators $\sigma_+ = \sigma^{12}$, $\sigma_- = \sigma^{21}$ as well as the projector $\hat{P}_- = \sigma^{22}$. These operators were used in chapter 4 to derive the commutator relations and the Ehrenfest ODE systems in first- and second-order expansion. It is also possible to derive equivalent ODE systems by utilizing the Pauli-matrices $\sigma_x, \sigma_y, \sigma_z$ (see discussion in chapter 4). We changed the default-settings in QuantumCumulants.jl to the Pauli-settings and received the same results (see toy-model in section A.6).
- Since QuantumCumulants.jl is mostly used for quantum-optical problems, we could

run into issues considering commutator relations or similar. We derived the mathematics in chapter 4, implemented the resulting commutator relations in *Mathematica* and compared the obtained solutions with the ones received by QuantumCumulants.jl for $\omega \in \{15, 21, 33, 39\}$. The solutions coincide with each other almost perfectly. A more precise discussion is presented in section 6.1.

Possible Problems: Numerical Computation Since the analysis of the divergences grew more and more in numerical complexity, we discussed the obtained knowledge with the two mathematicians Univ.-Prof. Dr. Alexander Ostermann and Univ.-Prof. Lukas Einkemmer, PhD from the University of Innsbruck.

- To solve a given ODE system numerically, we utilize the Julia package DifferentialEquations.jl [34]. Here, we have multiple options to compute the solutions. It might be important to choose the solvers, the relative tolerances (reltol) as well as the absolute tolerances (abstol) more carefully. One can also use adaptive step-size control for specific solvers. Hence, we can set the time steps dt to a fixed value and allow the examination of the divergences from a slightly different angle. For all acquired results in the previous chapters we used the Runge-Kutta-4-method [35] with the default tolerances. In section 6.2 we change the settings and discuss the results.
- Important information about the Ehrenfest ODE system can be received by examining the eigenvalues of the system's underlying Jacobi matrix. The imaginary parts of the eigenvalues tell us, how fast the real parts of the eigenvalues oscillate. Since the Ehrenfest ODE system is nonlinear non-autonomous and coupled, this permits to gather information of internal dynamics of the system under consideration.We discuss the results in section 6.3.
- We know from subsection 2.4.2 that the joint cumulant is assumed to be equal to 0. This was necessary to receive a recursive expression for the n-th order average. We can introduce a way to examine how close to zero the joint cumulants of all possible operator combinations actually are. The results help to determine, especially, which joint cumulants become very large. Therefore, we need the n-th order averages of both the full quantum dynamics and the QuantumCumulants.jl. This is discussed more thoroughly in section 6.4.

We consider now the more precise discussions starting with the examination of QuantumCumulants.jl.

6.1 Julia vs Mathematica

We need to consider that QuantumCumulants.jl might be the origin of the divergences. QuantumCumulants.jl is a package mostly utilized for quantum-optical problems, however, the bi-prime factorization is of purely non-quantum-optical nature. Maybe QuantumCumulants.jl has difficulties to compute the correct commutator relations or other kinds of

issues occur. We can prove that this is not the case by using the results from chapter 4 and implementing them into a different software, in this case *Mathematica*. The implementations of the theoretical discussions in section 4.1 and section 4.2 in Mathematica-code provide the exact same Ehrenfest ODE systems as the systems received by QuantumCumulants.jl. This implies, that QuantumCumulants.jl utilizes the same commutator relations as in chapter 4. Thus, QuantumCumulants.jl should not be the origin of the divergences. We present the comparisons between the measurements of the bit-digits, received by Mathematica and QuantumCumulants.jl, for $\omega = 15$ and $\omega = 21$, respectively, in first-order expansion at $T = 10$. The results are presented in Figure 6.1. Furthermore, in Figure 6.2 we observe the case $\omega = 15$ in second-order expansion at $T \in \{5, 10\}$. We plot also the second-order expansions for $\omega = 33$ and $\omega = 39$ at $T = 10$ in Figure 6.3.

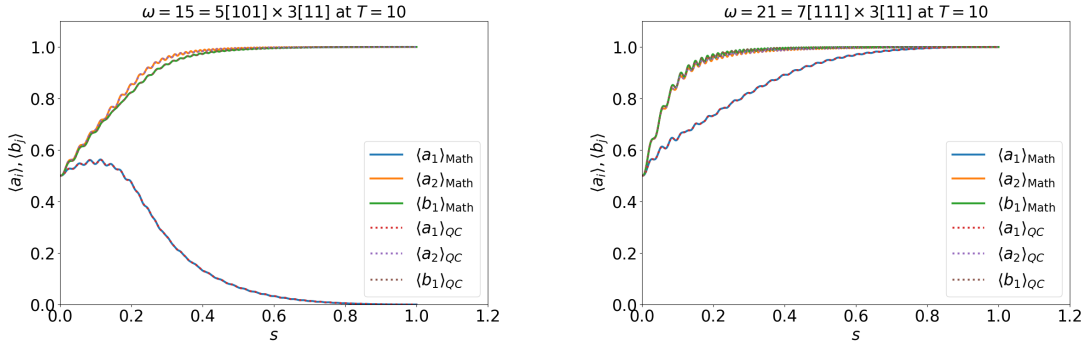

(a) (b)

Figure 6.1: Comparison of the mean-field bit-digit measurements between Mathematica (full lines) and QuantumCumulants.jl (dotted lines) for $\omega = 15$ in (a) and for $\omega = 21$ in (b) at $T = 10$.

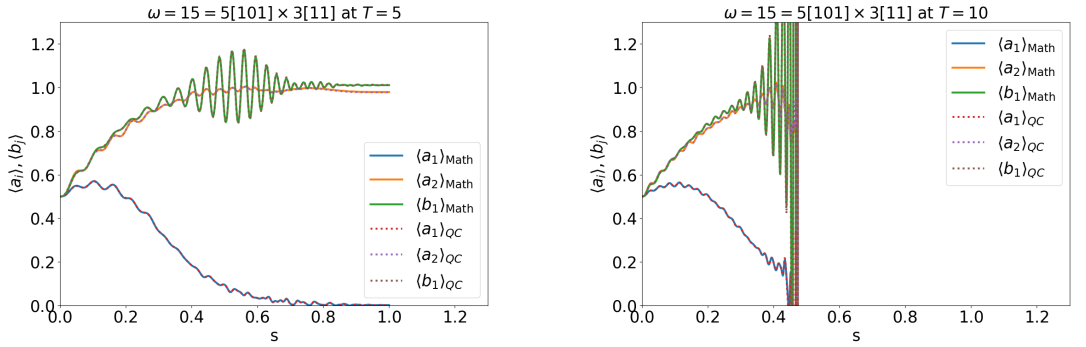

(a) (b)

Figure 6.2: Comparison of the second-order results between Mathematica (full lines) and QuantumCumulants.jl (dotted lines) for $\omega = 15$ at $T = 5$ in (a) and at $T = 10$ in (b). In the latter we observe that the evaluation is aborted at the divergent s for $T = 10$.

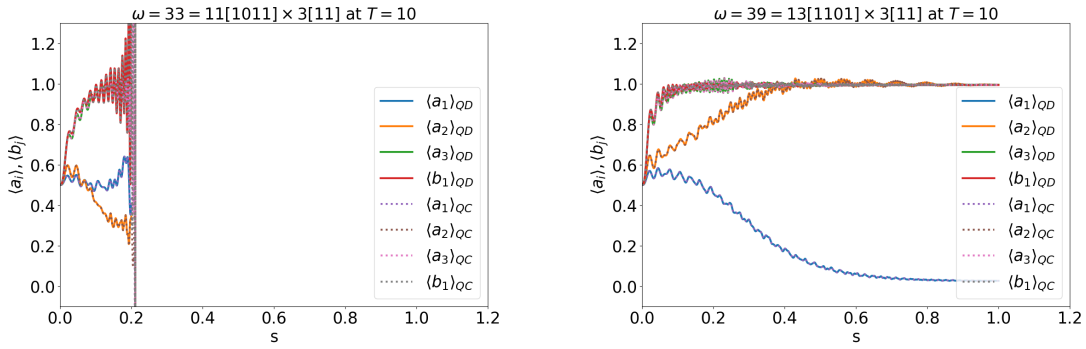

(a) (b)

Figure 6.3: Comparison of the second-order methods between Mathematica (full lines) and QuantumCumulants.jl (dotted lines) for $\omega = 33$ in (a) and for $\omega = 39$ in (b) at $T = 10$.

In Figure 6.1 we can observe that the solutions in the mean-field expansion for $\omega = 15$ and $\omega = 21$, respectively, coincide up to a numerical error. Also, Figure 6.2 and Figure 6.3 show, that the measurements of all cases obtained by both softwares overlap up to an error of numerical nature. Interestingly, the solutions of the cumulants approach in second-order for $\omega = 15$ at $T = 5$ inherits a finite oscillation, which has already grown larger than 1. Increasing T to $T = 10$ gives divergent behaviors for Mathematica as well as QuantumCumulants.jl. In Figure 6.3, we can observe similar divergences for $\omega = 33$, whereas $\omega = 39$ stays finite. It is now clear that QuantumCumulants.jl computes the commutator relations correctly, thus, provides the correct Ehrenfest ODE system. In the further discussion we analyze the numerical computations of the Ehrenfest ODE systems more thoroughly, since we used the default solvers so far.

6.2 Solvers and Tolerances

We use the Julia package *DifferentialEquations.jl* [34] to solve the Ehrenfest ODE system numerically. Here, we have different possibilities to actually solve a system of ODEs. For instance, we can choose a specific solver from a bunch of different explicit or implicit solvers. We can also change the tolerances absolute tolerance (abstol) and relative tolerance (reltol), which allow to dictate the precision of a numerical solution. In general, the smaller the tolerances the more precise the solutions. However, this also means an increase in computation time. Many other options are available as well to solve an ODE system. For example, one can set the numerical time-steps dt to a fixed value, hence, one turns off the adaptive step-size control. Since we assume that the solver choice, the tolerances and the step-size control are options, which influence the numerical computation the most and could allow the removal of the occurring divergences, we restrict the numerical analysis to these settings. Considering *line 86* in Appendix C as a template, we can define different solve-options by the following code:

```
solve(prob,RK4(),abstol = 1e-8, reltol = 1e-4, dt = 1e-6)
```

where *prob* defines a given ODEProblem with certain initial conditions. We use the explicit *Runge-Kutta-4 (RK4)* method [35], which we utilized to determine the results in the previous chapters, to solve the problem and define the tolerances *abstol* and *reltol* as well as the time-steps *dt* accordingly.

We start our examination measurements obtained via Julia. Therefore, we reconsider a problem, where we already know the correct results, and compare the RK4 solutions with the results obtained by utilizing a different solver called *Tsitouras 5/4 (Tsit5)* [36]. This solver is tightly related to the *Runge-Kutta-Fehlberg-4(5) (RKF4(5))* scheme [37]. The derivation of the Tsit5 Butcher tableau considers slightly different assumptions than the one for RKF4(5). We choose the bi-prime problem $\omega = 51$ (see Figure 3.4e) at $T \in \{10, 100\}$. The results are presented in Figure 6.4.

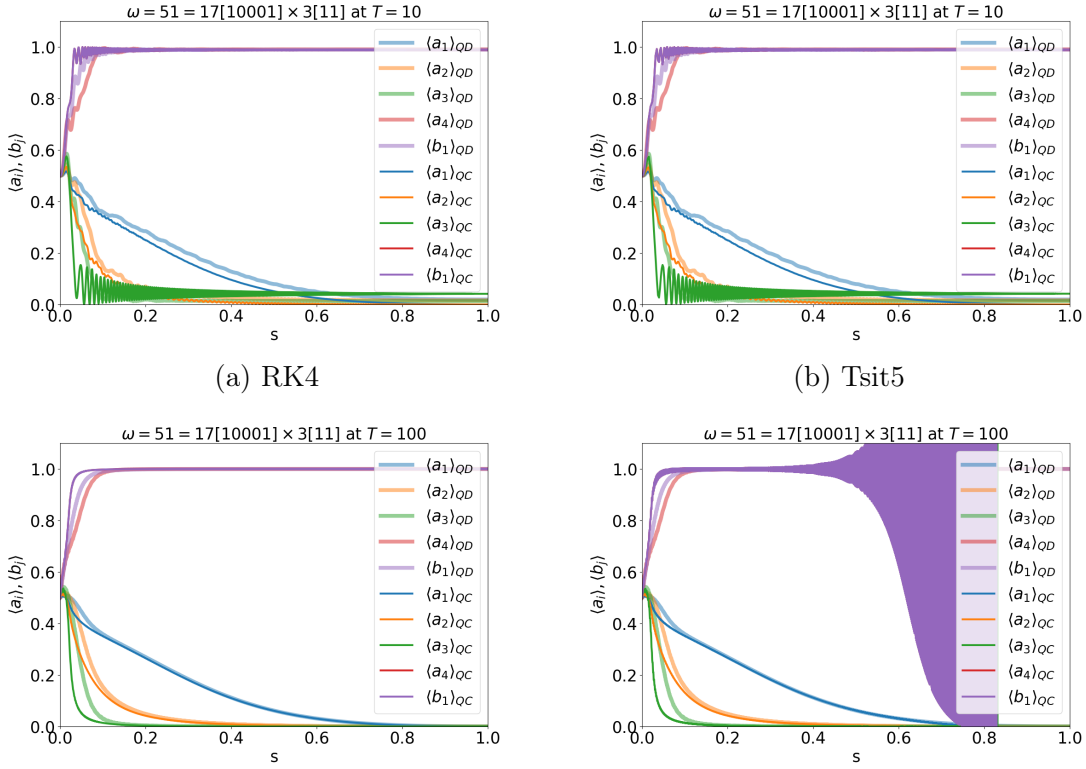

(a) RK4 (b) Tsit5

(c) RK4 (d) Tsit5

Figure 6.4: Comparison between the two solvers RK4 and Tsit5 in [(a),(c)] and [(b),(d)], respectively, with default tolerances and adaptive time-steps, where $\omega = 51[110011] = 17[10001] \times 3[11]$ at $T \in \{10, 100\}$. QD stands for the full quantum dynamics and QC for the QuantumCumulants.jl-solution.

Figure 6.4 reveals that at $T = 10$ both RK4 and Tsit5 provide, qualitatively, the same

results. However, at $T = 100$ the Tsit5 solutions suddenly develop divergences, whereas the RK4 solution remains stable and gives a better result. By default, we have abstol = 1e-6 and reltol = 1e-3. Decreasing the tolerances to abstol=1e-8=reltol yields the correct Tsit5-result. This can be observed in Figure 6.5.

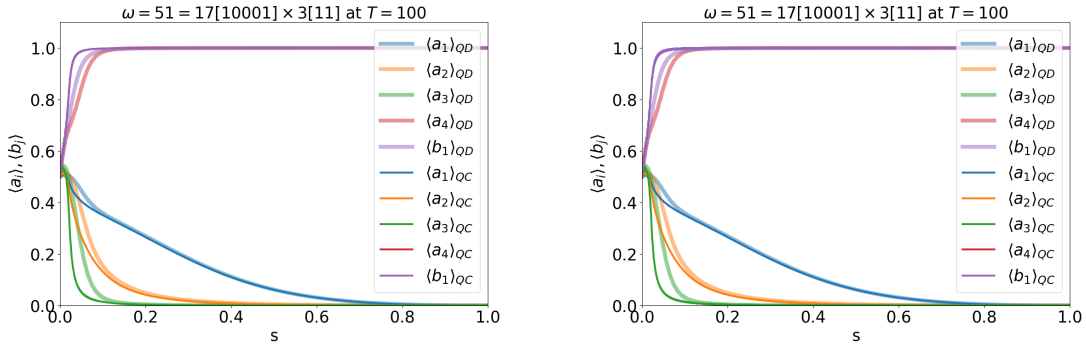

(a) RK4 (b) Tsit5

Figure 6.5: Comparison between the two solvers RK4 and Tsit5 in (a) and (b), respectively, for $\omega = 51[110011] = 17[10001] \times 3[11]$ at $T = 100$. One uses the default tolerances for RK4, whereas the tolerances are set to abstol=1e-8=reltol for Tsit5.

Thus, Figure 6.5 indicates, that it can be important to adjust the tolerances for a given solver. We consider now the expansion orders from second-order up to the maximal order for the strongly divergent cases $\omega \in \{15, 33\}$ at $T = 10$. In section 6.3 we talk about the possible stiffness of the Ehrenfest systems. Hence, we utilize a stiff solver as well. Since the RK4-method provides good solutions for the lowest and maximal order expansions, we discuss only the RK4 scheme as non-stiff solver where we adjusted the tolerances. We choose the stiff solver *TRBDF2* [38], which is claimed to be a reliable solver for large ODE systems [34]. The results for $\omega = 15$ are given in Figure 6.6 and for $\omega = 33$ in Figure 6.7.

The results in both Figure 6.6 and Figure 6.7 show, that adjusting the tolerances for the solver RK4 yields finite, but still strongly oscillating trajectories beyond the physical upper boundary 1. The lower physical boundary 0 is still fulfilled. We adjust the tolerances by hand and try out different combinations. It turns out that only around the combination abstol = reltol = 0.025 a finite oscillation is possible for $\omega = 15$. If abstol = reltol $<$ 0.025 we obtain the same divergences, whereas for abstol = reltol $>$ 0.025 the divergences possess a different global form. It seems, that around abstol = reltol = 0.025 an island of stability emerges. The tolerances are relatively large and there is only one stable tolerance-combination, which is not intuitive. Normally, the tolerances should be chosen smaller to acquire a better result. Therefore, the received results are strong indications for a numerical integration problem. Considering now TRBDF2 we find something similar. Here, we obtain a very good solution, however, also only for the same tolerance-combination. The same applies for the case $\omega = 33$ at abstol = reltol = 0.075. We tried this method of "optimizing" the tolerances for $\omega \in \{21, 39, 51, 57\}$ as well. We received finite solutions

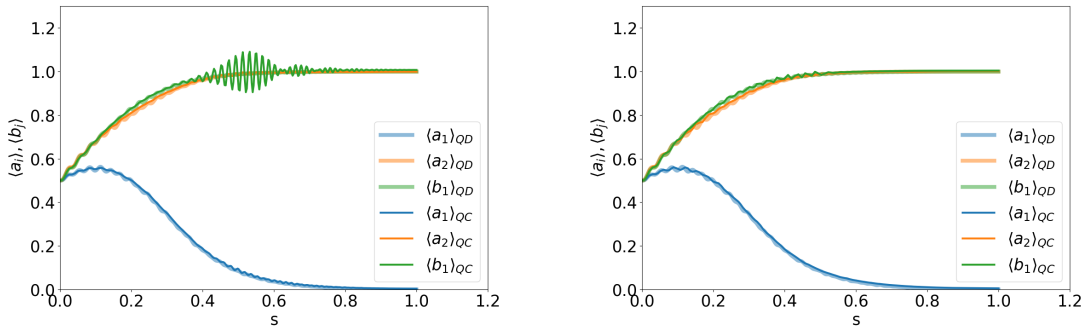

(a) RK4, second-order

(b) TRBDF2, second-order

(c) RK4, third-order

(d) TRBDF2, third-order

Figure 6.6: Bit-digit measurements for $\omega = 15[1111] = 5[101] \times 3[11]$ in second- and third(maximal)-order expansion using RK4 in [(a),(c)] and TRBDF2 [(b),(d)], respectively, with abstol = reltol = 0.025 and at $T = 10$.

only for $\omega = 21$ (absol = reltol = 0.025) and $\omega = 39$ (absol = reltol = 0.075). The results for $\omega \in \{15, 21, 33, 39\}$ at the respective tolerance-combinations remain stable if T is increased. We found tolerance-combinations for the cases $\omega = 51$ and $\omega = 57$, where the solutions were finite, but still larger than 1. For increasing T these solutions diverge immediately.

One possibility to examine the assumed numerical integration problem is to use non-adaptive dt. Since the numerical time-steps are non-changing the oscillations could be removed. For $\omega = 15$, the results are given in Figure 6.8. Figure 6.8 visualizes that for fixed time-steps dt =1e-5 the solution coincides with the adaptive approach.

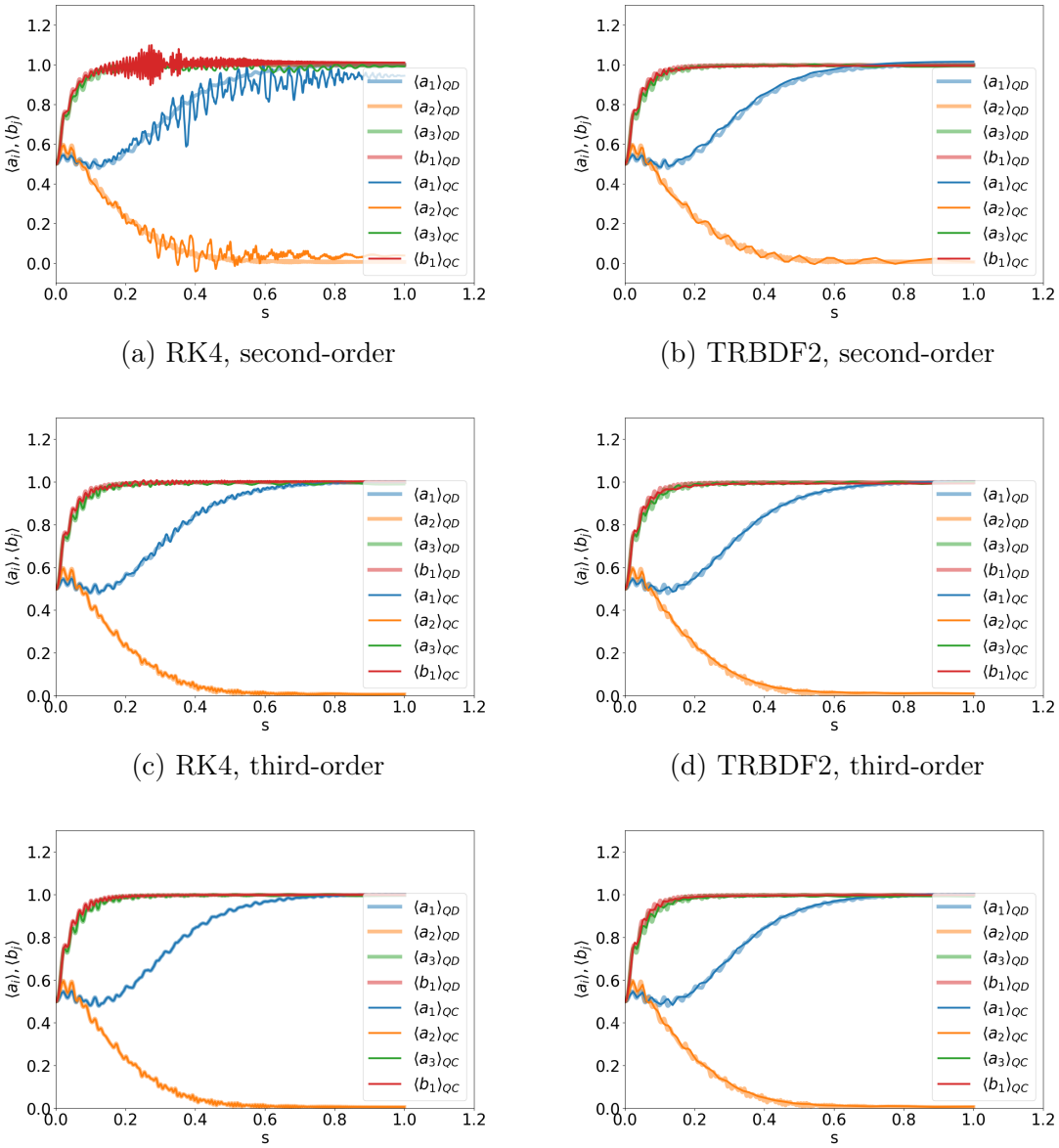

(a) RK4, second-order

(b) TRBDF2, second-order

(c) RK4, third-order

(d) TRBDF2, third-order

(e) RK4, fourth-order

(f) TRBDF2, fourth-order

Figure 6.7: Bit-digit measurements for $\omega = 33[100001] = 11[1011] \times 3[11]$ in second-, third- and fourth(maximal)-order expansion using RK4 in [(a),(c),(e)] and TRBDF2 in [(b),(d),(f)], respectively, with abstol = reltol = 0.075 and at $T = 10$.

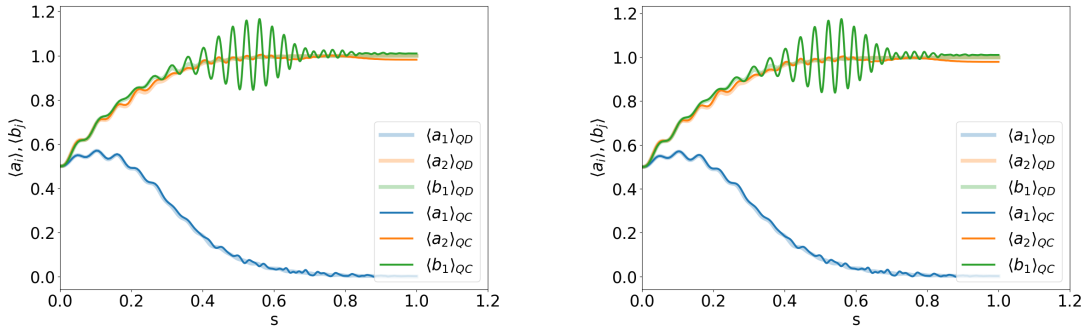

(a) RK4, dt = adaptive

(b) RK4, dt = 1e-5

Figure 6.8: Solving the bi-prime problem $\omega = 15[1111] = 5[101] \times 3[11]$ in second-order expansion using RK4 at default tolerances and $T = 5$. We compare the solution with adaptive step-size in (a) with the fixed step-size dt =1e-5 in (b).

We see that the choice of the solver, adjusting the tolerances and using fixed time-steps dt can be important, however, in our case we cannot tell if the divergences are implications of these choices or if they emerge due to properties of the expanded Ehrenfest system. We continue our analysis by examining the eigenvalues of the Jacobian matrices of the respective Ehrenfest ODE systems for the bi-prime factorization problem.

6.3 Jacobi Matrix Analysis

In this section we compute and plot the eigenvalues of the Jacobi matrix discussed in section 2.5 $\forall s \in [0, 1]$. We consider a divergent ($\omega = 15$ at $T \in \{5, 5.7\}$) as well as a non-divergent ($\omega = 21$ at $T = 10$) case for a three-qubit system, i.e. $n = 3$. Since we obtain divergent solutions for $\omega = 15$ in second-order expansion, we treat only this case. According to section A.1, the Ehrenfest ODE system has the system size $N = 3 \cdot 3/2(3 \cdot 3 - 1) = 36$. Hence, the Jacobian is a 36×36 complex matrix, i.e. $\mathcal{J}_{\mathbf{x}_0(s)}\mathbf{f}(\mathbf{x}(s), s) \in \mathrm{Mat}_{36\times 36}(\mathbb{C})$. It might be interesting to see how the Jacobian develops for expectation values governed by the Schrödinger equation, since the Schrödinger equation provides the full quantum dynamics using a different approach than solving an ODE system. Hence, we also implement and plot the theoretical discussion to approximate the Jacobian in section 2.5. In Figure 6.9, Figure 6.10 and in Figure 6.11, we compare the results of the eigenvalues λ for $\omega = 15$ and $\omega = 21$, respectively.

Figure 6.9 is the divergent case at $T = 5$. The imaginary eigenvalues of the Jacobian received by utilizing QuantumCumulants.jl oscillate, whereas those obtained by Schrödinger do not. Nevertheless, the imaginary parts are in the same regime, i.e., have similar absolute values and thus have the same global structure. The real parts are quite different. The global structure seems to be still the same, however, the oscillations are much stronger for the QC.jl solution. The four branches in the Schrödinger plot at medium s exist also in the

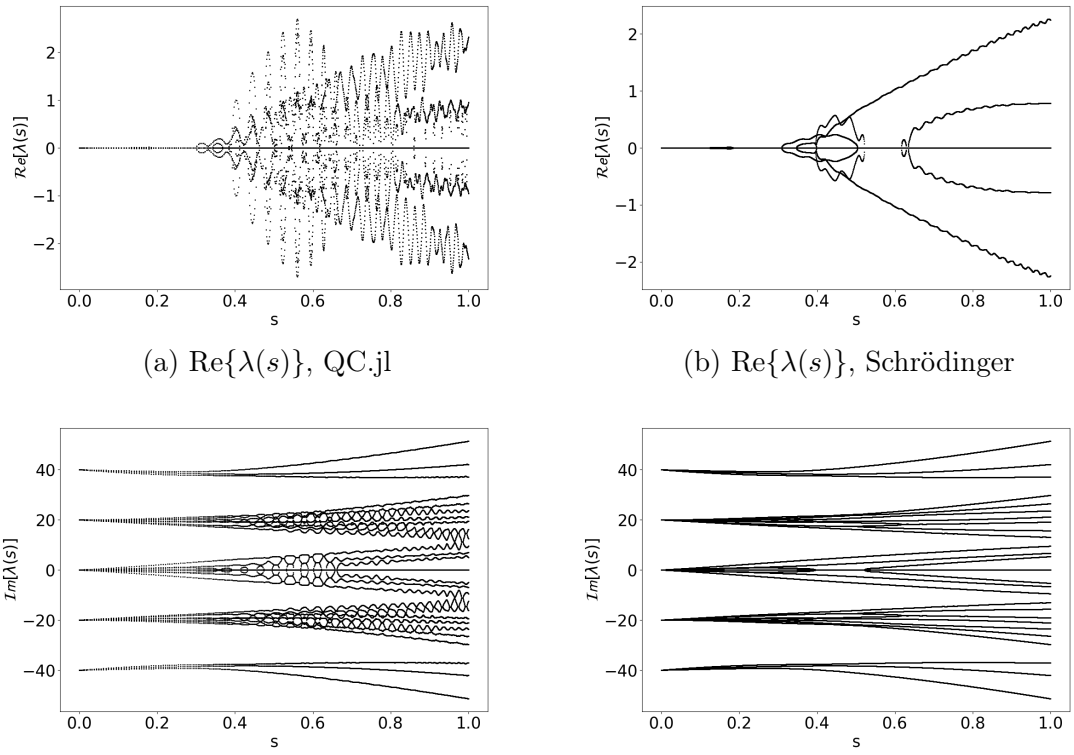

(a) Re$\{\lambda(s)\}$, QC.jl

(b) Re$\{\lambda(s)\}$, Schrödinger

(c) Im$\{\lambda(s)\}$, QC.jl

(d) Im$\{\lambda(s)\}$, Schrödinger

Figure 6.9: Comparison between the real and imaginary parts of the Jacobian eigenvalues $\lambda_i(s)$ for $\omega = 15$ at $T = 5$ determined by QuantumCumulants.jl (QC.jl) and Schrödinger, respectively.

QC.jl plot, but they are much more chaotic here. The circle-like shape in the Schrödinger plot, emerging at $s \approx 0.4$, is exchanged by a beat-shaped oscillation. Figure 6.10 shows that increasing T to $T = 5.7$ results in a growth of the real beat-shaped oscillation as well as the real branches, whereas the imaginary shapes look similar as for the case $T = 5$. The divergences are embedded within the Jacobian eigenvalues, but no direct implication can be made.

The non-divergent case $\omega = 21$ in Figure 6.11 shows that we obtain for both the real and the imaginary parts of the eigenvalues $\lambda_i(s)$ the same structures and regimes. This tells us, that the divergences somehow introduce oscillations that influence the global structure and regimes of the eigenvalues chaotically. According to [39], if the Re$\{\lambda_i(s)\}$ is large and negative almost certainly stiffness is present. We can define the stiffness ratio [40]:

$$r(s) = \frac{\max_{1\leq i\leq n} |Re\lambda_i(s)|}{\min_{1\leq i\leq n} |Re\lambda_i(s)|}. \tag{6.1}$$

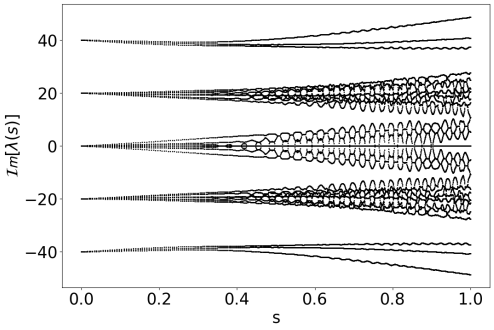

(a) Im$\{\lambda(s)\}$, QC.jl

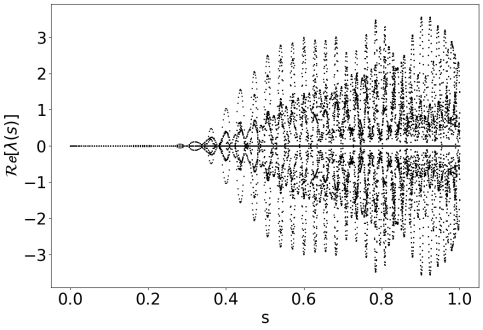

(b) Re$\{\lambda(s)\}$, QC.jl

Figure 6.10: Comparison between the real and imaginary parts of the Jacobian eigenvalues $\lambda_i(s)$ for $\omega = 15$ at $T = 5.7$ determined by QuantumCumulants.jl (QC.jl).

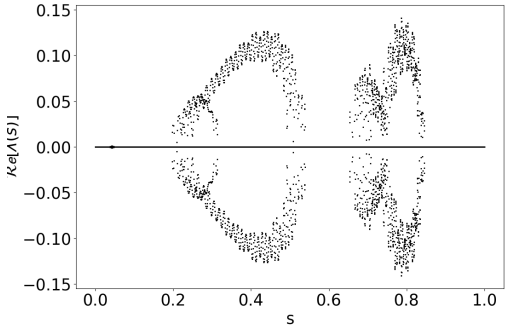

(a) Re$\{\lambda(s)\}$, QC.jl

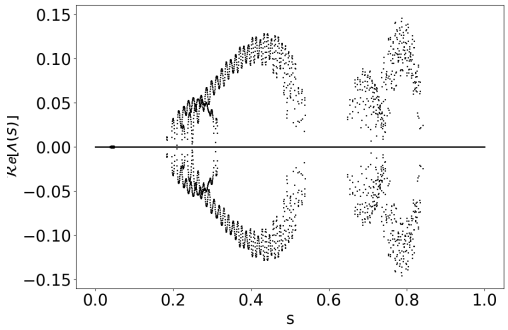

(b) Re$\{\lambda(s)\}$, Schrödinger

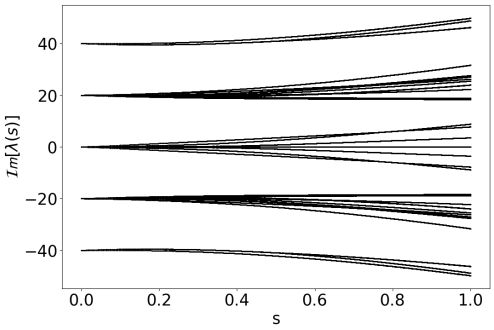

(c) Im$\{\lambda(s)\}$, QC.jl

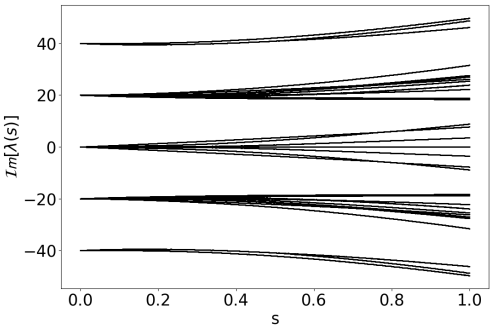

(d) Im$\{\lambda(s)\}$, Schrödinger

Figure 6.11: Comparison between the real and imaginary parts of the Jacobian eigenvalues $\lambda_i(s)$ for $\omega = 21$ at $T = 10$ determined by QuantumCumulants.jl (QC.jl) and Schrödinger, respectively.

The above expression is a quantitative measure of the stiffness, where the system is stiff

if r(s) diverges. One needs to be careful with this definition, because if eigenvalues $\lambda_i(s)$ are small, $r(s)$ becomes large which does not necessarily imply the stiffness of the system under consideration. According to Figure 6.9 and Figure 6.11 we obtain divergent values for $r(s)$ although $\omega = 21$ is certainly not stiff. Therefore a different measure of stiffness should be studied, e.g., as provided in discussions about stiffness for linear and non-linear ODE systems [40]. We will not discuss the stiffness here further, because this is beyond the scope of this thesis.

So far, in section 6.2 we have found a strong indicator for a numerical integration problem. But this is only the case if one rules out the divergent oscillations to be correct, since the divergent solutions are the results for all examinations done, that should prove the non-existence of a numerical integration problem. However, we assumed that adjusting the solver, tolerances or numerical time-steps are the options influencing the solutions the most. In this section, we have found that the divergences are reflected in the trajectories of the Jacobian eigenvalues depending on s, but we cannot say for certain that the divergences come from the underlying Ehrenfest systems and whether the system under consideration is stiff. The obtained information is not conclusive to determine a clear numerical or mathematical nature of the occurring divergences. The latter would originate from the generalized cumulant expansion method applied to the bi-prime factorization problem. We focus now on the last section of the examination of the divergences.

6.4 Joint Cumulants Analysis

In subsection 2.4.2 we assume the joint cumulants of n-th order to be equal to zero. This allows us to receive the recursive relation to describe the n-th order average in terms of lower-order averages. In this section, we plot the joint cumulants to see how close to zero these terms are. Therefore, we use Equation 2.62. It is also interesting to compare the results with the same joint cumulants, but now determined with Schrödinger expectation values, i.e. we change $\langle X_1 X_2 \cdots X_n \rangle_{C,o}(s) \to \langle X_1 X_2 \cdots X_n \rangle_{S,o}(s)$. This means, we use the same relation with the same recursive expansions, but we exchange the QuantumCumulants.jl with Schrödinger averages. We use section A.1 and consider $\omega = 15$ with n qubits. We have then $N = 3^2 n/2 \cdot (2 - 3n + n^2) = 3^3 = 27$ joint cumulants. In Figure 6.12 we visualize the joint cumulants for $\omega = 15$ at $T \in \{5, 10\}$ considering the cumulant expansion orders $o = \{1, 3\}$. In Figure 6.13 we examine the joint cumulants for $\omega = 15$ at $T \in \{5, 10\}$ as well but now for the divergent order $o = 2$.

In Figure 6.12 one can observe the non-divergent expansion orders $o = \{1, 3\}$. The global shapes and the regimes of the joint cumulant in first-order expansion $o = 1$ are for both the QuantumCumulants.jl and Schrödinger relatively similar at $T \in \{5, 10\}$. Interestingly, not all joint cumulants are constant for $s \to 1$. Especially, the combinations $\langle \sigma_+^{(1)} \hat{P}_{2,-} \sigma_-^{(3)} \rangle_{C,1}$ and $\langle \sigma_-^{(1)} \hat{P}_{2,-} \sigma_+^{(3)} \rangle_{C,1}$ oscillate strongly around zero. This is the case for QuantumCumulants.jl as well as Schrödinger. The reason for this is the choice of T. The overall evolution-time T is a good choice, however, it is still a rather fast transition. This means,

that we do not entirely stay in the ground state of our factoring Hamiltonian. Thus, the state contains small contributions to different sub-Hilbert spaces, i.e. an oscillation between higher energetic states and the ground state. Increasing T to $T = 100$ makes these oscillations very small. This is demonstrated in section A.7. For $o = 3$ and QC.jl we obtain results within a regime, which comes probably from numerical errors between the QuantumCumulants.jl and Schrödinger solution. The Schrödinger case is perfectly zero due to the fact, that for $o = 3$ no cumulant expansion is required.

In Figure 6.13, the global shape of the Schrödinger solution has changed, but the regime remains the same. The results of the divergent QuantumCumulants.jl solution show, that the oscillating terms, now $\langle \sigma_+^{(1)} \hat{P}_{2,-} \sigma_-^{(3)} \rangle_{C,2}$ and $\langle \sigma_-^{(1)} \hat{P}_{2,-} \sigma_+^{(3)} \rangle_{C,2}$, from before are clearly non-zero and grow larger for increasing T. Additionally at $T = 5$, the combinations $\langle \sigma_+^{(1)} \hat{P}_{2,-} \sigma_+^{(3)} \rangle_{C,2}$ and $\langle \sigma_-^{(1)} \hat{P}_{2,-} \sigma_-^{(3)} \rangle_{C,2}$ appear to have similar behaviors. The values for $\sigma_\pm \hat{P} \sigma_\mp$ increase more and more in amplitude. It seems, that these combinations are the reason for the divergences. A more precise investigation is provided in section A.7.

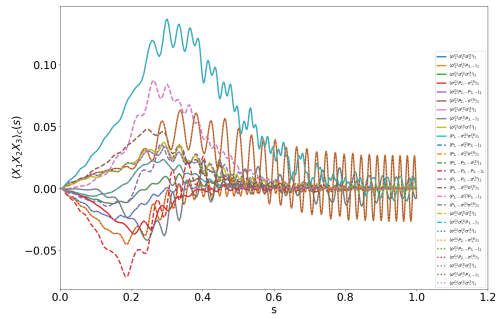

(a) $T = 5, o = 1$, QC.jl

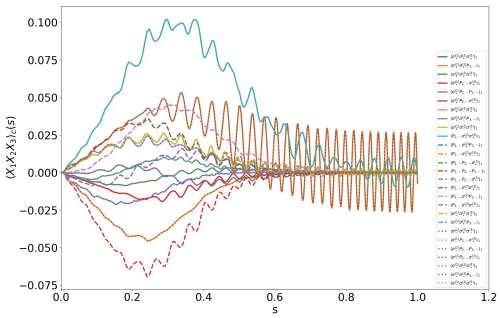

(b) $T = 5, o = 1$, Schrödinger

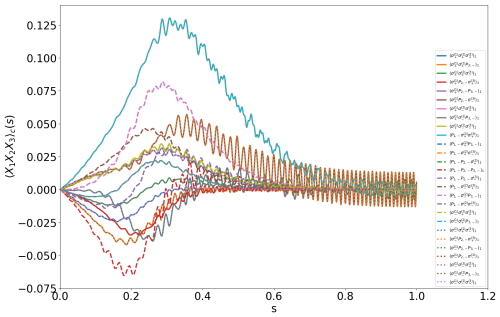

(c) $T = 10, o = 1$, QC.jl

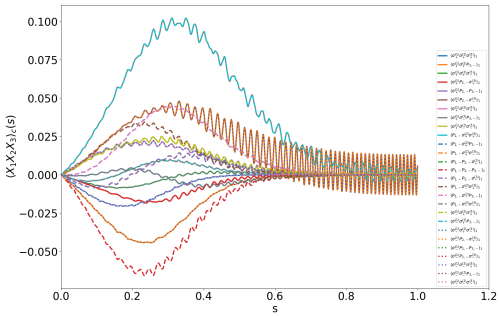

(d) $T = 10, o = 1$, Schrödinger

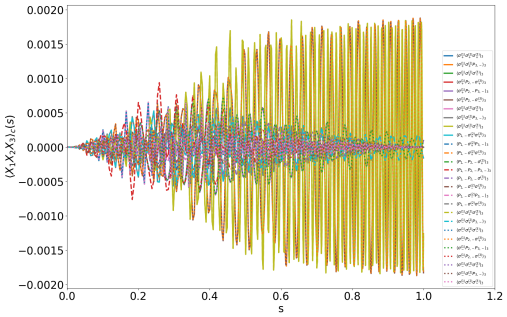

(e) $T = 5, o = 3$, QC.jl

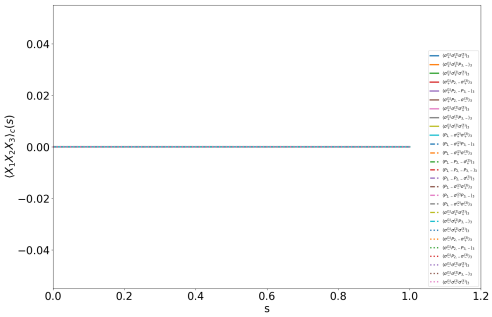

(f) $T = 5, o = 3$, Schrödinger

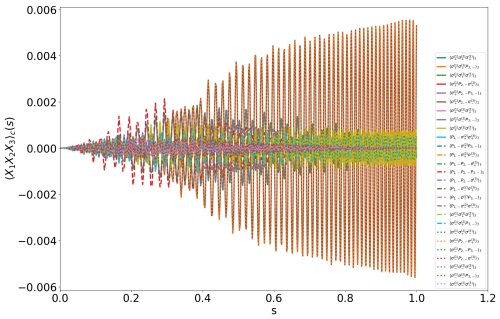

(g) $T = 10, o = 3$, QC.jl

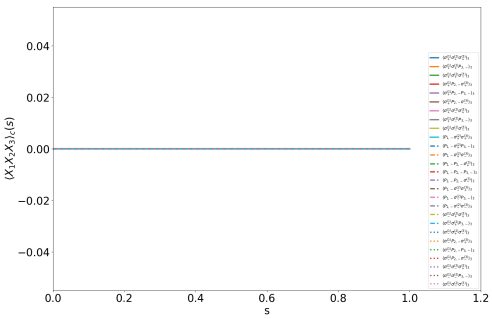

(h) $T = 10, o = 3$, Schrödinger

Figure 6.12: Comparison of the joint cumulants determined by QuantumCumulants.jl (QC.jl) and Schrödinger, respectively, for $\omega = 15$ with expansion order $o \in \{1, 3\}$ at $T \in \{5, 10\}$.

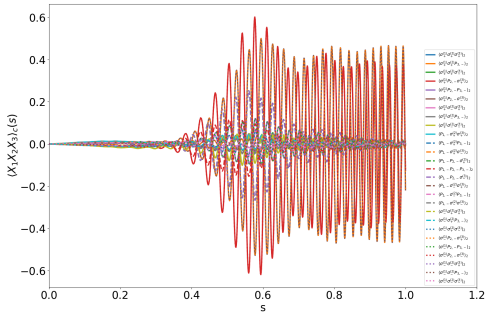

(a) $T = 5$, QC.jl

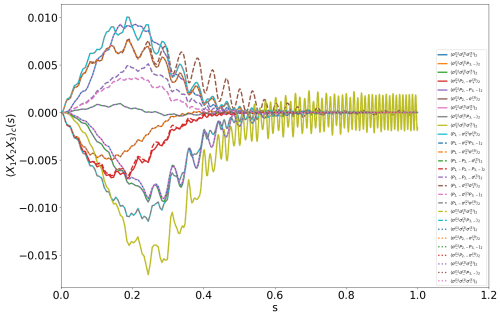

(b) $T = 5$, Schrödinger

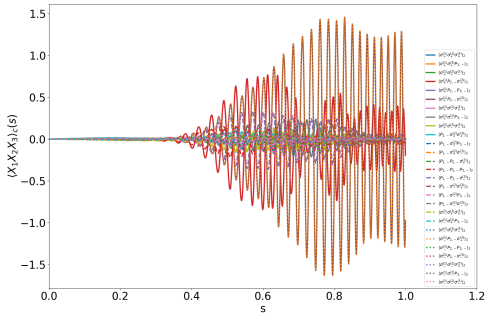

(c) $T = 5.7$, QC.jl

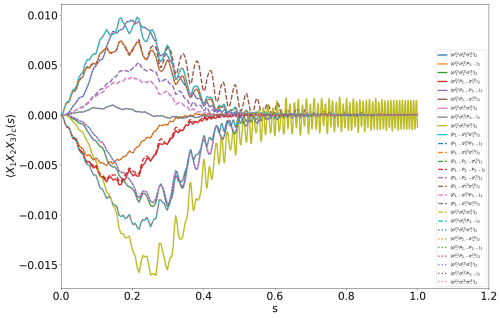

(d) $T = 5.7$, Schrödinger

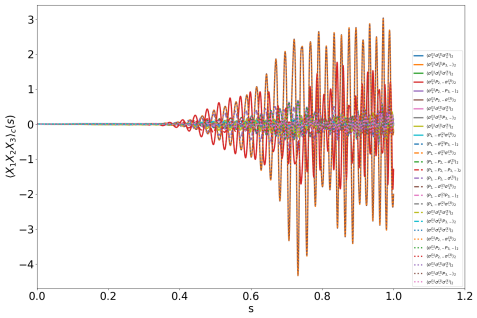

(e) $T = 5.9$, QC.jl

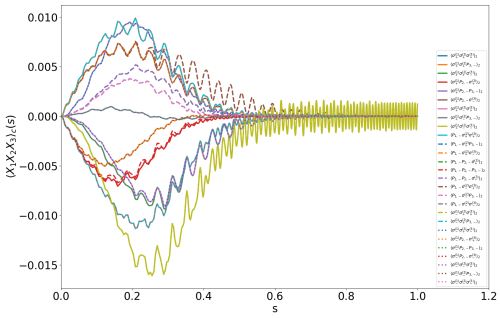

(f) $T = 5.9$, Schrödinger

Figure 6.13: Comparison of the joint cumulants determined by QuantumCumulants.jl (QC.jl) and Schrödinger, respectively, for $\omega = 15$ with expansion order $o = 2$ at $T \in \{5, 5.7, 5.9\}$.

Chapter 7

Conclusion and Outlook

In this thesis we have presented a procedure how the bi-prime factorization problem described as a classical optimization problem in terms of classical bit-digits within a cost function can be treated quantum mechanically. To obtain a quantum mechanical optimization problem, we have exchanged the classical bits with spins acting as qubits, thus, introduced observables. Also, we considered the cost function as a ground state problem by using a corresponding problem-Hamiltonian. The classical bit-digits are acquired by measuring the respective observables describing the spin orientation of the qubits. The goal is to obtain the ground state of the problem-Hamiltonian, which we computed by utilizing the adiabatic theorem. Everything together describes the quantum annealing of the bi-prime factorization problem. The correct expectation values of the factor bit-digits for the bi-primes $\{15, 21, 33, 39, 51, 57, 93, 265\}$ have been received solving the corresponding time-dependent Schrödinger equation without any problems. This shows us, that the quantum description indeed works. However, we also have found a specific case, for the bi-prime 95, where the adiabatic evolution gives the false solution for large evolution times, due to a very small minimal gap. We examined the fidelity, the *remaining in the ground state* (probability, that during the adiabatic evolution the respective state remains in the ground state of the adiabatic Hamiltonian), entropy of entanglement and bipartite quantum mutual information.
Since the system-Hamiltonian scales exponentially with the total qubit number, we approximated the full quantum dynamics by considering the Ehrenfest theorem as well as the generalized cumulant expansion method. Since we use the Ehrenfest theorem for each observable necessary to determine the bit-digit expectation values, we obtain a closed coupled nonlinear Ehrenfest ODE system in first-order. In a first step, we try to find a quantum advantage for the bi-prime factorization problem. Therefore, we constructed the Ehrenfest system in first-order cumulant expansion, also known as mean-field approach. Hence, we discard all quantum mechanical correlations. For small system-sizes both the cumulants solution as well as the full quantum dynamics provide the correct factors equally fast. Increasing the total number of qubits eventually shows that the cumulants solution

needs a larger overall adiabatic evolution-time to provide the correct factors. This is, indeed, a clear hint that a quantum advantage of the bi-prime factorization problem should to be taken seriously. We show this by considering the bi-prime 265.
The cumulant expansion can be used to gradually include quantum correlations step by step by including higher order correlations. We assumed that the expansion order successively approaches the full quantum dynamics. In a sense this is the case, because if the expansion order coincides with or is larger than the number of qubits, then, we receive the full quantum dynamics. However, almost all of the results with expansion orders larger than the mean-field expansion and smaller than the total qubit number possess divergent behavior. This is very surprising, because it seems that only the mean-field or the full quantum solution, in general, provide non-divergent solutions.
In the last chapter, we discuss thoroughly the possible origins of these divergences, but it turns out, that the exact reason for these results is not clear. We narrowed it down to three possibilities, which we give here as an outlook for further investigation. The first one is that, although a very careful investigation of the numerical evaluation took place, there still is a numerical error for the semi-classical cases. The second possibility considers that the generalized cumulant expansion method does not entirely work for the bi-prime factorization problem with the problem-Hamiltonian we used. There are many different possibilities to receive more efficient cost-functions for the factoring problem. Maybe using a different initial and problem Hamiltonian can resolve the issue. The third possibility tells us, that the bi-prime factorization problem cannot be expanded in such a manner due to possible properties such as that it is either NP or NP-complete.

Bibliography

[1] Wolfgang Sartorius von Waltershausen and Carl Friedrich Gauß. *Gauss zum Gedächtniss*. Hirzel, Leipzig, 1856.

[2] Carl Friedrich Gauss. *Disquisitiones arithmeticae*, volume 1. K. Gesellschaft der Wissenschaften zu Göttingen, 1870.

[3] Kenneth H Rosen. *Elementary number theory*. Pearson Education London, 2011.

[4] Harald Helfgott. An improved sieve of eratosthenes. *Mathematics of Computation*, 89(321):333–350, 2020.

[5] R Sherman Lehman. Factoring large integers. *Mathematics of Computation*, 28(126):637–646, 1974.

[6] James McKee. Turning euler's factoring method into a factoring algorithm. *Bulletin of the London Mathematical Society*, 28(4):351–355, 1996.

[7] Peter W Shor. Algorithms for quantum computation: discrete logarithms and factoring. In *Proceedings 35th annual symposium on foundations of computer science*, pages 124–134. Ieee, 1994.

[8] Arjen K. Lenstra. *Integer Factoring*, pages 611–618. Springer US, Boston, MA, 2011.

[9] Ronald L Rivest, Adi Shamir, and Leonard Adleman. A method for obtaining digital signatures and public-key cryptosystems. *Communications of the ACM*, 21(2):120–126, 1978.

[10] Juyoung Park, Seokho Jeong, Minhyuk Kim, Kangheun Kim, Andrew Byun, Louis Vignoli, Louis-Paul Henry, Loïc Henriet, and Jaewook Ahn. Rydberg-atom experiment for the integer factorization problem. *Phys. Rev. Res.*, 6:023241, Jun 2024.

[11] Edward Farhi, Jeffrey Goldstone, Sam Gutmann, and Michael Sipser. Quantum computation by adiabatic evolution. *arXiv preprint quant-ph/0001106*, 2000.

[12] Gernot Schaller and Ralf Schützhold. The role of symmetries in adiabatic quantum algorithms. *arXiv preprint arXiv:0708.1882*, 2007.

[13] Xinhua Peng, Zeyang Liao, Nanyang Xu, Gan Qin, Xianyi Zhou, Dieter Suter, and

Jiangfeng Du. Quantum adiabatic algorithm for factorization and its experimental implementation. *Phys. Rev. Lett.*, 101:220405, Nov 2008.

[14] Albert Messiah. *Quantum mechanics*. Courier Corporation, 2014.

[15] Leslie E Ballentine. *Quantum mechanics: a modern development*. World Scientific Publishing Company, 2014.

[16] Ryogo Kubo. Generalized cumulant expansion method. *Journal of the Physical Society of Japan*, 17(7):1100–1120, 1962.

[17] David Plankensteiner, Christoph Hotter, and Helmut Ritsch. Quantumcumulants. jl: A julia framework for generalized mean-field equations in open quantum systems. *Quantum*, 6:617, 2022.

[18] Sebastian Krämer, David Plankensteiner, Laurin Ostermann, and Helmut Ritsch. Quantumoptics. jl: A julia framework for simulating open quantum systems. *Computer Physics Communications*, 227:109–116, 2018.

[19] Lloyd Strickland and Harry Lewis. *Leibniz on Binary: The Invention of Computer Arithmetic*. 10 2022.

[20] Edwin KP Chong and Stanislaw H Żak. *An introduction to optimization*, volume 75. John Wiley & Sons, 2013.

[21] Max Born and Vladimir Fock. Beweis des adiabatensatzes. *Zeitschrift für Physik*, 51(3):165–180, 1928.

[22] Satoshi Morita and Hidetoshi Nishimori. Mathematical foundation of quantum annealing. *Journal of Mathematical Physics*, 49(12), 2008.

[23] Roman Martoňák, Giuseppe E Santoro, and Erio Tosatti. Quantum annealing of the traveling-salesman problem. *Physical Review E*, 70(5):057701, 2004.

[24] Mark W Johnson, Mohammad HS Amin, Suzanne Gildert, Trevor Lanting, Firas Hamze, Neil Dickson, Richard Harris, Andrew J Berkley, Jan Johansson, Paul Bunyk, et al. Quantum annealing with manufactured spins. *Nature*, 473(7346):194–198, 2011.

[25] Mark M. Wilde. *Quantum Information Theory*. Cambridge University Press, 2013.

[26] Thomas Hartman. Lectures on quantum gravity and black holes. *Cornell University*, 21, 2015.

[27] Asutosh Kumar. Multiparty quantum mutual information: An alternative definition. *Phys. Rev. A*, 96:012332, Jul 2017.

[28] Ugo Fano. Description of states in quantum mechanics by density matrix and operator techniques. *Reviews of modern physics*, 29(1):74, 1957.

[29] Heinz-Peter Breuer and Francesco Petruccione. *The theory of open quantum systems*. OUP Oxford, 2002.

[30] Bert E Fristedt and Lawrence F Gray. *A modern approach to probability theory*. Springer Science & Business Media, 2013.

[31] Giovanni Peccati and Murad S. Taqqu. Moments, cumulants and diagram formulae for non-linear functionals of random measures, 2008.

[32] Julian Moser. Symbolic indices and summations in quantumcumulants. jl.

[33] Sadri Hassani. *Mathematical physics: a modern introduction to its foundations*. Springer Science & Business Media, 2013.

[34] Christopher Rackauckas and Qing Nie. Differentialequations. jl–a performant and feature-rich ecosystem for solving differential equations in julia. *Journal of open research software*, 5(1):15–15, 2017.

[35] J.C. Butcher. A history of runge-kutta methods. *Applied Numerical Mathematics*, 20(3):247–260, 1996.

[36] Charalampos Tsitouras. Runge-kutta pairs of order 5(4) satisfying only the first column simplifying assumption. *Computers & Mathematics with Applications*, 62:770–775, 07 2011.

[37] E. Fehlberg. *Low-order Classical Runge-Kutta Formulas with Stepsize Control and Their Application to Some Heat Transfer Problems*. NASA technical report. National Aeronautics and Space Administration, 1969.

[38] ME Hosea and LF Shampine. Analysis and implementation of tr-bdf2. *Applied Numerical Mathematics*, 20(1-2):21–37, 1996.

[39] John Charles Butcher. *Numerical methods for ordinary differential equations*. John Wiley & Sons, 2016.

[40] Julyan HE Cartwright. Nonlinear stiffness, lyapunov exponents, and attractor dimension. *Physics Letters A*, 264(4):298–302, 1999.

Appendix A

Supplementary Material

A.1 Determination of System Size N

We know, that the Ehrenfest system consists of time-derivatives of expectation values of operator multiplications up to a truncation-order. In this section we derive a general formula which determines the system size N for Ehrenfest systems up to third order.

Let $\hat{\mathcal{O}}_{i'} \in \bigcup_{m=1}^{n} \{\sigma_+^{(m)}, \sigma_-^{(m)}, \hat{P}_{m,-}\}$ with $i' = (i, r)$, where $i \in \{1, 2, \cdots, n\}$ and r tells which kind of operator is used on the respective Hilbert space $\mathcal{H}_i$. In first-order expansion we receive $3 \cdot n$ expectation values of single operators with the shape $\langle \hat{\mathcal{O}}_{i'} \rangle$. This is discussed more precisely in chapter 4. The second-order expansion is a little more complicated. We know from chapter 4 that we effectively get two-operator expectation values $\langle \hat{\mathcal{O}}_{i'} \hat{\mathcal{O}}_{j'} \rangle$ if $i' \neq j'$. Else, the two operators can be written as one operator on the same Hilbert space due to non-trivial commutator relations. This is discussed more thoroughly in chapter 4. Considering $i' \neq j'$ we obtain for second-order averages

$$\left.\begin{array}{l} \left.\begin{array}{l} \langle \hat{\mathcal{O}}_1 \hat{\mathcal{O}}_2 \rangle \to 3 \cdot 3 \\ \vdots \\ \langle \hat{\mathcal{O}}_1 \hat{\mathcal{O}}_n \rangle \to 3 \cdot 3 \end{array}\right\} \Rightarrow 3^2(n-1) \\ \left.\begin{array}{l} \langle \hat{\mathcal{O}}_2 \hat{\mathcal{O}}_3 \rangle \to 3 \cdot 3 \\ \vdots \\ \langle \hat{\mathcal{O}}_2 \hat{\mathcal{O}}_n \rangle \to 3 \cdot 3 \end{array}\right\} \Rightarrow 3^2(n-2) \\ \vdots \\ \langle \hat{\mathcal{O}}_{n-1} \hat{\mathcal{O}}_n \rangle \Rightarrow 3^2 \end{array}\right\} \Rightarrow 3^2 \sum_{i=1}^{n-1} (n-i) = \frac{3^2}{2} n(n-1) \tag{A.1}$$

In sake of simplicity, we use here, e.g., $i', j' \in \{1, 2, \cdots, n\}$, because the respective kinds of operators are not important in this case. The Ehrenfest system size N of a bi-prime with n qubits in second-order expansion is given by

$$N = 3n + \frac{3^3 n}{2}(n-1) = \frac{3n}{2}(3n-1). \tag{A.2}$$

Proceeding similarly for the third-order expansion, we obtain the system size

$$N = 3n + \frac{3^2 n}{2}(n-1) + \frac{3^2 n}{2}(2 - 3n + n^2) = \frac{3n}{2}(5 - 6n + 3n^2). \tag{A.3}$$

This can be done for arbitrary expansion order. We can compare the results in this section with the system sizes received by QuantumCumulants.jl. The results are shown in Table A.1.

Table A.1: Here, we show that the derived polynomial formulas in n calculate the necessary system size N to receive a complete Ehrenfest system for the respective expansion order.

n	1st	2nd	3rd	QC.jl
3	9	36	63	✓
4	12	66	174	✓
5	15	105	375	✓

Interestingly, we see that the increase of the order results in a growth in the polynomial power. In a fixed order k, the system scales with n^k.

A.2 Commutator Relation of Hamiltonian With N Operators

Let $\hat{H}$ be a Hamiltonian and let $\hat{X}_1, \hat{X}_2, \cdots, \hat{X}_N$ be N observables. One starts from the commonly known commutator relation:

$$[\hat{H}, \hat{X}_1\hat{X}_2] = \hat{H}\hat{X}_1\hat{X}_2 + \hat{X}_1\hat{H}\hat{X}_2 - \hat{X}_1\hat{H}\hat{X}_2 - \hat{X}_1\hat{X}_2\hat{H} \tag{A.4}$$

$$= [\hat{H}, \hat{X}_1]\hat{X}_2 + \hat{X}_1[\hat{H}, \hat{X}_2]. \tag{A.5}$$

The goal is now to derive a rule, which generalizes above relation for $N > 2$. Considering $[\hat{H}, \prod_{i=1}^{N} \hat{X}_i]$ and utilizing Equation A.5 yields

$$\begin{aligned}
[\hat{H}, \prod_{i=1}^{N} \hat{X}_i] &= [\hat{H}, \left(\prod_{i=1}^{N-1} \hat{X}_i\right) \hat{X}_N] \\
&= \hat{H}\left(\prod_{i=1}^{N-1} \hat{X}_i\right) \hat{X}_N - \left(\prod_{i=1}^{N-1} \hat{X}_i\right) \hat{X}_N\hat{H} + \left(\prod_{i=1}^{N-1} \hat{X}_i\right) \hat{H}\hat{X}_N - \left(\prod_{i=1}^{N-1} \hat{X}_i\right) \hat{H}\hat{X}_N \\
&= [\hat{H}, \left(\prod_{i=1}^{N-1} \hat{X}_i\right)]\hat{X}_N + \left(\prod_{i=1}^{N-1} \hat{X}_i\right) [\hat{H}, \hat{X}_N] \\
&= [\hat{H}, \left(\prod_{i=1}^{N-2} \hat{X}_i\right)]\hat{X}_{N-1}\hat{X}_N + \left(\prod_{i=1}^{N-2} \hat{X}_i\right) [\hat{H}, \hat{X}_{N-1}]\hat{X}_N + \left(\prod_{i=1}^{N-1} \hat{X}_i\right) [\hat{H}, \hat{X}_N] \\
&\vdots \\
[\hat{H}, \prod_{i=1}^{N} \hat{X}_i] &= [H, \hat{X}_1] \left(\prod_{i=2}^{N} \hat{X}_i\right) + \sum_{i=2}^{N-1} \left(\prod_{j=1}^{i-1} \hat{X}_j\right) [\hat{H}, \hat{X}_i] \left(\prod_{k=i+1}^{N} \hat{X}_k\right) + \left(\prod_{i=1}^{N-1} \hat{X}_i\right) [\hat{H}, \hat{X}_N]
\end{aligned}$$

We prove Equation A.6 by induction.

Proof. Let the following induction hypothesis (IH) be given

$$[\hat{H}, \prod_{i=1}^{N} \hat{X}_i] = [H, \hat{X}_1] \left(\prod_{i=2}^{N} \hat{X}_i\right) + \sum_{i=2}^{N-1} \left(\prod_{j=1}^{i-1} \hat{X}_j\right) [\hat{H}, \hat{X}_i] \left(\prod_{k=i+1}^{N} \hat{X}_k\right) + \left(\prod_{i=1}^{N-1} \hat{X}_i\right) [\hat{H}, \hat{X}_N], \tag{A.6}$$

where $N > 2$.

Base case $N = 3$:

$$\begin{aligned}[\hat{H}, \prod_{i=1}^{3} \hat{X}_i] &= [\hat{H}, \hat{X}_1\hat{X}_2\hat{X}_3] \overset{Equation\ A.5}{=} [\hat{H}, (\hat{X}_1\hat{X}_2)]\hat{X}_3 + (\hat{X}_1\hat{X}_2)[\hat{H}, \hat{X}_3] \\ &= [\hat{H}, \hat{X}_1]\hat{X}_2\hat{X}_3 + \hat{X}_1[\hat{H}, \hat{X}_2]\hat{X}_3 + \hat{X}_1\hat{X}_2[\hat{H}, \hat{X}_3] \\ &\overset{\checkmark}{=} [\hat{H}, \hat{X}_1]\left(\prod_{i=2}^{3} \hat{X}_i\right) + \sum_{i=2}^{2}\left(\prod_{j=1}^{i-1} \hat{X}_j\right)[\hat{H}, \hat{X}_i]\left(\prod_{k=i+1}^{3} \hat{X}_k\right) + \left(\prod_{i=1}^{2} \hat{X}_i\right)[\hat{H}, \hat{X}_3]\end{aligned}$$

Let $N > 2$ and let the (IH) be valid:

$$[\hat{H}, \prod_{i=1}^{N} \hat{X}_i] = [H, \hat{X}_1]\left(\prod_{i=2}^{N} \hat{X}_i\right) + \sum_{i=2}^{N-1}\left(\prod_{j=1}^{i-1} \hat{X}_j\right)[\hat{H}, \hat{X}_i]\left(\prod_{k=i+1}^{N} \hat{X}_k\right) + \left(\prod_{i=1}^{N-1} \hat{X}_i\right)[\hat{H}, \hat{X}_N]$$

Induction step $N \to N + 1$:

$$\begin{aligned}[\hat{H}, \prod_{i=1}^{N+1} \hat{X}_i] &= [\hat{H}, \left(\prod_{i=1}^{N} \hat{X}_i\right)\hat{X}_{N+1}] \overset{Equation\ A.5}{=} [\hat{H}, \prod_{i=1}^{N} \hat{X}_i]\hat{X}_{N+1} + \left(\prod_{i=1}^{N} \hat{X}_i\right)[\hat{H}, \hat{X}_{N+1}] \\ &\overset{(IH)}{=} [H, \hat{X}_1]\left(\prod_{i=2}^{N} \hat{X}_i\right)\hat{X}_{N+1} + \sum_{i=2}^{N-1}\left(\prod_{j=1}^{i-1} \hat{X}_j\right)[\hat{H}, \hat{X}_i]\left(\prod_{k=i+1}^{N} \hat{X}_k\right)\hat{X}_{N+1} \\ &\quad + \left(\prod_{i=1}^{N-1} \hat{X}_i\right)[\hat{H}, \hat{X}_N]\hat{X}_{N+1} + \left(\prod_{i=1}^{N} \hat{X}_i\right)[\hat{H}, \hat{X}_{N+1}] \\ &= [H, \hat{X}_1]\left(\prod_{i=2}^{N+1} \hat{X}_i\right) + \sum_{i=2}^{N}\left(\prod_{j=1}^{i-1} \hat{X}_j\right)[\hat{H}, \hat{X}_i]\left(\prod_{k=i+1}^{N+1} \hat{X}_k\right) + \left(\prod_{i=1}^{N} \hat{X}_i\right)[\hat{H}, \hat{X}_{N+1}].\end{aligned}$$

This completes the proof.

□

A.3 Operator Relations in Heisenberg Picture

The Heisenberg operator $\hat{A}_{\mathrm{H}}(t)$ is defined as

$$\hat{A}_{\mathrm{H}}(t) = \hat{U}^{\dagger}(t, t_0)\hat{A}_{\mathrm{S}}\hat{U}(t, t_0), \tag{A.7}$$

where $\hat{U}(t, t_0)$ denotes the unitary time-evolution operator in Equation 2.37 and $\hat{A}_{\mathrm{S}}$ is the corresponding Schrödinger-picture operator. Let $\hat{A}_{\mathrm{S},1}, \hat{A}_{\mathrm{S},2}$ be given. Then, we obtain

$$\begin{aligned}
\hat{A}_{\mathrm{S},1}\hat{A}_{\mathrm{S},2} &= \hat{U}(t, t_0)\hat{U}^{\dagger}(t, t_0)\hat{A}_{\mathrm{S},1}\hat{U}(t, t_0)\hat{U}^{\dagger}(t, t_0)\hat{A}_{\mathrm{S},2}\hat{U}(t, t_0)\hat{U}^{\dagger}(t, t_0) && \text{(A.8)}\\
&= \hat{U}(t, t_0)\hat{A}_{\mathrm{H},1}(t)\hat{A}_{\mathrm{H},2}(t)\hat{U}^{\dagger}(t, t_0) && \text{(A.9)}\\
\Rightarrow \hat{A}_{\mathrm{H},1}(t)\hat{A}_{\mathrm{H},2}(t) &= \hat{U}^{\dagger}(t, t_0)\hat{A}_{\mathrm{S},1}\hat{A}_{\mathrm{S},2}\hat{U}(t, t_0). && \text{(A.10)}
\end{aligned}$$

The relations in Equation 4.33 translate directly into the Heisenberg picture.

A.4 Equivalence for Commuting Operators

The index sets $\mathcal{I}_A$ and $\mathcal{I}_B$ are defined in chapter 4. The same applies for the operators $\hat{\mathcal{O}}_{m_1}$ and $\hat{\mathcal{O}}_{m_2}$. Let $m_1 = m + 1$ and $m_2 = m$, where $m \in \mathcal{I}_A \cup (\mathcal{I}_B \backslash \{k + l\})$. The operators $\hat{\mathcal{O}}_m$ and $\hat{\mathcal{O}}_{m+1}$ act on different sub-Hilbert space, hence, they commute. Equation 4.29 takes the form

$$\frac{d}{dt}\langle(\hat{\mathcal{O}}_{m+1}\hat{\mathcal{O}}_m)(t)\rangle = \hat{i}\left\langle[\hat{H}(t), \hat{\mathcal{O}}_{m+1}\hat{\mathcal{O}}_m]\right\rangle = \hat{i}\left\langle[\hat{H}(t), \hat{\mathcal{O}}_m\hat{\mathcal{O}}_{m+1}]\right\rangle = \frac{d}{dt}\langle(\hat{\mathcal{O}}_m\hat{\mathcal{O}}_{m+1})(t)\rangle. \tag{A.11}$$

One could also justify this by utilizing the cyclic property of the trace:

$$\begin{aligned}
\frac{d}{dt}\langle(\hat{\mathcal{O}}_{m+1}\hat{\mathcal{O}}_m)(t)\rangle &= \hat{i}\left\langle[\hat{H}(t), \hat{\mathcal{O}}_{m+1}]\hat{\mathcal{O}}_m\right\rangle + \hat{i}\left\langle\hat{\mathcal{O}}_{m+1}[\hat{H}(t), \hat{\mathcal{O}}_m]\right\rangle && \text{(A.12)}\\
&= \hat{i}\left\langle\hat{\mathcal{O}}_m[\hat{H}(t), \hat{\mathcal{O}}_{m+1}]\right\rangle + \hat{i}\left\langle[\hat{H}(t), \hat{\mathcal{O}}_m]\hat{\mathcal{O}}_{m+1}\right\rangle = \frac{d}{dt}\langle(\hat{\mathcal{O}}_m\hat{\mathcal{O}}_{m+1})(t)\rangle. && \text{(A.13)}
\end{aligned}$$

A.5 Initial-Value Vector of Ehrenfest Systems

In order to solve the Ehrenfest system of arbitrary expansion order, we need the correct initial values for all required averages $(\langle\sigma_+^{(1)}\rangle, \langle\hat{P}_{1,-}\rangle, \langle\sigma_-^{(1)}\rangle, \langle\sigma_+^{(2)}\rangle, \cdots, \langle\sigma_+^{(1)}\sigma_+^{(2)}\rangle, \cdots, \langle\sigma_+^{(1)}\sigma_+^{(2)}\sigma_+^{(3)}\rangle, \cdots)^T$. According to subsection 2.2.2, the ground state at $s = 0$ is given by

$$|\psi(0)\rangle = |\psi_0\rangle = \bigotimes_{m=1}^{n} \frac{1}{\sqrt{2}}(|0\rangle_m + |1\rangle_m) \tag{A.14}$$

where n is the number of total dynamical qubits. Thus, we simply compute the relations for the operators acting on the l-th Hilbert space

$$\langle\sigma_+^{(l)}(0)\rangle = \frac{1}{2^n}\bigotimes_{i=1}^{n}({}_j\langle 0| + {}_j\langle 1|)\sigma_+^{(l)}\bigotimes_{j=1}^{n}(|0\rangle_i + |1\rangle_i) = \frac{1}{2^n}2^{n-1}({}_l\langle 0| + {}_l\langle 1|)\sigma_+^{(l)}(|0\rangle_l + |1\rangle_l) \tag{A.15}$$

$$= \frac{1}{2}({}_l\langle 0| + {}_l\langle 1|)|0\rangle_l = \frac{1}{2} = \langle\sigma_-^{(l)}(0)\rangle \tag{A.16}$$

$$\langle\hat{P}_{l,-}(0)\rangle = \frac{1}{2^n}2^{n-1}({}_l\langle 0| + {}_l\langle 1|)\hat{P}_{l,-}(|0\rangle_l + |1\rangle_l) = \frac{1}{2}. \tag{A.17}$$

We define then the operators $\hat{\mathcal{O}}^{(l)} \in \bigcup_{m=1}^{n}\{\sigma_\pm^{(m)}, \hat{P}_{m,-}\}$ and find

$$\langle(\hat{\mathcal{O}}^{(\alpha_1)}\cdots\hat{\mathcal{O}}^{(\alpha_k)})(0)\rangle = \left(\frac{1}{2}\right)^k, \tag{A.18}$$

where $\alpha_1, \cdots \alpha_k \in \{1, 2, \cdots, n\}$ and $\alpha_1 \neq \cdots \neq \alpha_k$. The initial-value vector up to arbitrary expansion order is given by

$$(\langle\sigma_+^{(1)}\rangle, \langle\hat{P}_{1,-}\rangle, \langle\sigma_-^{(1)}\rangle, \langle\sigma_+^{(2)}\rangle, \cdots, \langle\sigma_+^{(1)}\sigma_+^{(2)}\rangle, \cdots, \langle\sigma_+^{(1)}\sigma_+^{(2)}\sigma_+^{(3)}\rangle, \cdots)^T = \left(\frac{1}{2}, \frac{1}{2}, \frac{1}{2}, \frac{1}{2}, \ldots, \frac{1}{4}, \cdots, \frac{1}{8}, \cdots\right)^T \tag{A.19}$$

A.6 QuantumCumulants.jl Utilizing Pauli-Matrices

In chapter 4 we mention the possibility to change the default settings from QuantumCumulants.jl using the transition operators $\sigma_{\pm}^{(m)}$ as well as the projective operators $\hat{P}_{m,-}$ to considering the Pauli-matrices $\sigma_x^{(m)}, \sigma_y^{(m)}$ and $\sigma_z^{(m)}$. We did the computations and found the exact same results for both methods, which are presented in Figure A.1 for the bi-prime problem $\omega = 15$ at $T = 5$.

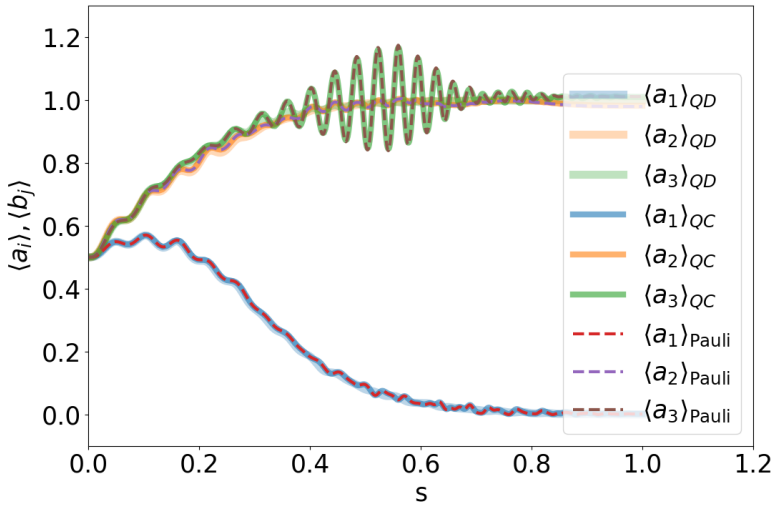

Figure A.1: Bit-digit measurements of $\omega = 15[1111] = 5[101] \times 3[11] = 5[101] \times 3[11]$ using the full quantum dynamics (QD), the default settings of QuantumCumulants.jl (QC) as well as the Pauli-matrix (Pauli) QuantumCumulants.jl settings.

In Figure A.1 we can clearly see that QuantumCumulants.jl provides the same results for both the transition-projector as well as the Pauli-matrix settings. This should be the case, because in section 6.1 we prove that QuantumCumulants.jl calculates the commutator relations correctly. Hence, the origin of the divergences can be either of numerical nature or the generalized cumulant expansion method fails in the case of a semi-classical model with expansion orders higher than the mean-field approach and smaller than the maximal order.

A.7 Further Investigation on Joint Cumulants

In this section we show some additional results of the discussion of the joint cumulants in section 6.4. In Figure A.2, one visualizes the joint cumulants for $\omega = 15$ at a very large $T = 100$ with expansion order $o = 1$ received by utilizing QuantumCumulants.jl and Schrödinger, respectively.

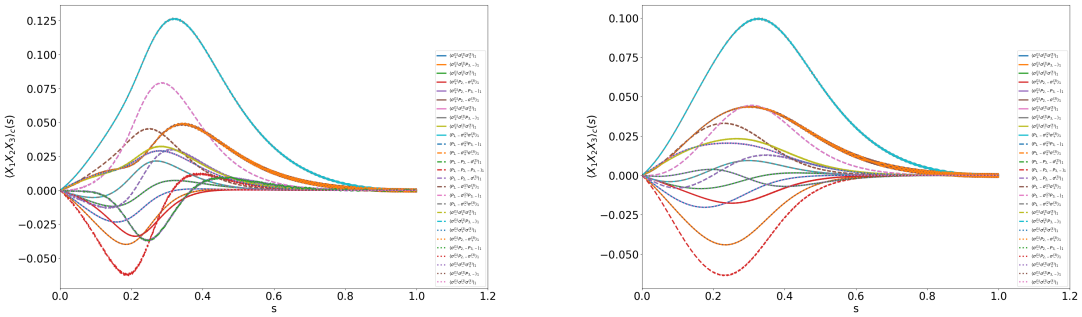

(a) QC.jl (b) Schrödinger

Figure A.2: Comparison of the joint cumulants determined by QuantumCumulants.jl (QC.jl) and Schrödinger, respectively, for $\omega = 15$ with expansion order $o = 1$ at $T = 100$.

Figure A.2 shows that the larger T, the smaller the oscillating combinations in both cases discussed in section 6.4. Hence, less contributions of higher-energy levels.

We know from Equation 2.59 that each n-th order average is a superposition of products of sub-averages of order up to l if the expansion order is equal to l. We plot in Figure A.3 the sub-averages from the combinations $\langle \sigma_+^{(1)} \hat{P}_{2,-} \sigma_-^{(3)} \rangle_{C,2} = \langle \sigma_-^{(1)} \hat{P}_{2,-} \sigma_+^{(3)} \rangle_{C,2}$ and $\langle \sigma_+^{(1)} \hat{P}_{2,-} \sigma_+^{(3)} \rangle_{C,2} = \langle \sigma_-^{(1)} \hat{P}_{2,-} \sigma_-^{(3)} \rangle_{C,2}$ discussed in section 6.4. Each combination consists of six different sub-averages:

$$\langle \sigma_+^{(1)} \hat{P}_{2,-} \sigma_-^{(3)} \rangle_{C,2} = \langle \sigma_+^{(1)} \rangle \langle \hat{P}_{2,-} \sigma_-^{(3)} \rangle + \langle \hat{P}_{2,-} \rangle \langle \sigma_+^{(1)} \sigma_-^{(3)} \rangle + \langle \sigma_-^{(3)} \rangle \langle \sigma_+^{(1)} \hat{P}_{2,-} \rangle - 2 \langle \sigma_+^{(1)} \rangle \langle \hat{P}_{2,-} \rangle \langle \sigma_-^{(3)} \rangle \tag{A.20}$$

$$\langle \sigma_+^{(1)} \hat{P}_{2,-} \sigma_+^{(3)} \rangle_{C,2} = \langle \sigma_+^{(1)} \rangle \langle \hat{P}_{2,-} \sigma_+^{(3)} \rangle + \langle \hat{P}_{2,-} \rangle \langle \sigma_+^{(1)} \sigma_+^{(3)} \rangle + \langle \sigma_+^{(3)} \rangle \langle \sigma_+^{(1)} \hat{P}_{2,-} \rangle - 2 \langle \sigma_+^{(1)} \rangle \langle \hat{P}_{2,-} \rangle \langle \sigma_+^{(3)} \rangle. \tag{A.21}$$

These terms are plotted in Figure A.3.

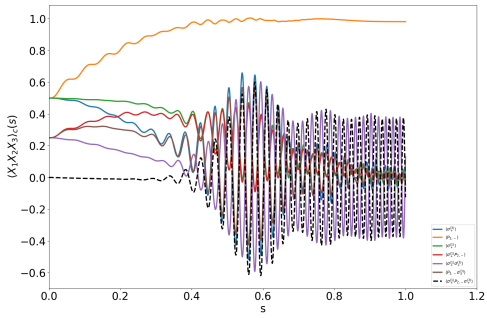

(a) $\langle \sigma_+^{(1)} \hat{P}_{2,-} \sigma_+^{(3)} \rangle_{C,2}$, QC.jl

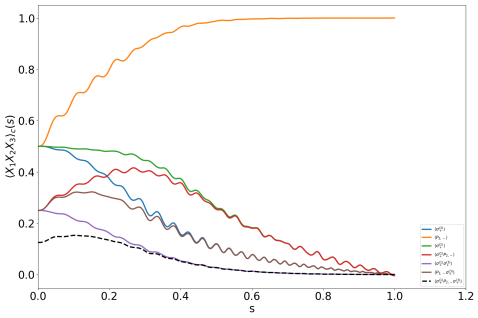

(b) $\langle \sigma_+^{(1)} \hat{P}_{2,-} \sigma_+^{(3)} \rangle_{C,2}$, Schrödinger

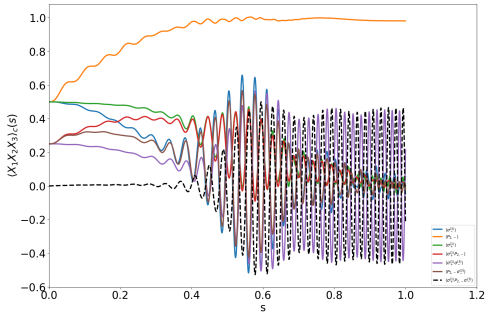

(c) $\langle \sigma_+^{(1)} \hat{P}_{2,-} \sigma_-^{(3)} \rangle_{C,2}$, QC.jl

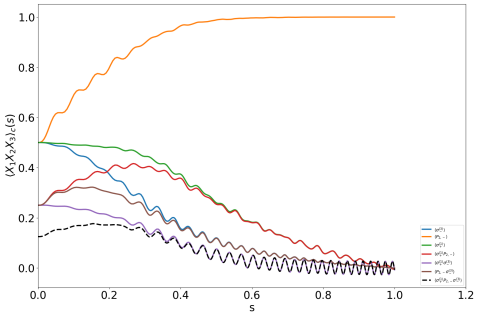

(d) $\langle \sigma_+^{(1)} \hat{P}_{2,-} \sigma_-^{(3)} \rangle_{C,2}$, Schrödinger

Figure A.3: Sub-averages of the combinations $\langle \sigma_+^{(1)} \hat{P}_{2,-} \sigma_-^{(3)} \rangle_{C,2} = \langle \sigma_-^{(1)} \hat{P}_{2,-} \sigma_+^{(3)} \rangle_{C,2}$ and $\langle \sigma_+^{(1)} \hat{P}_{2,-} \sigma_+^{(3)} \rangle_{C,2} = \langle \sigma_-^{(1)} \hat{P}_{2,-} \sigma_-^{(3)} \rangle_{C,2}$ for $\omega = 15$ at $T = 5$ in expansion order $o = 2$.

Appendix B

Mathematica Script of $\omega = 15$

```
(*Include some libraries*)
Needs["Combinatorica`"]
Needs["DifferentialEquations`NDSolveProblems`"];
Needs["DifferentialEquations`NDSolveUtilities`"];
(*Start with numbers of dynamical qubits*)
k = 2;
l = 1;
Remove[V2, v0]
(*Define the EXPECTATION VALUES of the bits, i.e., \langle a^{12} \rangle= a12*)
AllOperators = {{a12, a22, a21}, {b12, b22, b21}, {c12, c22, c21}};
AllOperatorst = {{a12[t], a22[t], a21[t]}, {b12[t], b22[t],
   b21[t]}, {c12[t], c22[t], c21[t]}};
AllOperators0 = {{a12[0], a22[0], a21[0]}, {b12[0], b22[0],
   b21[0]}, {c12[0], c22[0], c21[0]}};
AllOperatorsder = {{a12'[t], a22'[t], a21'[t]}, {b12'[t], b22'[t],
   b21'[t]}, {c12'[t], c22'[t], c21'[t]}};
(*Define the necessary partitions to obtain a complete Ehrenfest ODE system
(see Berechnungen 7)*)
(*We assume that Mathematica cannot handle Conjugate[a12] = a21,
hence, we derive a bigger system where we calculate these expressions
as well*)
V1 = Table[{Table[
    Table[{AllOperators[[i]][[1]], AllOperators[[r]][[k]]}, {k, 1,
      Length[AllOperators[[r]]]}], {r, i + 1,
     Length[AllOperators]}],
   Table[
    Table[{AllOperators[[i]][[2]], AllOperators[[r]][[k]]}, {k, 1,
      Length[AllOperators[[r]]]}], {r, i + 1,
     Length[AllOperators]}],
   Table[
    Table[{AllOperators[[i]][[3]], AllOperators[[r]][[k]]}, {k, 1,
      Length[AllOperators[[r]]]}], {r, i + 1,
     Length[AllOperators]}]}, {i, 1, Length[AllOperators] - 1}];
VOperatos = Flatten[V1];
VOp = {Flatten[AllOperators],
  Table[{VOperatos[[2*r - 1]], VOperatos[[2*r]]}, {r,
    1, (Length[VOperatos])/2}]};
VOpder = {Flatten[AllOperatorsder],
  Table[{(Symbol /@
```

```
        ToString /@
         Row /@ {{VOperatos[[2*r - 1]], VOperatos[[2*r]]}})[[1]]'[
    t]}, {r, 1, Length[VOperatos]/2}]};
VOpt = {Flatten[AllOperatorst],
  Table[{(Symbol /@
       ToString /@
        Row /@ {{VOperatos[[2*r - 1]], VOperatos[[2*r]]}})[[1]][
    t]}, {r, 1, Length[VOperatos]/2}]};
(*Define some convenient vectors for later*)
Numbers =
 Flatten[Table[{Table[
    Table[{{i, 1}, {r, k}}, {k, 1, Length[AllOperators[[r]]]}], {r,
     i + 1, Length[AllOperators]}],
    Table[
     Table[{{i, 2}, {r, k}}, {k, 1, Length[AllOperators[[r]]]}], {r,
     i + 1, Length[AllOperators]}],
    Table[
     Table[{{i, 3}, {r, k}}, {k, 1, Length[AllOperators[[r]]]}], {r,
     i + 1, Length[AllOperators]}]}, {i, 1,
    Length[AllOperators] - 1}]];
Numbers =
 Table[{Numbers[[2*r - 1]], Numbers[[2*r]]}, {r, 1,
   Length[Numbers]/2}];
R = Table[Numbers[[r]][[1]], {r, 1, Length[Numbers]}];
kind = Table[Numbers[[r]][[2]], {r, 1, Length[Numbers]}];
V0neu = (Flatten[{Flatten[AllOperators0],
    Table[{(Symbol /@
         ToString /@
          Row /@ {{VOperatos[[2*r - 1]], VOperatos[[2*r]]}})[[1]][
      0]}, {r, 1, Length[VOperatos]/2}]}]);
v0 = Flatten[{Table[0.5, {r, 1, 9}],
   Table[0.25, {r, 1, Length[Flatten[VOpt]] - 9}]}];
v0begin = Table[V0neu[[r]] == v0[[r]], {r, 1, Length[v0]}]
{a12[0] == 0.5, a22[0] == 0.5, a21[0] == 0.5, b12[0] == 0.5,
 b22[0] == 0.5, b21[0] == 0.5, c12[0] == 0.5, c22[0] == 0.5,
 c21[0] == 0.5, a12b12[0] == 0.25, a12b22[0] == 0.25,
 a12b21[0] == 0.25, a12c12[0] == 0.25, a12c22[0] == 0.25,
 a12c21[0] == 0.25, a22b12[0] == 0.25, a22b22[0] == 0.25,
 a22b21[0] == 0.25, a22c12[0] == 0.25, a22c22[0] == 0.25,
 a22c21[0] == 0.25, a21b12[0] == 0.25, a21b22[0] == 0.25,
 a21b21[0] == 0.25, a21c12[0] == 0.25, a21c22[0] == 0.25,
 a21c21[0] == 0.25, b12c12[0] == 0.25, b12c22[0] == 0.25,
 b12c21[0] == 0.25, b22c12[0] == 0.25, b22c22[0] == 0.25,
 b22c21[0] == 0.25, b21c12[0] == 0.25, b21c22[0] == 0.25,
 b21c21[0] == 0.25}
 (*Parameters*)
Time = 5.; (*Time for the adiabatic evolution*)
\[HBar] = 1.;
\[Omega] = 15;
\[Xi] = 10;
(*Definitions*)
(*Generalized cumulant expansion method in 2nd order*)
(*Define symbolic expressions like a12b12*)
\[Chi]2[X1_, X2_, r1_, r2_] :=
 Which[r1 == r2, 0,
  r1 < r2, (Symbol /@ ToString /@ Row /@ {{X1, X2}})[[1]][t],
  r2 < r1, (Symbol /@ ToString /@ Row /@ {{X2, X1}})[[1]][t]]
(*++++++++++++++++++++++++++++++++++++++++++++++++++++++++++++++++*)
```

```
(*Three-operator-expansion*)
\[Chi]3[X1_, X2_, X3_, r1_, r2_,
  r3_] := (X1[t]*\[Chi]2[X2, X3, r2, r3] +
   X2[t]*\[Chi]2[X1, X3, r1, r3] + X3[t]*\[Chi]2[X1, X2, r1, r2] -
   2*X1[t]*X2[t]*X3[t])
(*++++++++++++++++++++++++++++++++++++++++++++++++++++++++++++++*)
(*Four-operator-expansion*)
\[Chi]4[X1_, X2_, X3_, X4_, r1_, r2_, r3_,
  r4_] := (\[Chi]2[X1, X2, r1, r2]*\[Chi]2[X3, X4, r3, r4] + \[Chi]2[
     X1, X3, r1, r3]*\[Chi]2[X2, X4, r2, r4] + \[Chi]2[X1, X4, r1,
     r4]*\[Chi]2[X2, X3, r2, r3] - 2*X1[t]*X2[t]*X3[t]*X4[t])
(*++++++++++++++++++++++++++++++++++++++++++++++++++++++++++++++*)
(*Five-operator-expansion*)
\[Chi]5[X1_, X2_, X3_, X4_, X5_, r1_, r2_, r3_, r4_,
   r5_] := (\[Chi]2[X1, X4, r1, r4]*\[Chi]2[X2, X5, r2, r5]*
     X3[t] + \[Chi]2[X2, X5, r2, r5]*\[Chi]2[X3, X4, r3, r4]*
     X1[t] + \[Chi]2[X1, X4, r1, r4]*\[Chi]2[X3, X5, r3, r5]*
     X2[t] + \[Chi]2[X2, X4, r2, r4]*\[Chi]2[X3, X5, r3, r5]*
     X1[t] + \[Chi]2[X1, X3, r1, r3]*\[Chi]2[X2, X5, r2, r5]*X4[t] -
    2*X1[t]*X3[t]*
     X4[t]*\[Chi]2[X2, X5, r2, r5] + \[Chi]2[X1, X2, r1, r2]*\[Chi]2[
      X3, X5, r3, r5]*X4[t] -
    2*X1[t]*X2[t]*
     X4[t]*\[Chi]2[X3, X4, r3, r5] + \[Chi]2[X1, X3, r1, r3]*\[Chi]2[
      X4, X5, r4, r5]*
     X2[t] + \[Chi]2[X2, X3, r2, r3]*\[Chi]2[X4, X5, r4, r5]*
     X1[t] + \[Chi]2[X1, X2, r1, r2]*\[Chi]2[X4, X5, r4, r5]*X3[t] -
    2*X1[t]*X2[t]*X3[t]*\[Chi]2[X4, X5, r4, r5] +
    X5[t]*(\[Chi]2[X1, X2, r1, r2]*\[Chi]2[X3, X4, r3, r4] + \[Chi]2[
        X1, X3, r1, r3]*(\[Chi]2[X2, X4, r2, r4] - 2*X2[t]*X4[t]) -
       2*(\[Chi]2[X1, X4, r1, r4]*X2[t]*X3[t] +
          X3[t]*X4[t]*\[Chi]2[X1, X2, r1, r2] +
          X1[t]*(\[Chi]2[X2, X4, r2, r4]*
             X3[t] + \[Chi]2[X3, X4, r3, r4]*
             X2[t] + \[Chi]2[X2, X3, r2, r3]*X4[t] -
            3*X2[t]*X3[t]*X4[t]))) + \[Chi]2[X1, X5, r1,
      r5]*(\[Chi]2[X2, X4, r2, r4]*X3[t] +
      X2[t]*(\[Chi]2[X3, X4, r3, r4] - 2*X3[t]*X4[t]) + \[Chi]2[X2,
        X3, r2, r3]*(X4[t] +
        X5[t])));
(*Expressions for the correct expansion (see mathematical \
derivation)*)
Momone1[X1_, r1_] :=
 X1[t] + Sum[
   2^j*\[Chi]2[X1, VOp[[1]][[3*(j + k - 1) + 2]], r1, j + k], {j, 1,
    l}]
Momone2[X1_, r1_] :=
 X1[t] + Sum[
   2^(j + 1)*(1 + 2^(j - 1))*\[Chi]2[X1,
     VOp[[1]][[3*(j + k - 1) + 2]], r1, j + k], {j, 1, l}] +
  Sum[Sum[Which[j1 == j2, 0, j1 != j2,
     2^(j1 + j2)*\[Chi]3[X1, VOp[[1]][[3*(j1 + k - 1) + 2]],
      VOp[[1]][[3*(j2 + k - 1) + 2]], r1, j1 + k, j2 + k]], {j1, 1,
     l}], {j2, 1, l}]
Momone3[X1_, X2_, r1_, r2_] := \[Chi]2[X1, X2, r1, r2] +
  Sum[2^(j + 1)*(1 + 2^(j - 1))*\[Chi]3[X1, X2,
     VOp[[1]][[3*(j + k - 1) + 2]], r1, r2, j + k], {j, 1, l}] +
  Sum[Sum[Which[j1 == j2, 0, j1 != j2,
```

```
    2^(j1 + j2)*\[Chi]4[X1, X2, VOp[[1]][[3*(j1 + k - 1) + 2]],
     VOp[[1]][[3*(j2 + k - 1) + 2]], r1, r2, j1 + k, j2 + k]], {j1,
    1, l}], {j2, 1, l}]
Momone4[X1_, r1_] :=
 X1[t] + Sum[
   2^i*\[Chi]2[X1, VOp[[1]][[3*(i - 1) + 2]], r1, i], {i, 1, k}]
Momone5[X1_, r1_] :=
 X1[t] + Sum[
   2^(i + 1)*(1 + 2^(i - 1))*\[Chi]2[X1, VOp[[1]][[3*(i - 1) + 2]],
    r1, i], {i, 1, k}] +
  Sum[Sum[Which[i1 == i2, 0, i1 != i2,
    2^(i1 + i2)*\[Chi]3[X1, VOp[[1]][[3*(i1 - 1) + 2]],
     VOp[[1]][[3*(i2 - 1) + 2]], r1, i1, i2]], {i1, 1, k}], {i2, 1,
   k}]
Momone6[X1_, X2_, r1_, r2_] := \[Chi]2[X1, X2, r1, r2] +
  Sum[2^(i + 1)*(1 + 2^(i - 1))*\[Chi]3[X1, X2,
    VOp[[1]][[3*(i - 1) + 2]], r1, r2, i], {i, 1, k}] +
  Sum[Sum[Which[i1 == i2, 0, i1 != i2,
    2^(i1 + i2)*\[Chi]4[X1, X2, VOp[[1]][[3*(i1 - 1) + 2]],
     VOp[[1]][[3*(i2 - 1) + 2]], r1, r2, i1, i2]], {i1, 1, k}], {i2,
    1, k}]
(*++++++++++++++++++++++++++++++++++++++++++++++++++++++++++++++++*)
(*Ehrenfest theorem with operator multiplied from the right*)
(*r1 <= k*)
Mom3r1[X1_, X2_, r1_, r2_, k2_] := \[Chi]2[X1, X2, r1, r2] +
  Sum[2^j*Which[
    j + k != r2, \[Chi]3[X1, X2, VOp[[1]][[3*(j + k - 1) + 2]], r1,
     r2, j + k], j + k == r2,
    Which[k2 == 1, 0, k2 == 2, \[Chi]2[X1, X2, r1, r2],
     k2 == 3, \[Chi]2[X1, X2, r1, r2]]], {j, 1, l}]
Mom4r1[X1_, X2_, r1_, r2_, k2_] := \[Chi]2[X1, X2, r1, r2] +
  Sum[2^(j + 1)*(1 + 2^(j - 1))*
    Which[j + k != r2, \[Chi]3[X1, X2, VOp[[1]][[3*(j + k - 1) + 2]],
     r1, r2, j + k], j + k == r2,
    Which[k2 == 1, 0, k2 == 2, \[Chi]2[X1, X2, r1, r2],
     k2 == 3, \[Chi]2[X1, X2, r1, r2]]], {j, 1, l}] +
  Sum[Sum[Which[j1 == j2, 0, j1 != j2,
    2^(j1 + j2)*
     Which[j1 + k != r2 != j2 + k, \[Chi]4[X1, X2,
       VOp[[1]][[3*(j1 + k - 1) + 2]],
       VOp[[1]][[3*(j2 + k - 1) + 2]], r1, r2, j1 + k, j2 + k],
      j1 + k == r2 != j2 + k,
      Which[k2 == 1, 0,
       k2 == 2 || k2 == 3, \[Chi]3[X1, X2,
        VOp[[1]][[3*(j2 + k - 1) + 2]], r1, r2, j2 + k]],
      j1 + k != r2 == j2 + k,
      Which[k2 == 1, 0,
       k2 == 2 || k2 == 3, \[Chi]3[X1, X2,
        VOp[[1]][[3*(j1 + k - 1) + 2]], r1, r2, j1 + k]]]], {j1, 1,
    l}], {j2, 1, l}]
Mom5r1[X1_, X2_, X3_, r1_, r2_, r3_, k2_] :=
 Which[r2 != r3, \[Chi]3[X1, X2, X3, r1, r2, r3], r2 == r3,
  Which[k2 == 1, 0, k2 == 2 || k2 == 3, \[Chi]2[X1, X2, r1, r2]]] +
  Sum[2^(j + 1)*(1 + 2^(j - 1))*
    Which[j + k != r2 != r3, \[Chi]4[X1, X2, X3,
     VOp[[1]][[3*(j + k - 1) + 2]], r1, r2, r3, j + k],
    j + k == r2 != r3,
    Which[k2 == 1, 0, k2 == 2, \[Chi]3[X1, X2, X3, r1, r2, r3],
```

```
     k2 == 3, \[Chi]3[X1, X2, X3, r1, r2, r3]], j + k != r2 == r3,
    Which[k2 == 1, 0,
     k2 == 2, \[Chi]3[X1, X2, VOp[[1]][[3*(j + k - 1) + 2]], r1, r2,
      j + k], k2 == 3, \[Chi]3[X1, X2, VOp[[1]][[3*(j + k - 1) + 2]],
       r1, r2, j + k]]], {j, 1, l}] +
  Sum[Sum[Which[j1 == j2, 0, j1 != j2,
    2^(j1 + j2)*
     Which[j1 + k != r2 != r3 != j2 + k, \[Chi]5[X1, X2, X3,
      VOp[[1]][[3*(j1 + k - 1) + 2]],
      VOp[[1]][[3*(j2 + k - 1) + 2]], r1, r2, r3, j1 + k, j2 + k],
     j1 + k == r2 != r3 != j2 + k,
     Which[k2 == 1, 0,
      k2 == 2 || k2 == 3, \[Chi]4[X1, X2, X3,
       VOp[[1]][[3*(j2 + k - 1) + 2]], r1, r2, r3, j2 + k]],
     j1 + k != r2 == j2 + k != r3,
     Which[k2 == 1, 0,
      k2 == 2 || k2 == 3, \[Chi]4[X1, X2, X3,
       VOp[[1]][[3*(j1 + k - 1) + 2]], r1, r2, r3, j1 + k]],
     j1 + k != r2 == r3 != j2 + k,
     Which[k2 == 1, 0,
      k2 == 2 || k2 == 3, \[Chi]4[X1, X2,
       VOp[[1]][[3*(j1 + k - 1) + 2]],
       VOp[[1]][[3*(j2 + k - 1) + 2]], r1, r2, r3, j1 + k,
       j2 + k]]]], {j1, 1, l}], {j2, 1, l}]
(*k <= r1 <= k + l*)
Mom3r2[X1_, X2_, r1_, r2_, k2_] := \[Chi]2[X1, X2, r1, r2] +
  Sum[2^i*Which[
    i != r2, \[Chi]3[X1, X2, VOp[[1]][[3*(i - 1) + 2]], r1, r2, i],
    i == r2,
    Which[k2 == 1, 0, k2 == 2, \[Chi]2[X1, X2, r1, r2],
     k2 == 3, \[Chi]2[X1, X2, r1, r2]]], {i, 1, k}]
Mom4r2[X1_, X2_, r1_, r2_, k2_] := \[Chi]2[X1, X2, r1, r2] +
  Sum[2^(i + 1)*(1 + 2^(i - 1))*
   Which[i != r2, \[Chi]3[X1, X2, VOp[[1]][[3*(i - 1) + 2]], r1, r2,
     i], i == r2,
    Which[k2 == 1, 0, k2 == 2, \[Chi]2[X1, X2, r1, r2],
     k2 == 3, \[Chi]2[X1, X2, r1, r2]]], {i, 1, k}] +
  Sum[Sum[Which[i1 == i2, 0, i1 != i2,
    2^(i1 + i2)*
     Which[i1 != r2 != i2, \[Chi]4[X1, X2,
      VOp[[1]][[3*(i1 - 1) + 2]], VOp[[1]][[3*(i2 - 1) + 2]], r1,
      r2, i1, i2], i1 == r2 != i2,
     Which[k2 == 1, 0,
      k2 == 2 || k2 == 3, \[Chi]3[X1, X2,
       VOp[[1]][[3*(i2 - 1) + 2]], r1, r2, i2]], i1 != r2 == i2,
     Which[k2 == 1, 0,
      k2 == 2 || k2 == 3, \[Chi]3[X1, X2,
       VOp[[1]][[3*(i1 - 1) + 2]], r1, r2, i1]]]], {i1, 1, k}], {i2,
    1, k}]
Mom5r2[X1_, X2_, X3_, r1_, r2_, r3_,
  k2_] := \[Chi]3[X1, X2, X3, r1, r2, r3] +
  Sum[2^(i + 1)*(1 + 2^(i - 1))*
   Which[i != r2 != r3, \[Chi]4[X1, X2, X3,
     VOp[[1]][[3*(i - 1) + 2]], r1, r2, r3, i], i == r2 != r3,
    Which[k2 == 1, 0, k2 == 2, \[Chi]3[X1, X2, X3, r1, r2, r3],
     k2 == 3, \[Chi]3[X1, X2, X3, r1, r2, r3]], i != r2 == r3,
    Which[k2 == 1, 0,
     k2 == 2, \[Chi]3[X1, X2, VOp[[1]][[3*(i - 1) + 2]], r1, r2, i],
```

```
272       k2 == 3, \[Chi]3[X1, X2, VOp[[1]][[3*(i - 1) + 2]], r1, r2,
273        i]]], {i, 1, k}] +
274    Sum[Sum[Which[i1 == i2, 0, i1 != i2,
275      2^(i1 + i2)*
276       Which[i1 != r2 != r3 != i2, \[Chi]5[X1, X2, X3,
277        VOp[[1]][[3*(i1 - 1) + 2]], VOp[[1]][[3*(i2 - 1) + 2]], r1,
278        r2, r3, i1, i2], i1 == r2 != r3 != i2,
279       Which[k2 == 1, 0,
280        k2 == 2 || k2 == 3, \[Chi]4[X1, X2, X3,
281         VOp[[1]][[3*(i2 - 1) + 2]], r1, r2, r3, i2]],
282       i1 != r2 == i2 != r3,
283       Which[k2 == 1, 0,
284        k2 == 2 || k2 == 3, \[Chi]4[X1, X2, X3,
285         VOp[[1]][[3*(i1 - 1) + 2]], r1, r2, r3, i1]],
286       i1 != r2 == r3 != i2,
287       Which[k2 == 1, 0,
288        k2 == 2 || k2 == 3, \[Chi]4[X1, X2,
289         VOp[[1]][[3*(i1 - 1) + 2]], VOp[[1]][[3*(i2 - 1) + 2]], r1,
290         r2, r3, i1, i2]]]], {i1, 1, k}], {i2, 1, k}]
291  (*Ehrenfest theorem with operator multiplied from the left*)
292  (*r2 <= k*)
293  Mom3l1[X1_, X2_, r1_, r2_, k1_] := \[Chi]2[X1, X2, r1, r2] +
294    Sum[2^j*Which[
295      j + k != r1, \[Chi]3[X1, X2, VOp[[1]][[3*(j + k - 1) + 2]], r1,
296       r2, j + k], j + k == r1,
297      Which[k1 == 3, 0, k1 == 2, \[Chi]2[X1, X2, r1, r2],
298       k1 == 1, \[Chi]2[X1, X2, r1, r2]]], {j, 1, l}]
299  Mom4l1[X1_, X2_, r1_, r2_, k1_] := \[Chi]2[X1, X2, r1, r2] +
300    Sum[2^(j + 1)*(1 + 2^(j - 1))*
301      Which[j + k != r1, \[Chi]3[X1, X2, VOp[[1]][[3*(j + k - 1) + 2]],
302       r1, r2, j + k], j + k == r1,
303      Which[k1 == 3, 0, k1 == 2, \[Chi]2[X1, X2, r1, r2],
304       k1 == 1, \[Chi]2[X1, X2, r1, r2]]], {j, 1, l}] +
305    Sum[Sum[Which[j1 == j2, 0, j1 != j2,
306      2^(j1 + j2)*
307       Which[j1 + k != r1 != j2 + k, \[Chi]4[X1, X2,
308        VOp[[1]][[3*(j1 + k - 1) + 2]],
309        VOp[[1]][[3*(j2 + k - 1) + 2]], r1, r2, j1 + k, j2 + k],
310       j1 + k == r1 != j2 + k,
311       Which[k1 == 3, 0,
312        k1 == 2 || k1 == 1, \[Chi]3[X1, X2,
313         VOp[[1]][[3*(j2 + k - 1) + 2]], r1, r2, j2 + k]],
314       j1 + k != r1 == j2 + k,
315       Which[k1 == 3, 0,
316        k1 == 2 || k1 == 1, \[Chi]3[X1, X2,
317         VOp[[1]][[3*(j1 + k - 1) + 2]], r1, r2, j1 + k]]]], {j1, 1,
318      l}], {j2, 1, l}]
319  Mom5l1[X1_, X2_, X3_, r1_, r2_, r3_, k1_] :=
320   Which[r1 != r3, \[Chi]3[X1, X2, X3, r1, r2, r3], r1 == r3,
321    Which[k1 == 3, 0, k1 == 2 || k1 == 1, \[Chi]2[X1, X2, r1, r2]]] +
322    Sum[2^(j + 1)*(1 + 2^(j - 1))*
323      Which[j + k != r1 != r3, \[Chi]4[X1, X2, X3,
324       VOp[[1]][[3*(j + k - 1) + 2]], r1, r2, r3, j + k],
325      j + k == r1 != r3,
326      Which[k1 == 3, 0, k1 == 2, \[Chi]3[X1, X2, X3, r1, r2, r3],
327       k1 == 1, \[Chi]3[X1, X2, X3, r1, r2, r3]], j + k != r1 == r3,
328      Which[k1 == 3, 0,
329       k1 == 2, \[Chi]3[X1, X2, VOp[[1]][[3*(j + k - 1) + 2]], r1,
```

```
      r2, (j + k)],
     k1 == 1, \[Chi]3[X1, X2, VOp[[1]][[3*(j + k - 1) + 2]], r1,
      r2, (j + k)]]], {j, 1, l}] +
  Sum[Sum[Which[j1 == j2, 0, j1 != j2,
    2^(j1 + j2)*
     Which[j1 + k != r1 != r3 != j2 + k, \[Chi]5[X1, X2, X3,
      VOp[[1]][[3*(j1 + k - 1) + 2]],
      VOp[[1]][[3*(j2 + k - 1) + 2]], r1, r2, r3, j1 + k, j2 + k],
     j1 + k == r1 != r3 != j2 + k,
     Which[k1 == 3, 0,
      k1 == 2 || k1 == 1, \[Chi]4[X1, X2, X3,
       VOp[[1]][[3*(j2 + k - 1) + 2]], r1, r2, r3, j2 + k]],
     j1 + k != r1 == j2 + k != r3,
     Which[k1 == 3, 0,
      k1 == 2 || k1 == 1, \[Chi]4[X1, X2, X3,
       VOp[[1]][[3*(j1 + k - 1) + 2]], r1, r2, r3, j1 + k]],
     j1 + k != r1 == r3 != j2 + k,
     Which[k1 == 3, 0,
      k1 == 2 || k1 == 1, \[Chi]4[X1, X2,
       VOp[[1]][[3*(j1 + k - 1) + 2]],
       VOp[[1]][[3*(j2 + k - 1) + 2]], r1, r2, r3, j1 + k,
       j2 + k]]]], {j1, 1, l}], {j2, 1, l}]
(*k <= r2 <= k + l*)
Mom3l2[X1_, X2_, r1_, r2_, k1_] := \[Chi]2[X1, X2, r1, r2] +
  Sum[2^i*Which[
    i != r1, \[Chi]3[X1, X2, VOp[[1]][[3*(i - 1) + 2]], r1, r2, i],
    i == r1,
    Which[k1 == 3, 0, k1 == 2, \[Chi]2[X1, X2, r1, r2],
     k1 == 1, \[Chi]2[X1, X2, r1, r2]]], {i, 1, k}]
Mom4l2[X1_, X2_, r1_, r2_, k1_] := \[Chi]2[X1, X2, r1, r2] +
  Sum[2^(i + 1)*(1 + 2^(i - 1))*
   Which[i != r1, \[Chi]3[X1, X2, VOp[[1]][[3*(i - 1) + 2]], r1, r2,
     i], i == r1,
    Which[k1 == 3, 0, k1 == 2, \[Chi]2[X1, X2, r1, r2],
     k1 == 1, \[Chi]2[X1, X2, r1, r2]]], {i, 1, k}] +
  Sum[Sum[Which[i1 == i2, 0, i1 != i2,
    2^(i1 + i2)*
     Which[i1 != r1 != i2, \[Chi]4[X1, X2,
      VOp[[1]][[3*(i1 - 1) + 2]], VOp[[1]][[3*(i2 - 1) + 2]], r1,
      r2, i1, i2], i1 == r1 != i2,
     Which[k1 == 3, 0,
      k1 == 2 || k1 == 1, \[Chi]3[X1, X2,
       VOp[[1]][[3*(i2 - 1) + 2]], r1, r2, i2]], i1 != r1 == i2,
     Which[k1 == 3, 0,
      k1 == 2 || k1 == 1, \[Chi]3[X1, X2,
       VOp[[1]][[3*(i1 - 1) + 2]], r1, r2, i1]]]], {i1, 1, k}], {i2,
    1, k}]
Mom5l2[X1_, X2_, X3_, r1_, r2_, r3_,
  k1_] := \[Chi]3[X1, X2, X3, r1, r2, r3] +
  Sum[2^(i + 1)*(1 + 2^(i - 1))*
   Which[i != r2 != r3, \[Chi]4[X1, X2, X3,
     VOp[[1]][[3*(i - 1) + 2]], r1, r2, r3, i], i == r1 != r3,
    Which[k1 == 3, 0, k1 == 2, \[Chi]3[X1, X2, X3, r1, r2, r3],
     k1 == 1, \[Chi]3[X1, X2, X3, r1, r2, r3]], i != r1 == r3,
    Which[k1 == 3, 0,
     k1 == 2, \[Chi]3[X1, X2, VOp[[1]][[3*(i - 1) + 2]], r1, r2, i],
     k1 == 1, \[Chi]3[X1, X2, VOp[[1]][[3*(i - 1) + 2]], r1, r2,
      i]]], {i, 1, k}] +
```

```
  Sum[Sum[Which[i1 == i2, 0, i1 != i2,
    2^(i1 + i2)*
     Which[i1 != r1 != r3 != i2, \[Chi]5[X1, X2, X3,
       VOp[[1]][[3*(i1 - 1) + 2]], VOp[[1]][[3*(i2 - 1) + 2]], r1,
       r2, r3, i1, i2], i1 == r1 != r3 != i2,
      Which[k1 == 3, 0,
       k1 == 2 || k1 == 1, \[Chi]4[X1, X2, X3,
        VOp[[1]][[3*(i2 - 1) + 2]], r1, r2, r3, i2]],
      i1 != r1 == i2 != r3,
      Which[k1 == 3, 0,
       k1 == 2 || k1 == 1, \[Chi]4[X1, X2, X3,
        VOp[[1]][[3*(i1 - 1) + 2]], r1, r2, r3, i1]],
      i1 != r1 == r3 != i2,
      Which[k1 == 3, 0,
       k1 == 2 || k1 == 1, \[Chi]4[X1, X2,
        VOp[[1]][[3*(i1 - 1) + 2]], VOp[[1]][[3*(i2 - 1) + 2]], r1,
        r2, r3, i1, i2]]]], {i1, 1, k}], {i2, 1, k}]
(*The differential equations can be expressed more thoroughly by
introducing the RHS of equation as functions*)
(*Equations with only one-operator averages*)
f[x_, r_] :=
 I/\[HBar]*\[Xi]*(1 - 2*VOp[[1]][[3*(r - 1) + 2]][t])*(1 - t/Time) +
  I/\[HBar]*2^(r + 1)*(t/
    Time)*(\[Omega]*Momone1[x, r] - (1 + 2^(r - 1))*Momone2[x, r] -
    Sum[Which[i == r, 0, i != r,
      2^i*Momone3[x, VOp[[1]][[3*(i - 1) + 2]], r, i]], {i, 1, k}])
g[x_, r_] :=
 I/\[HBar]*\[Xi]*(1 - 2*VOp[[1]][[3*(r - 1) + 2]][t])*(1 - t/Time) +
  I/\[HBar]*2^(r - k + 1)*(t/
    Time)*(\[Omega]*Momone4[x, r] - (1 + 2^(r - k - 1))*
     Momone5[x, r] -
    Sum[Which[j == r - k, 0, j != r - k,
      2^j*Momone6[x, VOp[[1]][[3*(j + k - 1) + 2]], r, j + k]], {j,
      1, l}])
h[r_] := -I/\[HBar]*\[Xi]*(VOp[[1]][[3*(r - 1) + 1]][t] -
   VOp[[1]][[3*(r - 1) + 3]][t])*(1 - t/Time)

(*Equations with two-operator Averages*)
(*dO1/dt*O2*)
(*r1 <= k *)
Fr[x1_, x2_, r1_, r2_, k2_] :=
 I/\[HBar]*\[Xi]*(x2[t] -
    2*\[Chi]2[VOp[[1]][[3*(r1 - 1) + 2]], x2, r1, r2])*(1 -
    t/Time) +
  I/\[HBar]*2^(r1 + 1)*(\[Omega]*
     Mom3r1[x1, x2, r1, r2, k2] - (1 + 2^(r1 - 1))*
     Mom4r1[x1, x2, r1, r2, k2] -
    Sum[Which[i == r1, 0, i != r1,
      2^i*Mom5r1[x1, x2, VOp[[1]][[3*(i - 1) + 2]], r1, r2, i,
       k2]], {i, 1, k}])*(t/Time);
(*O1*dO2/dt*)
(*r2 <= k *)
Fl[x1_, x2_, r1_, r2_, k1_] :=
 I/\[HBar]*\[Xi]*(x1[t] -
    2*\[Chi]2[x1, VOp[[1]][[3*(r2 - 1) + 2]], r1, r2])*(1 -
    t/Time) +
  I/\[HBar]*2^(r2 + 1)*(\[Omega]*
     Mom3l1[x1, x2, r1, r2, k1] - (1 + 2^(r2 - 1))*
```

```
446       Mom4l1[x1, x2, r1, r2, k1] -
447      Sum[Which[i == r2, 0, i != r2,
448        2^i*Mom5l1[x1, x2, VOp[[1]][[3*(i - 1) + 2]], r1, r2, i,
449         k1]], {i, 1, k}])*(t/Time);
450 (*dO1/dt*O2*)
451 (*k <= r1 <= k + l*)
452 Gr[x1_, x2_, r1_, r2_, k2_] :=
453   I/\[HBar]*\[Xi]*(x2[t] -
454      2*\[Chi]2[VOp[[1]][[3*(r1 - 1) + 2]], x2, r1, r2])*(1 -
455      t/Time) +
456    I/\[HBar]*2^(r1 + 1 - k)*(\[Omega]*
457       Mom3r2[x1, x2, r1, r2, k2] - (1 + 2^(r1 - k - 1))*
458       Mom4r2[x1, x2, r1, r2, k2] -
459      Sum[Which[j + k == r1, 0, j + k != r1,
460        2^j*Mom5r2[x1, x2, VOp[[1]][[3*(j + k - 1) + 2]], r1, r2,
461         j + k, k2]], {j, 1, l}])*(t/Time);
462 (*O1*dO2/dt*)
463 (*k <= r2 <= k + l*)
464 Gl[x1_, x2_, r1_, r2_, k1_] :=
465   I/\[HBar]*\[Xi]*(x1[t] -
466      2*\[Chi]2[x1, VOp[[1]][[3*(r2 - 1) + 2]], r1, r2])*(1 -
467      t/Time) +
468    I/\[HBar]*2^(r2 + 1 - k)*(\[Omega]*
469       Mom3l2[x1, x2, r1, r2, k1] - (1 + 2^(r2 - k - 1))*
470       Mom4l2[x1, x2, r1, r2, k1] -
471      Sum[Which[j + k == r2, 0, j + k != r2,
472        2^j*Mom5l2[x1, x2, VOp[[1]][[3*(j + k - 1) + 2]], r1, r2,
473         j + k, k1]], {j, 1, l}])*(t/Time);
474 Hr[x2_, r1_,
475    r2_] := -I/\[HBar]*\[Xi]*(\[Chi]2[VOp[[1]][[3*(r1 - 1) + 1]], x2,
476      r1, r2] - \[Chi]2[VOp[[1]][[3*(r1 - 1) + 3]], x2, r1, r2])*(1 -
477     t/Time);
478 Hl[x1_, r1_,
479    r2_] := -I/\[HBar]*\[Xi]*(\[Chi]2[VOp[[1]][[3*(r2 - 1) + 1]], x1,
480      r2, r1] - \[Chi]2[VOp[[1]][[3*(r2 - 1) + 3]], x1, r2, r1])*(1 -
481     t/Time);
482
483 (*Construction of Ehrenfest system*)
484 R = Table[Numbers[[r]][[1]], {r, 1, Length[Numbers]}];
485 kind = Table[Numbers[[r]][[2]], {r, 1, Length[Numbers]}];
486 R1 = Flatten[Table[R[[2*r - 1]], {r, 1, Length[Numbers]/2}]];
487 R2 = Flatten[Table[R[[2*r]], {r, 1, Length[Numbers]/2}]];
488 kind1 = Flatten[Table[kind[[2*r - 1]], {r, 1, Length[kind]/2}]];
489 kind2 = Flatten[Table[kind[[2*r]], {r, 1, Length[kind]/2}]];
490 (*O2 = identity and O1 = identity*)
491 Eqn1 = Flatten[{Table[{VOpder[[1]][[3*(i - 1) + 1]] ==
492       f[VOp[[1]][[3*(i - 1) + 1]], i],
493      VOpder[[1]][[3*(i - 1) + 2]] == h[i],
494      VOpder[[1]][[
495        3*(i - 1) + 3]] == -f[VOp[[1]][[3*(i - 1) + 3]], i]}, {i, 1,
496      k}], Table[{VOpder[[1]][[3*(j + k - 1) + 1]] ==
497       g[VOp[[1]][[3*(j + k - 1) + 1]], j + k],
498      VOpder[[1]][[3*(j + k - 1) + 2]] == h[j + k],
499      VOpder[[1]][[
500        3*(j + k - 1) + 3]] == -g[VOp[[1]][[3*(j + k - 1) + 3]],
501         j + k]}, {j, 1, l}]}];
502
503 (*O2 != identity and O1 != identity*)
```

```
Eqn2 = Table[
  VOpder[[2]][[w]][[
    1]] == (Which[kind1[[w]] == 1,
      Which[R1[[w]] <= k,
       Fr[VOp[[2]][[w]][[1]], VOp[[2]][[w]][[2]], R1[[w]], R2[[w]],
        kind2[[w]]], R1[[w]] > k,
       Gr[VOp[[2]][[w]][[1]], VOp[[2]][[w]][[2]], R1[[w]], R2[[w]],
        kind2[[w]]]], kind1[[w]] == 2,
      Which[R1[[w]] <= k, Hr[VOp[[2]][[w]][[2]], R1[[w]], R2[[w]]],
       R1[[w]] > k, Hr[VOp[[2]][[w]][[2]], R1[[w]], R2[[w]]]],
      kind1[[w]] ==
       3, -Which[R1[[w]] <= k,
        Fr[VOp[[2]][[w]][[1]], VOp[[2]][[w]][[2]], R1[[w]], R2[[w]],
         kind2[[w]]], R1[[w]] > k,
        Gr[VOp[[2]][[w]][[1]], VOp[[2]][[w]][[2]], R1[[w]], R2[[w]],
         kind2[[w]]]]]) + (Which[kind2[[w]] == 1,
      Which[R2[[w]] <= k,
       Fl[VOp[[2]][[w]][[1]], VOp[[2]][[w]][[2]], R1[[w]], R2[[w]],
        kind1[[w]]], R2[[w]] > k,
       Gl[VOp[[2]][[w]][[1]], VOp[[2]][[w]][[2]], R1[[w]], R2[[w]],
        kind1[[w]]]], kind2[[w]] == 2,
      Which[R2[[w]] <= k, Hl[VOp[[2]][[w]][[1]], R1[[w]], R2[[w]]],
       R2[[w]] > k, Hl[VOp[[2]][[w]][[1]], R1[[w]], R2[[w]]]],
      kind2[[w]] ==
       3, -Which[R2[[w]] <= k,
        Fl[VOp[[2]][[w]][[1]], VOp[[2]][[w]][[2]], R1[[w]], R2[[w]],
         kind1[[w]]], R2[[w]] > k,
        Gl[VOp[[2]][[w]][[1]], VOp[[2]][[w]][[2]], R1[[w]], R2[[w]],
         kind1[[w]]]]]), {w, 1, Length[VOp[[2]]]}];
Eqn = Flatten[{Eqn1, Eqn2}];
VOpt = Flatten[VOpt];
EQN = {Eqn, v0begin};
(*Define Butcher tableau for the Runge-Kutta-Fehlberg 4(5) method*)
Fehlbergamat = {
  {1 / 4}, {3 / 32, 9 / 32}, {1932 / 2197, -7200 / 2197,
   7296 / 2197}, {439 / 216, -8, 3680 / 513, -845 / 4104}, {-8 / 27,
   2, -3544 / 2565, 1859 / 4104, -11 / 40}};
Fehlbergbvec = {25 / 216, 0, 1408 / 2565, 2197 / 4104, -1 / 5, 0};
Fehlbergcvec = {81 / 4, 3 / 8, 12 / 13, 1, 1 / 2};
Fehlbergevec = {-1 /360, 0, 128 / 4275,
  2197 / 75240, -1 / 50, -2 / 55};
FehlbergCoefficients[4, p_] :=
 N[{Fehlbergamat, Fehlbergbvec, Fehlbergcvec, Fehlbergevec}, p];
(*Solve system*)
sol = NDSolve[EQN, VOpt, {t, 0, Time},
  Method -> {"ExplicitRungeKutta",
    "Coefficients" -> FehlbergCoefficients, "DifferenceOrder" -> 4,
    "EmbeddedDifferenceOrder" -> 5, "StiffnessTest" -> False}];
(*sol = NDSolve[EQN,VOpt,{t,0,Time},Method->Automatic];*)

(*General Ehrenfest ODE system obtained by Mathematica (equations coincide with
the ones obtained by Julia)*)
Eqn

(*Plot of the bit-averages in second-order cumulant expansion for
number 15 depending on s(coincides with Julia as well)*)

s = 1.2
```

```
562 Show[Plot[Re[Evaluate[VOpt[[2]] /. sol]], {t, 0, Time},
563   PlotStyle -> Red, PlotRange -> {{0, Time}, {-0.1*s, s*1.1}}],
564  Plot[Re[Evaluate[VOpt[[5]] /. sol]], {t, 0, Time}, PlotStyle -> Blue,
565    PlotRange -> {{0, Time}, {-0.1*s, s*1.1}}],
566  Plot[Re[Evaluate[VOpt[[8]] /. sol]], {t, 0, Time},
567   PlotStyle -> Green, PlotRange -> {{0, Time}, {-0.1*s, s*1.1}}]]
```

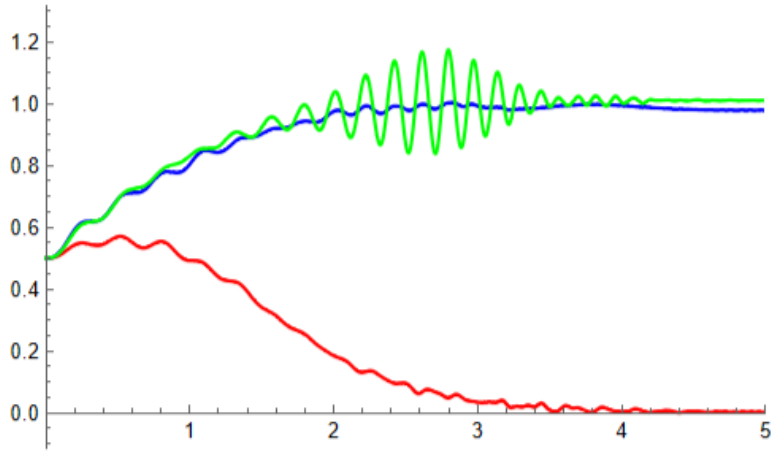

Figure B.1: Bi-prime factorization problem for $\omega = 15$ in second-order expansion obtained via Mathematica.

Appendix C

Implementation of The Quantum Dynamics and QuantumCumulants.jl

```julia
using QuantumCumulants
using QuantumOptics
using OrdinaryDiffEq, ModelingToolkit
using QuantumOpticsBase
using ForwardDiff

# Toy-model ω = 15

# Quantum Cumulants


# define parameters, variables as well as functions
@cnumbers ω n k l T ξ ħ
@syms t::Real
@register r(t)

# traget number, time as well as parameter ξ = Ξ
value = 15
Time = 10.
ξ= 10

# order of cumulant expansion
od = 1

# dynamical bits of a/b
K = 2
L = 1
# total number of dynamical bits
N = K + L

# define Hilbert space
Hn = [NLevelSpace(Symbol(:atom,i),2) for i=1:N]
H = S1(Hn...)

# define transition operators
σ(i,j,w) = Transition(H,Symbol(:σ, w),i,j,w)
```

```
37
38 # write primes in binary representation
39 a = 1 + sum(2^i*σ(2,2,i) for i=1:K)
40 b = 1 + sum(2^j*σ(2,2,j+K) for j=1:L)
41
42 # construct Hamiltonian H(t)
43 # initial Hamiltonian H0
44 H0 = -ξ*sum(σ(1,2,i) + σ(2,1,i) for i=1:N)
45
46 # define s variable as function
47 function S(t)
48    return t/Time
49 end
50
51 # target Hamiltonian Hp
52 Hp = (1*ω - a*b)^2
53
54 # full Hamiltonian H(t)
55 Ham = (1 - S(t))*H0 + S(t)*Hp
56
57 # operators for ODE system
58 ops1 = [σ(1,2,i) for i=1:N]
59 ops2 = [σ(2,2,i) for i=1:N]
60 ops = []
61
62 # 1st order
63 for i=1:N
64    push!(ops,ops1[i])
65    push!(ops,ops2[i])
66 end
67
68
69 me = meanfield(ops,Ham);
70 me_expanded = cumulant_expansion(me,od);
71 mean = complete(me_expanded);
72 mean
73
74 # initial value vector
75 if od == 1
76    u0 = zeros(ComplexF64, 2*N)
77    for i=1:2*N
78       u0[i] = 0.5
79    end
80 end
81
82 @named sys = ODESystem(me_expanded)
83
84 p0 = (ω=>value, n=>N,k=>K,l=>L,T=>Time,ξ=> Ξ,ħ=>1.)
85 prob = ODEProblem(sys,u0,(0.0,Time),p0)
86 sol = solve(prob,RK4())
87
88 t = sol.t;
89
90
91 # Quantum Dynamics
92
93
94 # basis for spin-1/2
```

```
onespin = SpinBasis(1//2);

# some parameters
L1 = Ξ
L2 = L1*1
W = length(t)
s = LinRange(0, 1, W );
Xi = 1.

# composite basis
allspin = onespin
for i=1:(N-1)
   allspin = tensor(allspin, onespin)
end

# Pauli matrices acting on one qubit
sz = sigmaz(onespin);
sx = sigmax(onespin);
sy = sigmay(onespin);

# transition operators
sp = 1/2*(sx + 1im*sy);
sm = 1/2*(sx - 1im*sy);

# identity operator
id = identityoperator(allspin);

# projector onto ith Hilbert space and its identity
opz = 1. /2*(identityoperator(onespin)-sz);
id2 = identityoperator(onespin)

#defining some operator vectors
Sz = []
Sp = []

for i=1:N
   push!(Sz,embed(allspin,i,opz))
end

for i=1:N
   push!(Sp,embed(allspin,i,sp))

end

# a and b in binary representation
A = id
B = id

for i=1:K
   A = A + (2^(i))*Sz[i]
end
for i=1:L
   B = B + (2^(i))*Sz[i+K]
end

# Problem Hamiltonian Hp
HpQ = (value*id-A*B)^2

# some matrices
```

```
sigx = zeros(N,length(s))
sigy = zeros(N,length(s))
sigz = zeros(N,length(s))
Opz = zeros(N,length(s))
Spl = zeros(N,length(s))

sigp = zeros(N)
sigm = zeros(N)

# construction of inital Hamiltonian H0
H0Q = -L1*(embed(allspin,1,sx))

for i=2:K-1
   H0Q = H0Q - L1*(embed(allspin,i,sx))
end
for i=K:N
   H0Q = H0Q - L2*Xi*(embed(allspin,i,sx))
end


# linear interpolation with s = t/T
# exact Energy spectrum of total Hamiltonian H = (1 -s)* H0+s*Hp
Eall = zeros(length(s), 2^N);
for i=1:length(s)
   HQ = (1-s[i])*H0Q+s[i]*HpQ;
   Eall[i,:] = eigenstates(DenseOperator(HQ))[1]
end

# exact ground state
psi_g = []
for i=1:length(s)
   HQ = (1-s[i])*H0Q+s[i]*HpQ;
   push!(psi_g,eigenstates(DenseOperator(HQ))[2][1])
end

# total evolution time
T = Time

# initial state , i.e. ground state of H0
psi0 = eigenstates(DenseOperator(H0Q))[2][1]

# time - dependent Hamiltonian as function
function Ht(t, psi)
return (1-t/T)*H0Q+t/T*HpQ
end

# time evolution using time-dependent SchrÃ¶dinger equation
tout1 , psi1 = timeevolution.schroedinger_dynamic(s*T, psi0 , Ht; maxiters=1e7);

# correct ground state solution of target Hamiltonian Hp
psiL = eigenstates(DenseOperator(HpQ))[2][1]

# overlaps, hence, fidelity and "remaining in ground state"
P_sol1 = [abs.((dagger(psi1[i])*psiL)).^2 for i = 1: length(s)]
P_sol2 = [abs.((dagger(psi1[i])*psi_g[i,1])).^2 for i = 1: length(s)]


```

```
for i=1:N
   for u=1:length(s)
      sigx[i,u]=real.(expect(embed(allspin,i,sx),psi1[u]))
      sigy[i,u]= real.(expect(embed(allspin,i,sy),psi1[u]))
      sigz[i,u]= real.(expect(embed(allspin,i,sz),psi1[u]))
      Opz[i,u]= real.(expect(Sz[i],psi1[u]))
      Spl[i,u]= real.(expect(Sp[i],psi1[u]))
   end
end


# Plots

using PyPlot

figure(figsize=[12, 8])
PyPlot.xticks(fontsize=25)
PyPlot.yticks(fontsize=25)
PyPlot.xlim(0,1.2)
PyPlot.ylim(0.,1.3)
PyPlot.xlabel("s",fontsize=25)
PyPlot.ylabel(L"⟨ a_i ⟩,⟨ b_j ⟩$",fontsize=25)
PyPlot.xticks(fontsize=25)
PyPlot.yticks(fontsize=25)

#Quantum Dynamics
for i=1:N
   if i == 1
      PyPlot.plot(s,Opz[i,:],linewidth=8,alpha=0.25,label = L"$⟨ a_1 ⟩_{QD}$",color = "C0"
          )
   elseif i ==2
      PyPlot.plot(s,Opz[i,:],linewidth=8,alpha=0.25,label = L"$⟨ a_2 ⟩_{QD}$",color = "C1"
          )
   else
      PyPlot.plot(s,Opz[i,:],linewidth=8,alpha=0.25,label = L"$⟨ b_i ⟩_{QD}$",color = "C2"
          )
   end
end

#Quantum Cumulants
for i=1:N
   if i == 1
      PyPlot.plot(t/T, real.(sol[σ(2,2,i)]),linewidth=3,alpha = 1,label = L"$⟨ a_1 ⟩_{QC}$
          ",color = "C0")
   elseif i == 2
      PyPlot.plot(t/T, real.(sol[σ(2,2,i)]),linewidth=3,alpha = 1,label = L"$⟨ a_2 ⟩_{QC}$
          ",color = "C1")
   else
      PyPlot.plot(t/T, real.(sol[σ(2,2,i)]),linewidth=3,alpha = 1,label = L"$⟨ b_1 ⟩_{QC}$
          ",color = "C2")
   end
end



legend(fontsize=25,loc=4)
savefig("Cumulants_1st_order_15.png")
```